THE ROLE OF CORTICAL SPREADING DEPOLARIZATIONS IN TRAUMATIC BRAIN INJURY OUTCOME

by

Refa't A Abo Ghazleh

Submitted in partial fulfilment of the requirements
for the degree of Doctor of Philosophy

at

Dalhousie University
Halifax, Nova Scotia
March 2020

TABLE OF CONTENTS

LIST OF FIGURES

ABSTRACT

Traumatic brain injury (TBI) is a blow to the head that disrupts normal brain function. Concussion is a common clinical syndrome that can follow mild TBI. Concussion is associated with a variety of disabling neurological symptoms that may last for months and even years. Despite growing interest in understanding the pathophysiology of concussion, the electrophysiological events that occur during mild TBI and underlie concussion are unknown.

To investigate the electrophysiological changes underlying concussion, we recorded epidurally from rats immediately following mild TBI. We confirmed that spreading depolarizations (SDs), and not seizures, are a common event after a mild TBI, and mostly occur within the first two minutes after an impact in one or both brain hemispheres. Animals with SDs required a longer time to resume mobility. Furthermore, TBI-induced SDs have a larger amplitude compared to triggered SDs in anesthetized and unanesthetized animals.

Next, we used intravital microscopy to study the effect of triggered SDs on blood-brain barrier (BBB) integrity and neurovascular coupling. TBI-exposed animals (but not control) showed a significant increase in BBB permeability within two hours after stimulation. The cerebral blood flow response to SDs in TBI-exposed rats was similar to that recorded in controls except the late hyperemia phase, which was significantly shorter in TBI.

To study sudden death in this TBI model, we recorded the electrical activity from the cortical hemispheres and brain stem. Within two minutes of impact, we observed SDs and non-spreading depression of electrical activity in both brain hemispheres and the brain stem. Respiration gradually slowed and eventually ceased when a depression of electrical activity was longer than 2 minutes. Cardiac arrest followed respiratory arrest and occurred around 18 minutes after TBI.

In summary, depression of brain activity is a common immediate electrophysiological change following mild TBI and may underlie signs and symptoms of concussion and be associated with immediate catastrophic death. My study proposes SD as a potential diagnostic and therapeutic target in TBI.

LIST OF ABBREVIATIONS USED

ACSF	Artificial Cerebrospinal Fluid
ASH	Aneurismal Subarachnoid Hemorrhage
BBB	Blood-Brain Barrier
BS	Brain Stem
BK_{Ca}	Calcium-Activated Potassium Channels
CNS	Central Nervous System
COX_2	Cyclooxygenase 2
CSDs	Cortical Spreading Depolarizations
CTE	Chronic Traumatic Encephalopathy
EB	Evans Blue
ECs	Endothelial Cells
ECoG	Electrocorticography
EEG	Electroencephalography
ECG	Electrocardiogram
ECM	Extracellular Matrix
iGluR	Ionotropic Glutamate Receptors
GABA	Gamma Aminobutyric Acid
KATP	ATP-Sensitive Potassium Channels
KCl	Potassium Chloride
LFP	Lateral Fluid Percussion
LDF	Laser Doppler Flowmeter
MMPs	Matrix Metalloproteinases
mGluR	Metabotropic Glutamate Receptors
mTBI	Mild Traumatic Brain Injury
Na-Flu	Sodium Fluorescein
NMDARs	N-Methyl-D-Aspartate Receptors
NO	Nitric Oxide
nNOS	NO Synthase
NVC	Neurovascular Coupling
NVU	Neurovascular Unit

PGE2	Prostaglandin E2
PTC	Post-Traumatic Coma
PTS	Post-Traumatic Seizures
PTE	Post-Traumatic Epilepsy
rCBF	Regional Cerebral Blood Flow
RR	Respiratory Rate
SC	Subcutaneous
SAH	Subarachnoid Hemorrhage
SDH	Subdural Hematomas
SDs	Spreading Depolarizations
TBI	Traumatic Brain Injury
TGF-β	Transforming Growth Factor-β
TSD	Terminal Spreading Depolarization
WD	Wallerian Degeneration

ACKNOWLEDGEMENT

I would like to express my deep gratitude to my supervisor, Prof. Alon Friedman, whose expertise, knowledge, and passion for science, has taught me how compelling and rewarding research can be. With your support through my PhD journey I learned that nothing is impossible; do not give up, take your time, think about it, and if they did it, we can do it. Your enthusiasm for research inspired and motivated me and your patience and generosity touched me. I consider you a brother and a friend. Thank you for this experience.

Thank you to my committee members Dr. William Baldridge, Dr. Victor Rafuse, and Dr. Kazue Semba for overseeing my work and contributing to my development as a researcher. Also, thank you all for the work and life advice you gave me during our occasional one-on-one conversations. Thank you so much for your time and invaluable efforts.

Dr. William Baldridge, thank you so much for your teaching and mentoring during the neuroscience course, I learned a lot, and you were amazing professor.

Thank you to my external examiner Dr. Jed Hartings for your time, efforts, and contribution to my thesis. I appreciate it.

Ms. Kay Murphy, thank you for your friendship, knowledge, and all the help with day-to-day challenges in the lab. We are so lucky in the lab to have a noble person like you. Your help is invaluable, your generosity beyond the imagination and your passion above the expectations. Thank you for your intellectual input and assistance with technical issues. Thank you for being my teacher, friend, advisor and sister. Words cannot express how grateful I am for your help and support over the four previous years. Thanks a lot.

Dr. Ofer Prager, thank you my friend for your time and help, I appreciate it.

Evyatar Swissa, thank you very much for teaching me the craniotomy.

Many thanks to current and past members of the Friedman lab.

I would like to give heart-felt thanks to my dear mother, family and friends for their ever-present support and unconditional love as I pursued personal endeavors in education.

I wish to dedicate this thesis with affection to the memory of my father, Ahmad Abo Ghazleh, who always believed in science and education. You are gone but your belief in me has made this journey possible. May Allah have mercy on your soul.

Chapter 1: Introduction

1.1 Traumatic Brain Injury

Traumatic brain injury (TBI) is an insult to the brain from an external mechanical force, and it can result in temporary or permanent impairment of cognitive, physical, and psychosocial functions (1). In the United States, TBI accounts for over 30% of all injury deaths (2). Canada is estimated to have a similar number of injuries, resulting in this problem reaching epidemic proportions. Approximately 160,000 people experience TBI annually, and 1.5 million Canadians live with the effects of TBI (3). In 2021, it is estimated that 640,100 people will suffer a TBI in Canada and in ten years this number is expected to exceed 730,300 (4).

Mild traumatic brain injury (mTBI) is very common. The global incidence of mTBI has been estimated to be 42 million people annually (5,6) TBI can be caused by various mechanical forces including direct physical insults, falls, motor vehicle collisions, and sport injuries. TBI is associated with neurophysiological and neurochemical changes lasting for days, months, and even years post-trauma. These changes vary in severities and include dysregulation of neurotransmitters, the release of inflammatory molecules, and brain cellular death (7). TBI is a significant threat to cognitive health and has short and long-term effects. TBI has adverse clinical outcomes; including the increase in risk of developing post traumatic epilepsy (PTE) (8), Alzheimer's disease (9,10), permanent disability, and even death (2). Despite a growing body of research, there is still an incomplete understanding of the etiology of TBI, with limited treatment interventions for those living with permanent disabilities.

1.2 TBI and Neuronal Injuries

There are several structural, physiological, and biochemical modifications that occur in the brain after a head injury and this may increase the susceptibility for further brain tissue damage.

A neuron is composed of a cell body, dendrites, and an axon. If the cell body is damaged, the probable result will be neuronal death due to the loss of proper function of the cell (11,12). Neuronal loss can also occur if there is injury to the axon close to the cell body, and ultimately both parts will deteriorate and degenerate, a process called retrograde

degeneration (12). In contrast, if the injury to the axon is away from the cell body, then the distal axonal segment will deteriorate and degenerate (Wallerian or anterograde degeneration) (12,13), and the remaining proximal axon stub will regrow and regenerate a new axon.

Wallerian degeneration (WD) is a process of degeneration of the axonal segment distal to the point of injury that is isolated from the soma, following a cut or crush to the nerve fibers in both the central nervous system (CNS) and the peripheral nervous system (PNS). In 1850 Augustus Waller observed that following a transection of a nerve, the distal portion of the nerve undergoes progressive degeneration (14,15). WD usually begins within 30 minutes of injury (13) and varies across species. The process of WD includes a cellular and molecular pattern of events, such as the breakdown of the axonal membrane, disassembling of the axonal cytoskeleton and degradation of its components, and invasion of phagocytic cells to the site of injury (16,17). WD is usually followed by regeneration of the injured axon in the PNS, but the failure of injured axons to regrow in the CNS is the dominant phenomenon (16). The rate of WD is faster in the PNS than the CNS due to the speed or failure of the CNS to remove myelin debris (18,19).

The molecular mechanism that regulates axon destruction is still unclear. An increase in intra-axonal calcium has been seen following axonal injury (20). The increase of Ca^{2+} influx leads to activation of the intracellular Ca^{2+}-dependent protease calpain, that leads to cleaving of the axonal neurofilament and microtubule components (tubulin) (21) and cytoskeleton destruction (22). Following the breakdown of the axonal membrane and the cytoskeleton (23), axonal loss triggers degeneration of the myelin sheath and macrophage influx (24).

Calcium channel inhibitors or chemical inhibition of calpain proteases prevent the increase in intra-axonal Ca^{2+} and attenuates axonal degeneration (22,25). It has been suggested that Na^+/K^+ ATPase failure and Na^+ influx through persistent Na^+ channels promote Ca^{2+} influx into the injured axon. While the depolarized membrane will open voltage-gated Ca^{2+} channels, the increase of intracellular [Na^+] will reverse the normal direction of Na^+/Ca^{2+} exchanger activity, leading to an increased influx of Ca^{2+} (26–28).

At the dendritic level, a study showed that dendrites in a *Drosophila* model were regenerated after being removed from a neuron (29). When a neuronal cell body is injured,

a process known as chromatolysis occurs. The chromatolysis is the dissolution of Nissl bodies in the neuronal soma, that is triggered following axotomy and neuronal injuries (30). Many significant morphological changes take place in nerve cells during chromatolysis including an increase in the size of the nucleus, the migration of the nucleus to the cell body periphery, a loss of the Golgi apparatus, and an increase in lysosomal structures, that can be followed by cell apoptosis (30–32). However, the significance of the chromatolysis and the changes linked to it are still unknown.

In the CNS, an oligodendrocyte myelinates several axons. However, oligodendrocytes have little or no ability to remove debris after axonal injury. When an oligodendrocyte loses its axonal contact after injury, programmed cell death of the oligodendrocyte can be initiated and the amount of debris increased. Furthermore, the blood-brain barrier prevents macrophages from entering the brain from the circulatory system (33). The debris releases many inhibitory molecules that prevent axonal growth such as myelin associated glycoprotein (MAG) and oligodendrocyte myelin glycoprotein (Omgp). The proximal stumps of the injured axons can only form a short sprout, they become swollen and are known as retraction bulbs that do not grow (18,34–36). Thus, there is a poor clearance of myelin, axonal fragments, oligodendrocytes, and other debris in the CNS, and this will decrease the chance of the regeneration process.

In the PNS, injured axons provoke neurons to activate Schwann cells via different signaling pathways (37). Schwann cells then divide and initiate phagocytosis of myelin and axonal debris. At the same time, Schwann cells secrete molecules to attract macrophages (38). Macrophages migrate and have access to the injured site to help Schwann cells clean and remove all debris (15,33,38). The distal part of the axon that separated from the soma will degenerate. Therefore, WD in the PNS leads to a rapid clearance of debris and enables rapid axon regeneration (23). The proximal part of the axon is still attached to the cell body and will be sustained with the myelin sheath and regrow in a Schwann cell-lined endoneurial tube (band of Bunger). Furthermore, Schwann cells produce growth factors that enhance axon growth within the tube. When the axons reach their targets, they are able to resume their functional connections (12,13,18,34,35,39–41). In the PNS, rapid WD results in an extracellular environment that promotes axon regeneration. Slow WD in the CNS results in a prolonged presence of myelin-associated inhibitors that likely contribute

to the failure of axons to regenerate (23). In addition, following injury, glutamate receptors are over activated, leading to the damage and death of neurons, a process known as excitotoxicity (42). Thus, over activation of these receptors increases intracellular Ca^{+2} (43), leading to the release of many enzymes, such as phospholipase (PLA) and protease. These enzymes damage different cell structures such as the cell membrane, DNA, and the cytoskeleton (44,45), and enhance the initiation of apoptosis.

1.3 Spreading Depolarizations

1.3.1 History

In 1944, the physiologist Leão while studying epilepsy in the rabbit, noticed a sudden temporary cessation of electrocorticographic (ECoG) activity accompanied by a large negative slow potential change recorded with extracellular electrodes, that later became known as spreading depolarizations (SDs) (46). The potential change was slowly propagating through the cerebral cortex. The depression of electrical activity across the cortex was described as a cortical spreading depression (46,47). The cortical spreading depolarization (CSD) and the depression of brain activity have been recognized as pathologic disruptions in cortical electrical activity that follow a variety of neurological diseases and brain injuries. CSD has been studied in animal models and recently in humans, and it has been recognized and described as a massive neuronal depolarization resulting in the loss of neuronal activity accompanied by significant changes in cerebral blood flow and brain tissue perfusion (48–50). Although there is a considerable amount of literature published about SDs since 1944, the biophysical mechanism of SDs is still not completely understood.

1.3.2 Definition and Characteristics of SDs

Spreading depolarizations is a generic term for the spectrum of waves initiated and propagated in the CNS, characterized by abrupt and near-complete sustained neuronal depolarization (48,51), observed as a large slow potential change in the extracellular space (52,53) and it propagates at 1-9.5 mm/min across the brain (54,55). During SDs, neurons cannot fire action potentials, as the sustained depolarization is above the threshold, and the membrane channels that generate action potentials are inactivated (56). The propagation of

SD waves in the gray matter of the CNS causes swelling of neurons, distortion of dendritic spines (48), and silencing of the brain's electrical activity (spreading depression) (46).
SDs were previously implicated as the relevant pathological waves propagated across a migraine brain (57). In 2002, Anthony Strong and colleagues recorded SDs for the first time from human brain following a TBI (58) and intracerebral hemorrhage (59). Furthermore, SDs occur abundantly in individuals with aneurismal subarachnoid hemorrhage (ASH), delayed ischemic stroke, subarachnoid hemorrhage (SAH) (52), or malignant hemispheric stroke (60).

1.3.3 Mechanisms of Initiation

SDs can be triggered experimentally in an animal model using mechanical or electrical methods as well as using various noxious conditions, such as potassium, glutamate, sodium pump inhibitors, hypoxia, and ischemia (48,61–64). However, it is unclear if there is any difference between SDs initiated spontaneously following a TBI and other neurological disorders and those triggered experimentally in labs. Grafstein in 1956 established a proposed mechanism for SDs. She suggested that during SDs, there is a efflux of K^+ from depolarized neurons to the extracellular space beyond the critical value (> 15 mM), and this has been the most accepted hypothesis (64). But assuming that K^+ is the major player in this process is at odds with decreasing extracellular K^+ during the time course of SDs (65). There are extreme changes in ion concentrations and neurotransmitters, most importantly glutamate, during SDs (66,67). There is an implicit assumption that during SDs there is a near complete neuronal depolarization accompanied by a loss of electrical activity (68). The assumption was disputed by a recent rodent study that recorded intra-somatic and intra-dendritic signals simultaneously from a hippocampal pyramidal neuron. The study revealed that not all parts of the neuron are inactivated during SDs, and that neurons can maintain their integrity and electrical function. At the dendritic level, just a specific part of its membrane depolarized during SD. Furthermore, the electrical response may still be intact in some parts of pyramidal cells engaged in SDs even if electrical activity is not detected in the soma (51). The activation of NMDARs located in dendrites of pyramidal cells is a key factor for initiation of SDs (69).
When brain tissue is exposed to stimuli that initiates SD, neurons will be depolarized, and

the concentration of K^+ in the extracellular space will increase (69,70). The minimum extracellular [K^+] at which SDs could be induced is 15 mM (71). It had been hypothesized that high extracellular [K^+] will activate and increase net inward current, resulting in a cycle that increases neuronal depolarization and extracellular [K^+]. While K^+ is released from the cells to the extracellular space (64), ions such as Na^+, Ca^{+2}, and Cl^- will enter cells followed by water influx, that will cause cell swelling (Figure 1.1). The extracellular [K^+] rapidly increases within 2-3 second to 55 mM, whereas extracellular [Na^+] rapidly decreases to 60 mM, [Cl^-] decreases to 75 mM, and [Ca^{+2}] also decreases to 0.08 mM (72).

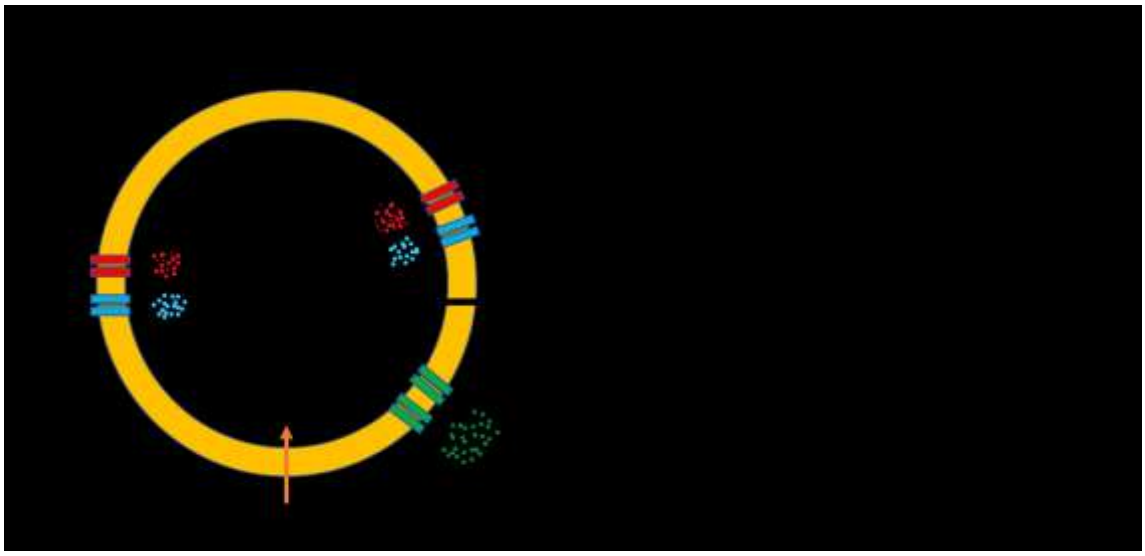

Figure 1.1. Mechanism of spreading depolarization in the neuron.
During SD, there is an abrupt-near complete sustained massive neuronal depolarization, observed as a slow potential change (SPC) in the extracellular space (ECS). Neurons cannot fire action potentials (AP), as the sustained depolarization is above the inactivation threshold, at which the membrane channels that generate AP are inactivated.

Activation of voltage-gated Ca^{+2} channels in presynaptic terminals will enhance the release of glutamate from cortical pyramidal cells synapses (73,74). Glutamate is well known as the main excitatory neurotransmitter activating N-methyl-D-aspartate receptors (NMDARs), leading to an increased net inward current that exacerbates neuronal depolarization (66,75,76). It is worth noting that activation of NMDARs will sustain and prolong the duration of the increase in dendritic Ca^{+2} following SDs. It is well known that an increase in intracellular [Ca^{+2}] will initiate acute neuronal injury and even neuronal death (77). Intracellular [Ca^{+2}] first increases in distal dendrites then propagates toward the

soma, but the intracellular [Ca^{+2}] returns to baseline first in the soma then after 2 minutes in the dendrites (78).

Astrocytes have a role in this process. The glial Na^{+}-K^{+} pump and inwardly rectifying K^{+} channels (KIR) have a role in buffering the increase in extracellular [K^{+}] (79). Furthermore, glutamate transporters on astrocytic end feet efficiently remove glutamate from the synapses (80).

As mentioned previously, SDs can be triggered and blocked experimentally. SDs can be initiated by activation of NMDARs (62). SDs triggered in the cerebral cortex using KCl or electrical stimulation have similar pharmacology, in which NMDAR antagonists can block SDs triggered using either methods (70,75,81). This may indicate that NMDARs are crucial for initiation of SDs (82), and at the same time they affect the propagation of SDs (81,83).

1.3.4 Mechanisms of Propagation

Depolarization waves spread throughout brain cells causing neuronal swelling, an acidic environment, and a global loss of hyperpolarization (46,84). The propagation of SDs across the cerebral cortex and the brain is still controversial. While many hypotheses have been suggested to explain this process, the diffusion of chemical substances is the most widely accepted to explain the slow propagation of SDs across the brain, specifically the diffusion of K^{+} within the interstitial space (64,72). Thus, the increase in the concentration of K^{+} and glutamate (66,73–76) in the extracellular space during SDs will cause excitability in neighboring neurons and enhance the propagation of SDs to the surrounding tissue across the brain (48,84). Kramer and his colleagues described the disruptive effect of SDs on normal cerebral vascular responses, in which hypoperfusion will dominate the surrounding areas, leaving the neurons in an energy deprived state. This state can cause the cessation of the transmembrane ionic exchanges. This injurious state that is created by SD waves, continues across the brain until healthy tissue with enough energy restores homeostasis and stops SD waves (67).

1.3.5 SDs in Brain Injury

Spontaneous CSDs have been described in sedated patients after severe injuries to the brain, including TBI (53,85,86) subarachnoid hemorrhage (52,87), and malignant stroke (54,88). Under these conditions, it has been shown that CSDs may be associated with an

impaired vascular response (54,89) and worse clinical outcome (90,91). SDs were recorded in 53% of TBI patients who received craniotomies for hematoma evacuation and decompression 1-week post-trauma (85). It has been suggested that prolonged duration of SDs is one of the major factors behind the formation of cortical lesions, that might be attributed to hypoperfusion and impaired neurovascular coupling during SDs (53). The monitoring and blockade of SDs is one of the major steps to assess a patient's progress and to avoid a secondary brain injury (85).

In addition to SDs, there are different clinical signs and symptoms reported immediately following TBI, that are known as a concussion. There still is an incomplete understanding of the etiology of these signs and symptoms (92). Although there is still considerable controversy surrounding the definition of concussion, there is a general consensus that the term concussion represents different types of head trauma associated with pathophysiological changes (93,94). Concussion is seen with variable clinical, cognitive signs and symptoms. It may occur with or without loss of consciousness, seizures, confusion, dizziness, and sometimes normal structural imaging (95). Many hypotheses were suggested to explain these signs and symptoms, but unfortunately none explained all the observed findings, especially the loss of consciousness after TBI.

1.3.6 SDs and Seizures

The relationship and interaction between SDs and seizures is still controversial. The hyperexcitable state and firing of groups of neurons during seizures and the neuronal deactivation state during SDs make the relationship more complex, especially since they are following each other interchangeably. While neurons fire action potentials synchronously during epileptic activity (96), spreading waves of electrical brain silence (spreading depression) are observed during SD (85,90,97).

Seizures and CSDs were reported following an acute injury to a human brain, and they both have a role in the exacerbation of tissue damage (58,98–100) by inducing inverse neurovascular coupling and decreasing the regional cerebral blood flow. Propagating of spreading depolarization into the penumbra of ischemia induces a decrease in cerebral blood flow and will increase the size of ischemia and expand it (85,100–102). Recent

ECoG recordings from patients with ASH and acute TBI demonstrated that SDs occur more frequently compared to seizures (58,90), and are associated with worse outcomes (90,91). In contrast to chronic epilepsy that favors an episode of ictal epileptic events over that of SDs, patients with acute brain injury and ASH were found to have the occurrence of SDs instead of ictal epileptic events (58,90). SDs and seizures can follow each other interchangeably in which SDs can precede or follow seizures (103). However, triggered SDs were found to enhance neuronal excitability and facilitate the seizure activity in epileptic human brain tissues (104–106). In anesthetized rats, triggered seizure activity can lead to single and repetitive SDs (106).

Mechanistically, NMDARs have an important role in both epileptiform activity and SDs. Antiepileptic antagonists of the NMDARs, such as ketamine, were found to halt SD activity. However, antiepileptics without NMDA properties, such as diazepam, did not affect SD activity (107).

1.4 The Blood-Brain Barrier (BBB)

The BBB is a unique anatomical and physiological selective protective barrier, formed in the CNS to separate it from the systemic circulation (108). The existence of this barrier in the brain was first described by Paul Ehrlich in 1885.

1.4.1 Anatomy and Physiology

The BBB is formed by endothelial cells (ECs) that act as a principle barrier unit; which are connected to each other via tight junctions (109). Cell to cell interactions together with other cellular elements such as astrocytes, pericytes, and neurons (Figure 1.2), help the BBB to protect the brain and maintain normal neuronal functions (110,111). The ECs and the surrounding cellular elements form a barrier and neurovascular unit that have many functions such as: (1) regulation and maintenance of the ionic and molecular components of the extracellular environment in the brain, (2) maintain the transport of oxygen and other nutrients between the brain and the blood stream and (3) protect the brain from different pathogens and toxins (109,112).

ECs are simple squamous epithelial cells derived from mesoderm, that line the interior surface of blood vessels and regulate the flow of substances into and out of the brain (113). The endothelial cells of BBB are 39% thinner than the endothelial cells of skeletal muscles

(114). ECs in the CNS are held together by extensive tight junctions that allow them to tightly regulate the movement of ions and molecules to and from the brain (115). Furthermore, the mitochondrial content of ECs in the CNS is greater than cells in all non-neural tissues, suggesting that this increase is due to the energy requirements needed to maintain the ion gradient between the blood plasma and brain extracellular fluid (116).

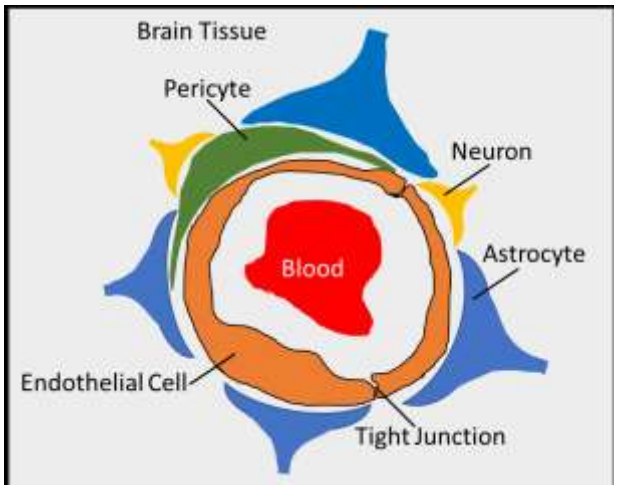

Figure 1.2. Endothelial cells (ECs) and BBB cellular components.
Schematic representation of the BBB. The BBB is formed primarily by brain endothelial cells, which are connected via tight junctions. The BBB maintains the appropriate ionic composition of the interstitial fluid of the brain and regulates selective diffusion of substances between the brain and the peripheral circulation.

1.4.2 BBB in Disease

BBB dysfunction is common in various neurological disorders, including status epilepticus, stroke, and TBI (117,118). Opening of the BBB can also induce epileptogenesis and sustains or even aggravates the epileptic condition (119,120). The low threshold for seizure and epilepsy has been suggested to be related to an increase in BBB permeability that can last for weeks and even years (111,121). However, the cascade of processes that occur during epileptiform activity and those that may affect BBB integrity are still a matter of investigation.

Albumin is a water soluble protein found in blood plasma, and normally cannot pass into the brain through the BBB (122). The leakage of albumin from the blood stream to brain tissue has been determined to be an indicator of BBB dysfunction (122–125). Albumin staining has been reported in the brains of patients with drug resistance epilepsy, cerebral

focal lesions (126,127), and vascular abnormalities (126). Moreover, Seiffert and colleagues showed that BBB disruption by direct cortical application of albumin can lead to epileptiform activity in rats (123).

Transforming growth factor-β (TGF-β) proteins are multifunctional cytokines that modulate a variety of functions including the regulation of cell growth, cell differentiation, and apoptosis (128). TGF-β is up-regulated in many acute or chronic central nervous system disorders including brain trauma (129) and vascular injury (121).

Albumin leakage from the blood to the brain occurs following impaired integrity of the BBB. Albumin then binds to the TGF-β receptors of astrocytes, resulting in a transformation and transcriptional change of astrocytes (129,130).

Activation of TGF-β signaling causes a down-regulation of inward-rectifying potassium (Kir 4.1) channels (131,132) and glutamate transporters (133). These changes in astrocytic function cause an increase in neuronal excitability as a result of an accumulation of extracellular K^+ and glutamate.

1.4.3 Measuring BBB Integrity

In 1885, Paul Ehrlich was the first to observe the lack of staining in the brain and spinal cord after an intravenous injection of intravital dyes while the peripheral organs were stained. Later in 1913, Edwin Goldmann (one of Ehrlich's students) found that the brain of an animal was stained, but not the rest of the body, after a dye injection into the cerebrospinal fluid (CSF), suggesting that there was a barrier between the brain and the rest of the body. In recent years, there has been increased interest in the BBB and its role in neurological disorders but to test the permeability of this delicate barrier requires appropriate tracing materials and methods. Different methods have been used to study BBB integrity, and the most common practical affordable method in experimental models is the intravenous injection of tracers with a molecular weight (MW) greater than 180 Da. The molecular weight of the tracer is an important factor to prevent passage across the BBB (134). There are tracers and software that can be used to evaluate the degree of the extravascular leakage (135). Among those tracers, Evans blue (MW 961 Da) is still the most commonly used tracer to verify BBB integrity (134,136,137). Sodium fluorescein (Na-Flu, MW 376 Da) is one of the smallest markers used for assessment of BBB integrity

(134,136–141). Both Na-Flu and EB have fluorescent properties, and they can be detected by a fluorescent microscope (excitation at 440 nm and emission at 525 nm) (136). Compared to Na-Flu, EB has a higher affinity for serum albumin and a high-molecular complex is formed (EBA 68500 Da) (138,142,143). The molecular complex that is formed between EB and serum albumin cannot pass through the BBB, making it a robust model to use as a marker for BBB integrity. Although EB is more commonly used, Na-Flu is less toxic (144). It is worth noting that EB is slowly excreted from the circulating blood by the liver (145). It is gradually eliminated from the plasma, and a rapid drop is achieved after 24 hours. After 3 days, it reaches a level insufficient for detection of BBB dysfunction (146). Na-Flu is metabolized by the kidneys and is excreted from the blood through the urine, and systemic clearance is complete 48-72 hours after the administration (138,147). Recently, BBB permeability was assessed in humans by quantitatively analyzing magnetic resonance imaging (MRI), with the advantage of localizing BBB leakage in the brain (148). There is a growing interest in the significance of BBB permeability as a biomarker and target for treatment in neurological disorders.

1.4.4 SDs and the BBB

The relationship between SDs and disruptions in the BBB is not well known. It has recently been suggested that there is a relationship between SDs and the BBB, and it is mediated by a family of proteolytic enzymes called matrix metalloproteinases (MMPs) (149).

MMPs are members of an enzyme family (proteolytic enzymes) that digest components of the extracellular matrix (ECM) such as the interstitial and basement membrane collagens and cell surface receptors (150). MMPs have multiple roles in the normal immune response to infection (151), and a key role in several processes at the cellular level such as cell proliferation, cell to cell interactions, differentiation, and cellular death (152).

An effect was observed after the release and activation of MMPs following intracerebral hemorrhage, stroke, brain tumor, and TBI (150,153–156) with an obvious effect on the integrity of the BBB. MMPs have been injected into the brains of rats, and increasing capillary permeability was observed (153). The change in the BBB permeability was attributed to the destruction of collagen in the basal lamina, and the damage is proportional

to the amount of enzyme activation and the MMPs inhibitors that reduce extracellular matrix proteolysis and protect the BBB (153).

It has been suggested that CSDs cause prolonged MMP-9 activity that leads to BBB dysfunction and vascular leakage that can be suppressed by an MMPs inhibitor (149). In the previous study, following 3-6 hours of triggered SDs, the level of MMP-9 was increased, reaching the maximum at 24 hours and lasting at least 48 hours. Cerebral vascular leakage of plasma protein was detected after 3 hours of SDs and lasted at least 24 hours. Protein leakage from cerebral vessels was not detected in MMP-9-null mice, indicating that MMPs were a predisposing factor for the initiation of the BBB disruption process. The study observed that MMP-9 activation was associated with the loss of the basement membrane and tight junction proteins, indicating disruption of the BBB (149). In another study, triggering CSDs in rats using 3 mg of solid KCl caused an increase in the number of pinocytic vesicles in endothelial cells and swelling of the end feet of astrocytes which indicates that there could be an alternative mechanism in which SDs contribute to BBB dysfunction (157). The increase in extravasation of plasma protein as a result of the KCl application itself was not excluded as a possible mechanism (158).

1.5 Neurovascular Coupling

1.5.1 History

Early theories suggested that the systemic circulation controlled the cerebral blood flow, and the brain played no role in controlling its own blood supply. In 1890, Roy and Sherrington discovered that the brain produced metabolites which diffused to the surrounding vessels and this increased the blood flow to the activated brain (159). In the early 20th century, Craigie's work supported the idea that increased blood flow to the brain increased the vascular density across different regions in the brain (160). The development of diffusible tracers provided a tool for quantitative measurement of the blood flow and provided evidence for the increase of CBF in response to an activated brain region (161). Recently MRIs have been used as a non-invasive technique for monitoring CBF in humans (162), particularly using the blood oxygenation-level dependent (BOLD), reflecting changes in cerebral blood flow and cerebral metabolic rate of oxygen consumption.

1.5.2 Definition and Characteristics

The brain uses approximately 20% of the body's energy which is the largest amount of any organ (163). Glucose is the form of energy used by the healthy brain to maintain and fuel cerebral activities. Lactate can also fuel brain activities but lactate passes through the BBB at a much slower rate as compared to glucose which crosses rapidly (164). During an increase in brain activities, blood flow to the brain will rise and can be accompanied by cerebral vasodilation to facilitate the response to the cells energy requirements.

The phenomenon of an increase in regional cerebral blood flow (rCBF) in response to physiological neuronal activation and a decrease rCBF in response to neuronal deactivation is called neurovascular coupling (NVC) (135,165–167). The coupling process is provided by cell structures that link and maintain dynamic interactions with each other, including neurons, astrocytes, pericytes, and vascular smooth muscle cells (VSMC) (168,169). All these components form a neurovascular unit (NVU), Figure 1.3.

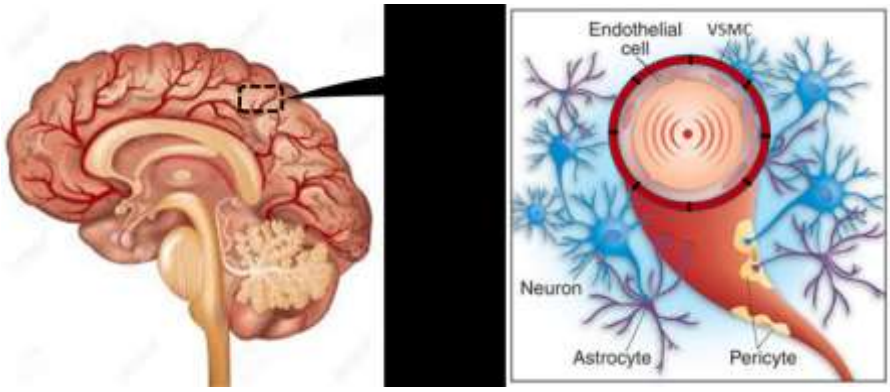

Figure 1.3. Schematic representation of the NVU.

The schematic drawings above show the components of the NVU: neurons, astrocytes, endothelial cells of BBB, vascular smooth muscle cells (VSMC), pericytes and extracellular matrix components. The NVU regulates the delivery of blood flow to the brain and is responsible for maintaining the homeostasis of the cerebral microenvironment, ensuring optimal functioning of neurons and other brain cells. (Modified from Flaumenhaft and Lo, 2006).

One of the most important functions of the NVU is to regulate the transport and diffusion of substances and molecules across the endothelial cells of the BBB depending on the energy requirements and metabolic status of the brain (170).

The link between brain activity and the increase in blood flow to the brain has been observed for decades (159), but there is controversy as to which component is dominant in the NVC process. There are many questions that require answers: Which component has the role of immediate vascular response (within a second) or late response within a few seconds following neuronal activation?

An explanation for the autoregulatory rapid response mechanism of NVC is neurotransmitters which have been proven to play an important role in controlling neuronal signaling (171). Neurons and astrocytes both respond to an increase in the neurotransmitter glutamate in the extracellular space, suggesting there are different mechanisms by which neuronal and astrocytic signaling controls cerebral blood flow in response to changes in brain activities (171–176).

1.5.3 Underlying Mechanisms

The anatomical association between neurons, astrocytes, and cerebral vessels led researchers to explore their role in the NVC process. In general, neurons and astrocytes respond to the increase in extracellular glutamate released from presynaptic terminals (171,176). When presynaptic terminals are stimulated, glutamate is released into the extracellular space, and this activates postsynaptic glutamate receptors in both neurons and astrocytes (171). In postsynaptic neurons, glutamate activates ionotropic glutamate receptors (iGluR), which increases the cytosolic calcium concentration (176). Intracellular Ca^{2+} will activate neuronal nitric oxide synthase (nNOS), that causes NO to act directly on the parenchymal arterioles as a dilator (172,177–179). It has been suggested that NO activates cyclic guanosine monophosphate (cGMP) in the smooth muscle of cerebral vessels leading to vasodilation (180), and inhibits 20-hydroxyeicosatetraenoic acid (20-HETE) in smooth muscle of the same vessels to inhibit vasoconstriction (181,182). In the same way, cyclooxygenase 2 (COX_2) is activated by an increase of cytosolic Ca^{2+} (183), which leads to the production of prostaglandin E2 (PGE2). It is unknown whether PGE2 acts directly on smooth muscle cells or indirectly on astrocytes to vasodilate cerebral vessels.

In astrocytes, glutamate activates metabotropic glutamate receptors (mGluR) (171), and similar to neurons, activation of mGluR leads to an increase of the intracellular calcium concentration (176). However, the increase in cytosolic Ca^{2+} also leads to activation of phospholipase A2 (PLA2), which generates arachidonic acid (AA). The AA produces PGE2 through COX1, and epoxyeicosatrienoic acid (EETs) through cytochrome P450 2C11 epoxygenase (CYP2C11), in which EETs mediate smooth muscle relaxation through an unknown mechanism (182,184). Close contact has been reported between perivascular astrocytic endfeet and cerebral vessels (185). Following an increase in cytosolic Ca^{2+} in astrocytes, potassium is released from calcium-activated potassium (BKca) channels in the endfeet of the plasma membrane (186,187) into the extracellular nanospace between the endfeet and the vascular smooth muscle. The increase in potassium concentration activates an inward rectifier potassium (Kir) channel on the smooth muscle, that leads to rapid hyperpolarization of smooth muscle (vasodilation), closure of voltage-dependent Ca^{2+} channels, and an increase of cerebral blood flow (188–190).

These explanations are the favored hypotheses for the NVC process, but there is disagreement. The involvement of astrocytes in NVC has been generally accepted, but recently it has been found that an increrase in intracelluar Ca^{2+} inside the astrocytes occurs after arteriolar dilation begins (191). Furthermore, normal hyperemic response was found in a mouse model lacking the ability to generate an increase in astrocytic intracellular Ca^{2+} (lacking astrocytic inositol triphosphate type-2) (191). Furthermore, astrocytes have no direct contact with pial arteries at the surface of the brain (192), and that excludes astrocytes from a role in the dilation of pial arteries.

It was accepted that the changes in the tone of the vascular smooth muscle was the only unique mediator for NVC process. This theory is accepted for pial vessels, but an explanation was required for the capillaries that are devoid of smooth muscle (193). However, after the discovery of pericytes (at ~50 μm intervals along capillaries), these were then identified as the mediator of regulation of cerebral blood flow at the capillary level (171). Pericytes are contractile cells, and one of the cellular elements surrounding endothelial cells in capillaries and venules in the brain (194), and they actively communicate with other cells of the neurovascular unit. Pericytes have a significant role in maintenance of BBB integrity and regulating capillary blood flow through either direct contact or through signaling pathways (195). It has been discovered that pericytes evoke capillary vasodilation in response to the neurotransmitter glutamate, mediated by NO and PGE2, and the arteriolar dilation was preceded by capillary response (196). The same study, showed that pericyte-induced capillary constriction was followed by pericyte death in response to ischemia, suggesting that prevention of irreversible capillary constriction may protect the BBB from disruption and maintain the NVC and blood flow.

1.5.4 SDs and NVC

SDs and to a lesser extent ictal epileptic activities have been recorded in acutely injured human brains and ASH (52,197), suggesting that SDs have a role in neuronal death, increasing the metabolic demands, and in inverse NVC. Both SDs and ictal epileptic events were accompanied by an increase in cerebral blood flow to compensate for the increase in energy demands, an occasional reverse in NVC and a decrease in cerebral blood flow.

The changes in cerebral blood flow whether hyperemia or oligemia in response to SDs has been studied previously (135,178,179,198–202). The response of cerebral vessels to SDs varied between healthy and pathological tissue. In healthy tissue, the physiological hemodynamic response was hyperemia, but in tissue at risk for progressive damage, oligemia was the hemodynamic response (48,89,203–205). NVC varied between TBI patients depending on the severity of the injuries. The variations in NVC response were physiological hyperemic, pathological inverse, and could change from physiological to pathological coupling (89). However, a decrease in the cerebral blood flow and an inverse in NVC were recorded with SDs following subarachnoid hemorrhage, TBI, or after brain injury (53,206–208), suggesting that inverse NVC exacerbates existing ischemic conditions and increases the duration of SDs.

SDs are accompanied by the release of glutamate, arachidonic acids, and production of NO, that ultimately led to vasodilation (209,210). Furthermore, during SD glucose and energy consumption are increased three fold, tissue ATP abundance decreases, and the extracellular concentration of sodium, chloride, and calcium are decreased (210–212).

Although there is an increase in rCBF during the early phase of SD to supply the tissue with the energy necessary to restore ionic equilibrium (86), tissue hypoxia can still be detected in brain regions that are distant from capillary supply (213). A rodent study monitored the blood flow in cortical cerebral vessels, and hyperemia during SDs was evident in small vessels and to a lesser extent in arterioles and venules (201).

The combined effect of TBI and SDs on rCBF in rats has been investigated (202). This study showed that compared to baseline, the TBI group had less rCBF before and even after SDs, suggesting a compromised NVC process. In the same study, the recovery of blood flow was longer with the TBI group, but the magnitude of hyperemia was decreased following recurrent and repeated SDs.

A description of the rCBF process recorded in response to SDs has been reported previously (214). The response of rCBF is divided into three phases. The first phase represents the hyperemic phase, which is dominant during the occurrence of SD (202,205,214). The duration of this phase is about 1-2 minutes, reaching a peak within a minute from the beginning of SD. The second phase is the late hyperemic phase, which starts after 3-5 minutes of SD and induces up to a 10 % increase in CBF (215). Following

different neurological conditions such as TBI or subarachnoid hemorrhage, oligemia can last for hours and it represents the third phase (53,89,202,205,214,216,217). However, variations in phases and durations of CBF within and across species have been reported, perhaps due to other factors such as the experimental conditions and the method used to measure the CBF. However, in general there is a consensus on the relationship between NVC and SDs in healthy and in neuropathological conditions.

1.6 Aims of the Study

Despite the enormous impact of concussion, the mechanism underlying the neurological symptoms and outcome are still only partly understood.
My overall goal was to improve our understanding of the electrophysiological activity underlying concussion and its potential implications. Specifically, I aimed to:

First: monitor the neurophysiological changes that occur immediately after traumatic brain injury (Chapter 2).

Second: study the changes in blood-brain barrier integrity and neurovascular coupling (Chapter 3).

Third: study the neurophysiological alteration underlying immediate catastrophic death following mild TBI (Chapter 4).

Chapter 2: Spreading Depolarization as the Electrophysiological Signature of Concussion

2.1 Introduction

Mild traumatic brain injury (TBI) is a major global health concern that has been estimated to affect over 40 million people annually (5,218). Concussion is a common neurological presentation that occurs frequently following mild TBI. While its definition is evolving, concussion is most often defined according to variable clinical symptoms (94). It may or may not include loss of consciousness, along with confusion and dizziness. In most cases of concussion, structural imaging reveals no pathology (219), and it is thought that transient functional disturbances underlie the symptoms of concussion (219,220). Accumulating evidence has suggested that repeated concussions may be linked to an increased risk of developing delayed neuropsychiatric complications, including depression (221), epilepsy (222), and neurodegenerative diseases, such as chronic traumatic encephalopathy (CTE) (223), Parkinson's disease (224), and Alzheimer's disease (10). Despite these devastating consequences, the pathophysiological mechanisms that underlie concussion are largely unknown. Electroencephalography (EEG) has been used to study the effect of TBI on the electrical activity of the brain (220,225), and immediate depression of EEG has been reported after TBI impact. Due to the methods used, spreading depolarization (SD) was not identified as the mechanism of silencing of the electrical activity of the brain. In the present study, we recorded electrophysiological changes from the cortical surface within seconds following repetitive mild TBI. Using a weight-drop model with rats that are pre-implanted with epidural electrodes, we show that cortical spreading depolarization is the earliest common pathophysiological event following mild TBI. We suggest that SDs are the electrophysiological hallmark of concussion.

2.2 Materials and Methods

All experiments were performed following institutionally approved protocols in accordance with the Canadian Council on Animal Care and were approved by the Dalhousie University Committee on Laboratory Animals.

2.2.1.1 Surgical Procedures

Surgical procedures for the rats were performed under deep anesthesia (3% isoflurane for induction and 1.5% for maintenance). Blood oxygen saturation (SpO2) was monitored continuously using a paw clip connected to an animal oximeter pod (ML325, ADInstruments, Sydney, Australia) and a PowerLab data acquisition device (PL3508, ADInstruments, Sydney, Australia). The rats were mounted in a stereotaxic frame and core body temperature was maintained at 37.3°C using a surgery heating pad (Physiotemp). Prior to surgery, the area of the incision was cleaned aseptically by wiping the skin with three alternating swipes of 90% alcohol and betadine. A midsagittal incision (2.5 cm) was made to expose the skull. Drilling was performed under saline cooling to avoid heat injury. For recording from freely behaving animals before and immediately after TBI, two holes (2x2 mm in diameter) were drilled for screw placement (stainless steel bone screws, Fine Science Tools, 0.86 mm x 4 mm) in the right parietal bone (2 mm posterior to bregma, 2 mm anterior to lambda, and 3 mm lateral to sagittal suture). A ground electrode was inserted into the neck subcutaneous tissue. Electrodes were constructed from Teflon insulated silver wire (280 μm diameter, A-M Systems, Inc.) and miniature connectors (Ginder Scientific, ABS plug, GS09PLG-220). The silver wires of the electrodes were then wrapped around the screws and were fixed to the skull using dental cement. In a subset of animals, two additional screws were inserted in the left parietal bone to record from both hemispheres. A cylindrical platform (1 cm in diameter and 1.5 cm in height), to receive a dropped weight, was formed above both sides of the frontal bone using dental cement (Figure 2.1A and B). For cortical surface imaging under deep anesthesia, a craniotomy (4x6 mm in diameter, 2 mm posterior to bregma, 2 mm anterior to lambda, and 2 mm lateral to sagittal suture) was performed as described previously (135). The cranial window was covered by a transparent plastic cover slip (Figure 2.1C), and a dental cement platform was constructed above the frontal bone for animals expected to receive TBI. In another group

of animals, and in addition to the right parietal cranial window, a right frontal bone window was prepared (2x2 mm in diameter, 2 mm lateral and 2 mm anterior to bregma) (Figure 2.1D) to trigger SDs in control and TBI-exposed animals. Following the surgical procedure, ketoprofen for analgesia (5 mg/kg, SC) was injected with lactate Ringer solution (5 mL). Animals were kept warm and under observation until recovery.

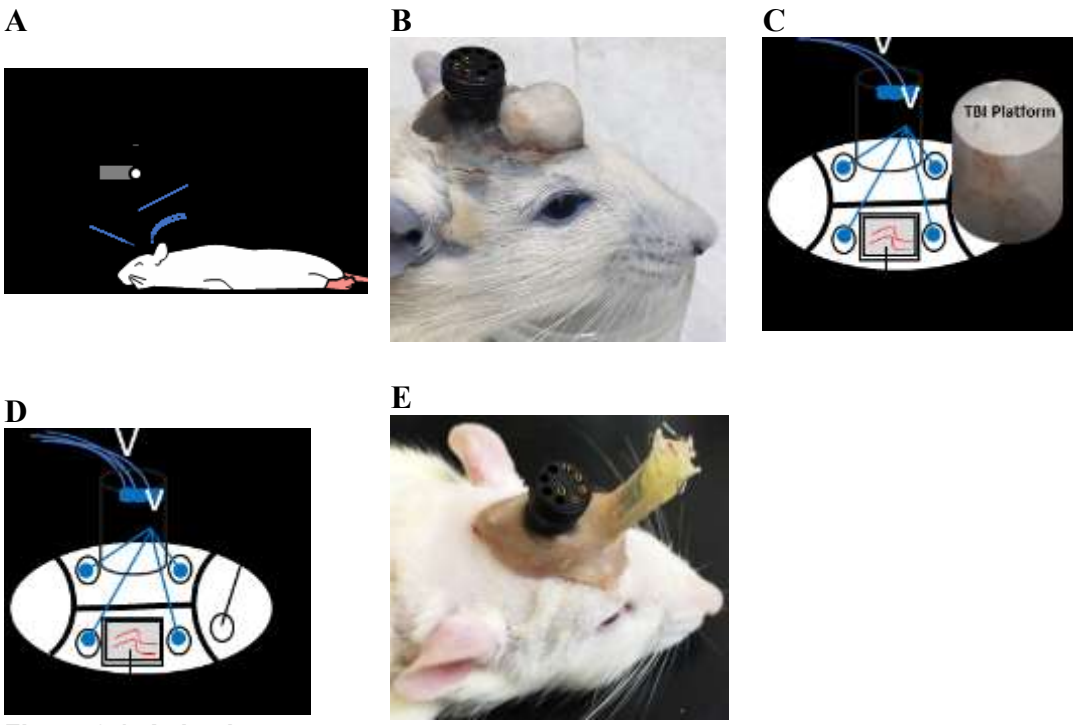

Figure 2.1. Animals groups.

The animal has a pre-implanted electrode for ECoG recording, and a dental cement platform oriented below the metal bolt to receive the dropped weight (**A** and **B**). Schematic drawings show the location of holes for ECoG, right parietal window for cortical monitoring, and frontally constructed platform for TBI (**C**) and with a frontal hole for electrical stimulation (**D**). The pre-implanted electrodes for ECoG and electrically triggering SDs in unanesthetized animals through the frontal hole (**E**).

2.2.1.2 Mild Traumatic Brain Injury

A weight drop TBI model was adapted by (Ellen Parker, 2019) from Mychasiuk (226), Marmarou et al. (227) and Kane et al. (228) with modifications for a mild TBI (Figure 2.2). Briefly, young (8-10 weeks) adult male Sprague Dawley rats were sedated using an induction chamber (3% isoflurane, 2 L/min O2), until the toe-pinch reflex was absent. Rats were then placed in the prone position on a sheet of aluminum foil taped to the top of a plastic box (30x30x20 cm in depth). A metal bolt (1 cm diameter x 10 cm length) was placed on the surgically constructed dental cement platform on the skull of the rat. TBI was induced using a weight (600 g) travelling vertically (1.2 m) along a metal guide rail. Following the impact, animals fell through the foil onto a foam pad placed at the bottom of the box. Sham controls had the same surgical procedure and anesthesia induction but did not receive a TBI.

Figure 2.2. Schematic drawing for mild TBI model.
(**1**) Animal is sedated using isoflurane and laid in a prone position on aluminum foil. As the animal is impacted, it breaks the foil and flips to the bottom of the box (**2** and **3**).

2.2.1.3 Electrocorticographic (ECoG) Recordings

TBI and recordings were acquired 24 to 72 hours after the surgical procedure. The animals were tethered to an Octal bio amplifier (ML138, ADInstruments, Sydney, Australia) for recording differential epidural ECoG signals. Near-direct current (DC) recordings were acquired (sampling rate of 1 kHz) with a high-pass filter of 0.02 Hz, a low-pass filter of 100 Hz, and a 60 Hz notch filter. A one-hour baseline recording was acquired in a recording box (60x30x30 cm). The animals were reconnected to the recording system within < 30 seconds of impact and recording continued for one hour. In a subset of animals (n=8), there was continuous recording for 24 hours. Another group of rats randomly divided into control (n=12) and TBI (n=10) groups had recording under isoflurane anesthesia (1.5-2%), and SDs were electrically triggered and monitored. ECoG data were analyzed using LabChart software (version 8) and MATLAB.

2.2.1.3.1 Recording in Freely Behaving Animals (Recovering from Anesthesia)

For the purpose of recording from freely behaving animals (TBI-awake group), and to study the neurophysiological changes that occur within seconds after repetitive mild TBI, Sprague-Dawley rats were impacted three times. On day 1, animals (n=23) were impacted for the first time, 20 out of 23 animals received a second impact on day 2, and 19 out of 20 received a third impact on day 3 (Figure 2.3). Following either the first or third impact, Evans blue was injected intravenously through the tail vein, and after 30 minutes the animals were deeply anesthetized using pentobarbital (Euthansol, intraperitoneally, 50 mg/kg), then perfused through the left ventricle of the heart with normal saline (0.9% saline) followed by 4% formaldehyde solution. Extracted brains were post-fixed in a 4% PFA solution at 4°C.

In addition, there was an unanesthetized electrically-triggered SD group (n=20), in which electrodes were implanted for ECoG recording from the right brain hemisphere and to electrically triggering SDs through the right frontal hole (Figure 2.1E). This group did not receive an impact (TBI). After 24 hours of recovery from surgery, these animals underwent an hour of baseline ECoG recording, followed by another hour of electrically triggering SDs and ECoG recording.

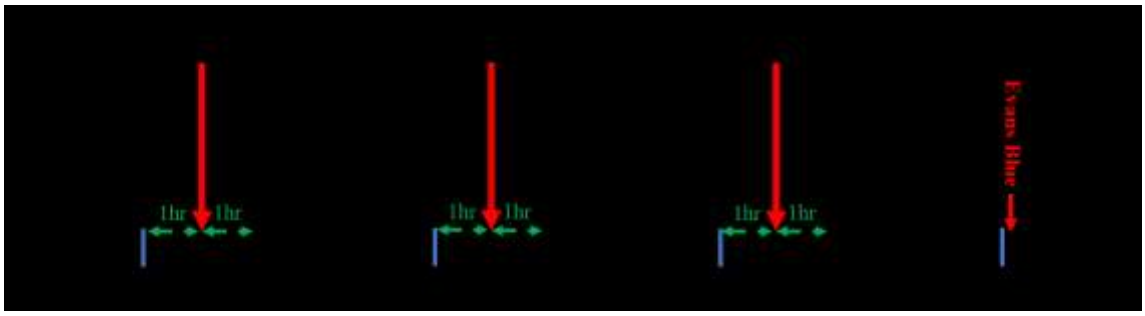

Figure 2.3. Schematic drawing shows the major steps for recording from the TBI-awake group.

Electrodes were implanted for epidural ECoG recording. After 24-72 hours of recovery, and for 1-3 consecutive days, the animals underwent two hours of ECoG recording. The first hour is baseline, followed by a TBI impact, and then one more hour of ECoG recording.

2.2.1.3.2 Recording in Deeply Anesthetized Animals

All procedures (craniotomy, ECoG recordings, and triggering SDs) were carried out under deep anesthesia using isoflurane (1.5-2%, 1 L/min O_2). Sprague-Dawley rats were divided randomly into control (n=12) and TBI groups (n=10). The TBI group, but not the control, was subjected to a single mild TBI once per day for 5 consecutive days before the craniotomy and recording procedures. SDs were triggered using electrical stimulation in both groups (Figure 2.1D). The same equipment and configurations of the recording mentioned previously were used for three hours of continuous ECoG recording from the deeply anesthetized animals. After an hour of a baseline recording, SDs were triggered during the second hour while monitoring the ECoG, followed by another hour of recording. Similarly, ECoG signals were also collected from another deeply anesthetized group before and immediately following TBI (Figure 2.1C), simultaneously with cortical surface imaging through the parietal window that is covered by a transparent plastic cover slip.

2.2.1.4 Electrically Triggered SDs

SDs were triggered epidurally as reported (75,87), using two stainless steel stimulation electrodes (0.5 mm in diameter). Stimulation parameters were: 20 volt (V) and 20 Hz for 2 seconds. Pulse duration was increased every 10 minutes from 5 to 20 ms, with 5 ms steps. SDs were triggered in deeply anesthetized (control and TBI) (Figure 2.1D) and unanesthetized group (Figure 2.1E).

2.2.1.5 Cortical Imaging

To allow cortical surface imaging immediately following TBI, the open parietal window was covered by a transparent plastic cover (Figure 2.1C). In a subset of animals (n=6), intravital microscopy (Axio Zoom, V16, Zeiss GmbH; Konigsallee, Germany) was performed immediately (< 30 sec) following impact. These rats were maintained under deep anesthesia (isoflurane 1.5%). Images were taken from the surface of the cortex at a rate of one image/sec using a scientific CMOS camera (PCO Edge 5.5 model, PCO-Tech Canada). The changes in intrinsic optical signal (IOS) were analyzed as reported (229,230) using MATLAB.

2.2.2 Statistical Analysis

Results are expressed as (if not otherwise stated) mean ± standard error of the mean. Differences between more than two groups were determined by Kruskal Wallis test or Friedman test, and between two groups were determined by Wilcoxon signed-rank test or Mann-Whitney U test. The differences were statistically significant at $P < 0.05$. All statistical analyses were performed using IBM SPSS Statistics, version 24.0.

2.3 Results

Three criteria were established and used to validate a mild TBI model with concussive-like injury: (1) mortality is rare; (2) a reduction in neurobehavioral performance can be observed during the first minutes to hours after injury, and a recovery can be documented 24 hours after the impact; and (3) brain MRI 24 hours after injury and gross post-mortem examination show no evidence of significant intracranial bleeding or gross structural injury. We selected a drop weight and height (600 g, 1.2 m) in which all the animals survived the injury and recovered from anesthesia.

2.3.1 SDs are Likely to Occur Following Mild TBI

Brain activity was recorded before and for >1 hour during recovery from a short period of anesthesia. In sham controls, cortical activity during recovery from anesthesia was characterized by increased amplitude and slowing compared to pre-anesthesia baseline, and returned to baseline within 4-5 minutes (Figure 2.4).

In contrast, the most common change in brain activity following mild TBI was the appearance of a large, long-duration, propagating potential, which was associated with a depression of cortical activity, as reported for spreading depolarization (SD) in rodents and humans (52,53,202,206).

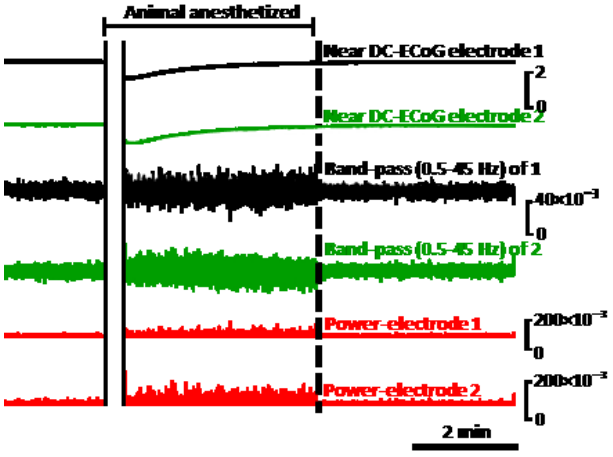

Figure 2.4. Recording from a non-injured sham control.

The upper two traces show raw ECoG recordings (band-pass: 0.02-100 Hz). The 3rd and 4th traces show band-pass (0.5-45 Hz) activity. Note the high amplitude activity during recovery from anesthesia.

All animals (n=23) had the first TBI impact, 20 animals had a second impact, and 19 animals had a third one. Animals were grouped according to the post-injury electrophysiological pattern, Figure 2.5. For the first time, SDs were recorded in unanesthetized animals immediately following mild TBI. TBI-induced SDs were recorded after the first (43.4%, in 10 of the 23), the second (55%, in 11 of the 20), and the third TBI (57.8%, in 11 of the 19). In contrast, convulsive seizures with no evidence for SDs were very rare and were recorded in only 2 animals after exposure to the second and third TBI, while one rat (4.34%) showed a seizure preceded and followed SD after the first TBI. There were no SDs or seizures clearly observed after the first (52.1%, in 12 of the 23), second (40%, in 8 of the 20), and third TBI (36.8%, in 7 of the 19), and in the sham control (n=10).

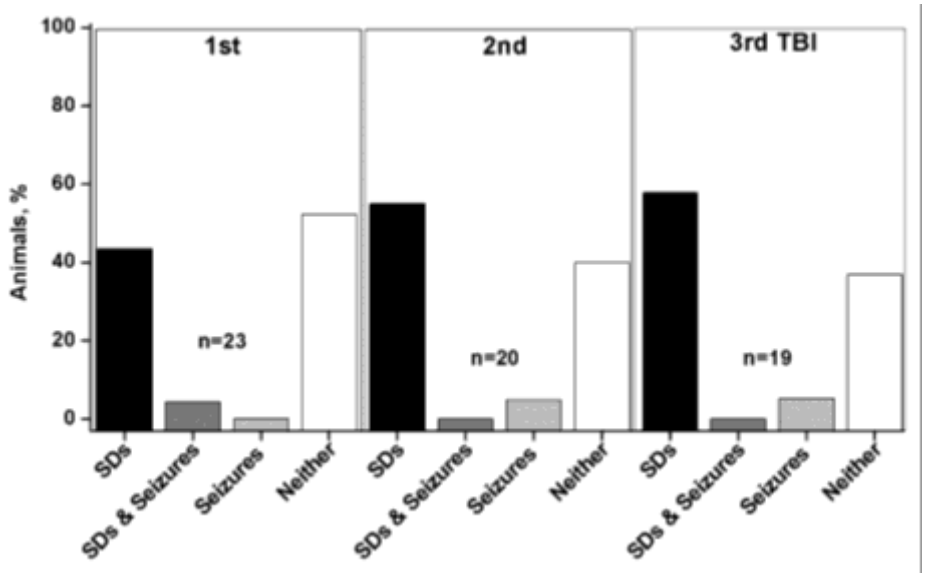

Figure 2.5. The percentage of SDs and seizures following repetitive mild TBI.
From left to right, animals were impacted for the first (1st), 2nd, and 3rd time.

The percentage of SDs or seizures occurring between the groups was almost similar after each impact. When all impacts were totaled (n=62 impacts), SDs were observed following 51.6% of the impacts (n=32 out of 62, Figure 2.6). Seizure activity associated with convulsions but without SD was observed in two animals (3.2%).

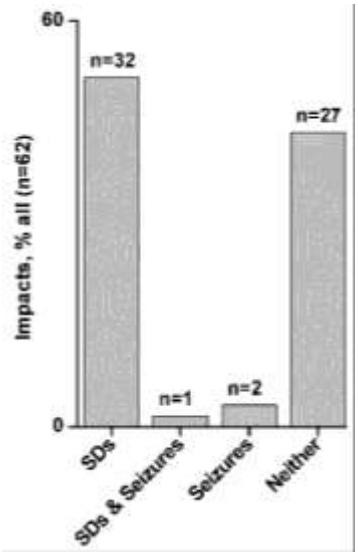

Figure 2.6. Occurrence rate of SDs and seizures following all impacts.

One animal (1.6%) displayed an electrographic seizure that preceded and followed the SD (Figure 2.7). In 27 impacts (43.6%), and in all sham controls (n=10) neither SDs nor seizures were observed. As no histological investigation of the brains was conducted, it is unknown whether there are differences between animals with and without SDs. Of the 33 SDs, 32 were recorded within the first 3 minutes (mean 125 ± 9 s, n=32) after the impact (Figure 2.7 and Figure 2.8). In one animal, a late SD was recorded 43 minutes after injury. In a subset of animals (n=8), recordings were continued for 24 hours with no additional SDs noted. In a subgroup of rats (n=10), recording electrodes were implanted above both hemispheres. In 7 out of 10 (70%) impacts, TBI-induced SDs were recorded in both hemispheres (Figure 2.8).

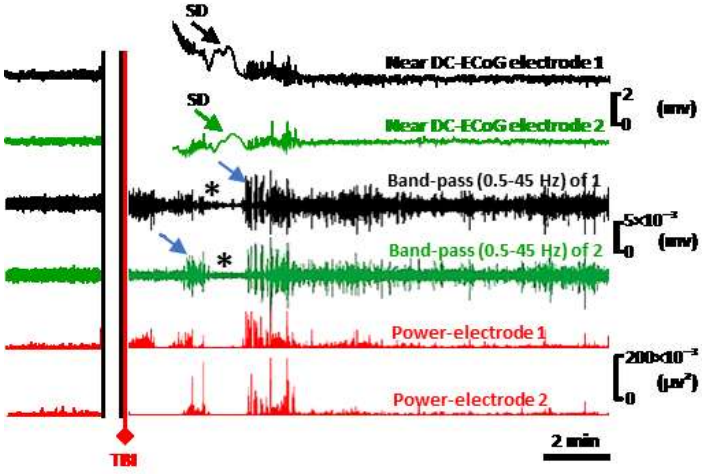

Figure 2.7. Epidural near DC-ECoG from right brain hemisphere.

Recordings of TBI-induced SDs and seizures from the right brain hemisphere following a mild TBI. First upper two traces represent the raw ECoG recordings (band-pass: 0.02-100 Hz) and show SDs recorded in both two neighboring electrodes 1 and 2. Seizures recorded before and after SDs (blue arrows). Traces 3 and 4 show the spontaneous brain activity in near DC-ECoG recordings (band-pass 0.5-45 Hz), in which spreading depression was observed in both electrodes (1 and 2) simultaneously during SDs (asterisk). The squared spontaneous activity (power near DC-ECoG) of both electrodes was used as another accurate measure to quantify the depression in spontaneous brain activity (52,53,231). After ~2 minutes of mild TBI, SDs and seizures are seen in electrode 1 and electrode 2.

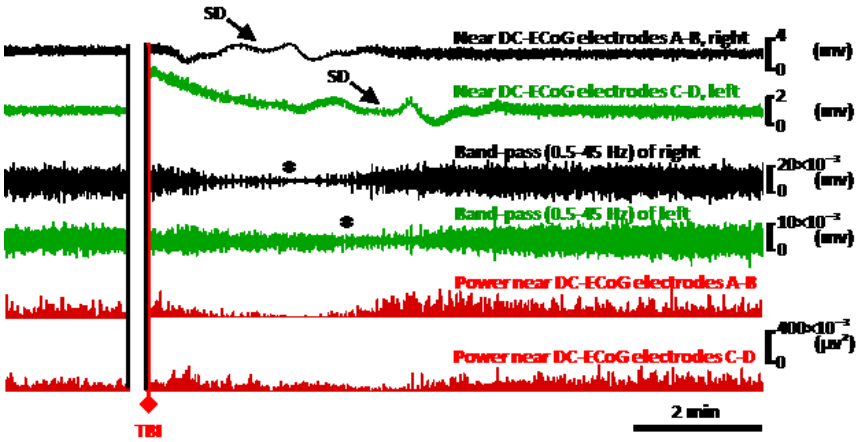

Figure 2.8. Epidural near DC-ECoG from both brain hemispheres.

TBI-induced SDs were recorded from both brain hemispheres following mTBI. First upper two traces show the raw ECoG recording (band-pass: 0.02-100 Hz) of two electrodes. Electrodes A-B record from the right hemisphere, whereas electrodes C-D record from the left hemisphere. Suppression of the brain activity (band-pass 0.5-45 Hz) is observed in both hemispheres (asterisk) as shown in traces 5 and 6.

The cortical surface in the right frontal window (the presumed region of maximal impact force) was electrically stimulated in order to induce SDs (75). One to two minutes (103 ± 29 s) following stimulation, SDs were recorded from the right parietal electrodes (n=20, Figure 2.9). The latency of electrically-triggered SDs was similar to that observed for TBI-induced SDs (n=32, 125 ± 9 s).

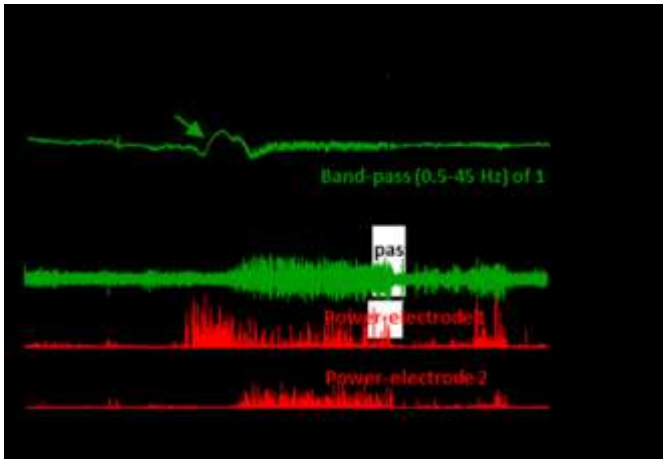

Figure 2.9. Electrically-triggered SDs propagated from the right frontal hole and recorded by right parietal electrodes in the unanesthetized group.

Cortical imaging during SD recordings (n=6) confirmed propagating changes in IOS (Figure 2.10A and B), as reported (229,232).

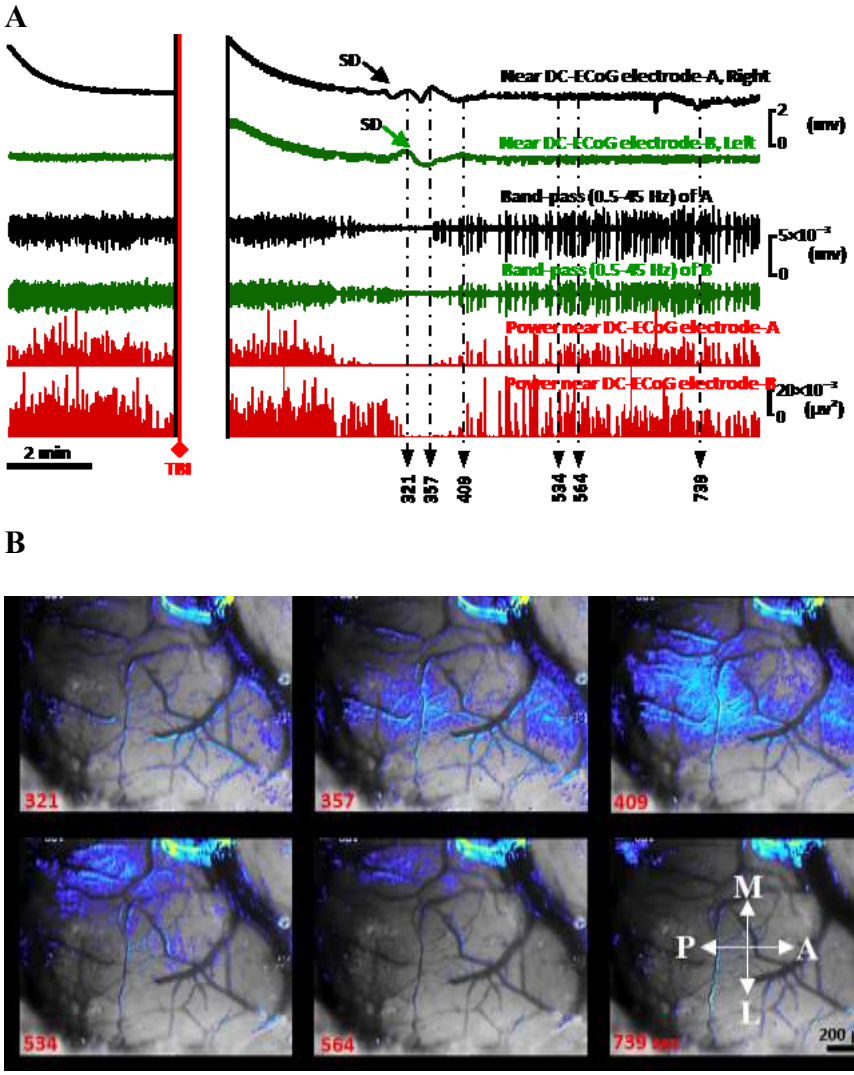

Figure 2.10. Intravital microscopy showing changes in intrinsic optical signals during SD. **(A)** ECoG recording from both brain hemispheres after a mild TBI showing bilateral SD occurrence. Perpendicular dotted arrows indicate the time of recording of the images shown below. (B) Images were acquired during ECoG recording from the surface of the brain at various time points after mild TBI. Changes in IOS are superimposed onto brain images. SDs were triggered in multiple cortical foci following impact and propagated medially toward the midline in the right hemisphere. A, anterior; P, posterior; L, lateral; M, medial. IOS=intrinsic optical signal.

2.3.2 TBI Animals Having SDs Need Longer Time to Resume Spontaneous Locomotion

Motor arrest was the most common behavioral phenotype during SDs, but occasionally unilateral or bilateral contractile rhythmic limb movements were noted, with slow extension of one or two limbs. Latency to resume spontaneous locomotion was significantly longer in animals with SDs (360 ± 26 s, n=32) compared to rats where no pathological brain activity (SDs or seizures) was recorded (196 ± 25 s, n=27, P=0.001), or to sham controls (67 ± 6 s, n=30, P< 0.0001, Figure 2.11A). Although there was no significant difference or relationship between the time to resume locomotion and the number of TBI impacts (Figure 2.11B), significant differences were found between control and all TBI animals regardless the number of impacts. Contrary to expectations, there was no relationship between the time needed to resume spontaneous mobility and the spreading depression duration or SD amplitude.

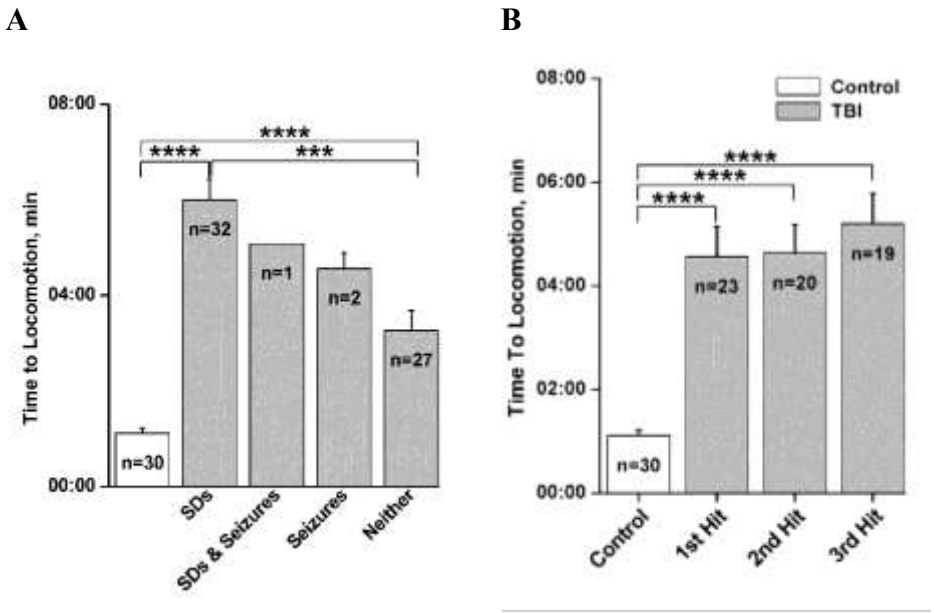

Figure 2.11. Time to resume spontaneous locomotion.

(A) Time to resume locomotion was the longest in animals having SDs. However, all TBI subgroups have longer duration to resume their voluntary activity compared to control. **(B)** There was no significant difference between animals exposed to one or more TBI impacts. *** P ≤ 0.001, and **** P ≤ 0.0001.

2.3.3 Repetitive (But Not Single) Mild TBI is Associated with Brain Contusions

A summary of the relationship between the brain contusions and number of TBI impacts is shown in Figure 2.12. The brain contusions are common in repetitive mild TBI. Evans blue (MW of 961 Da) is frequently used as a tracer to detect blood-brain barrier disruption and leakage. Evans blue was injected 30 minutes before perfusing the animals to detect any visible contusion formation or BBB disruption. No difference was observed between control (n=30) and animals exposed to a single TBI (n=4), in which both groups did not have contusions (Figure 2.12A, B, C, and G). We observed that 89.47 % of animals exposed to three repetitive mild TBI (17 out of 19) have brain contusions mainly in the inferior surface of the brain (Figure 2.12D, E, F, and G).

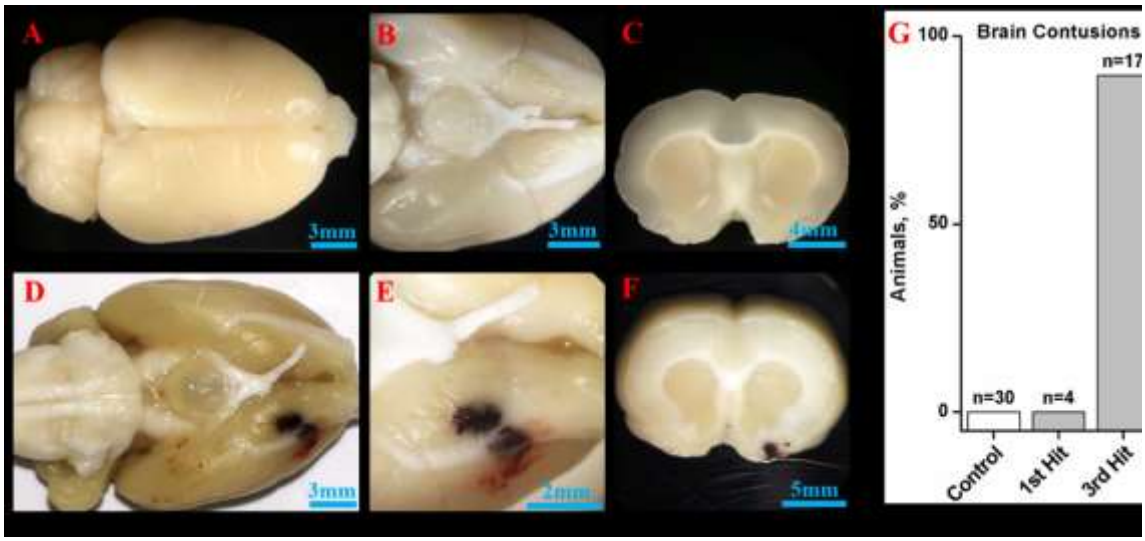

Figure 2.12. TBI and control brains.

Brain contusions were observed following three impacts (**D**), but not after one impact or in controls (**A**). Closer views for the inferior surfaces of the brains show no blood after one impact and in control (**B**), and brain contusions after exposure to three impacts (**E**). **C** and **F** are coronal sections for **B** and **E** respectively. (**G**) The percentage of contusions occurrence among control group and animals exposed to one and three impacts.

2.3.4 SDs Characteristics I: Amplitude

The amplitudes of the slow potential changes of SD waves were measured from peak to peak. Recordings were acquired using a near-DC amplifier with a high-pass filter of .02 Hz, that will distort the DC-shift of SD. However, the stereotyped slow potential change that serves as a hallmark signature of SD can be recorded. Thus amplitude and duration measurements should be interpreted with caution (231). The amplitude of electrically-induced SDs was larger in awake animals compared to anesthetized controls (awake: 1.04 ± 0.12 mV, n=20 vs. anesthetized: 0.26 ± 0.03 mV, n=12, $P<0.0001$), likely due to the suppression effect of anesthesia. Notably, injury-induced SDs were larger in amplitude compared to electrically-stimulated SDs recorded in awake animals (1.47 ± 0.14 mV, n=33, vs. 1.04 ± 0.12 mV, n=20; P=0.01). Electrically-induced SDs in rats after injury were smaller than trauma-induced SDs, but larger compared to electrically-induced SDs in anesthetized controls (P=0.02). However, depending on the number of impacts given to the animal, analysis showed that SDs had almost similar amplitudes between groups of animals that had one, two or three impacts; 1.47 ± 0.24 mV, 1.53 ± 0.26 mV, and 1.42 ± 0.23 mV respectively (Figure 2.13B).

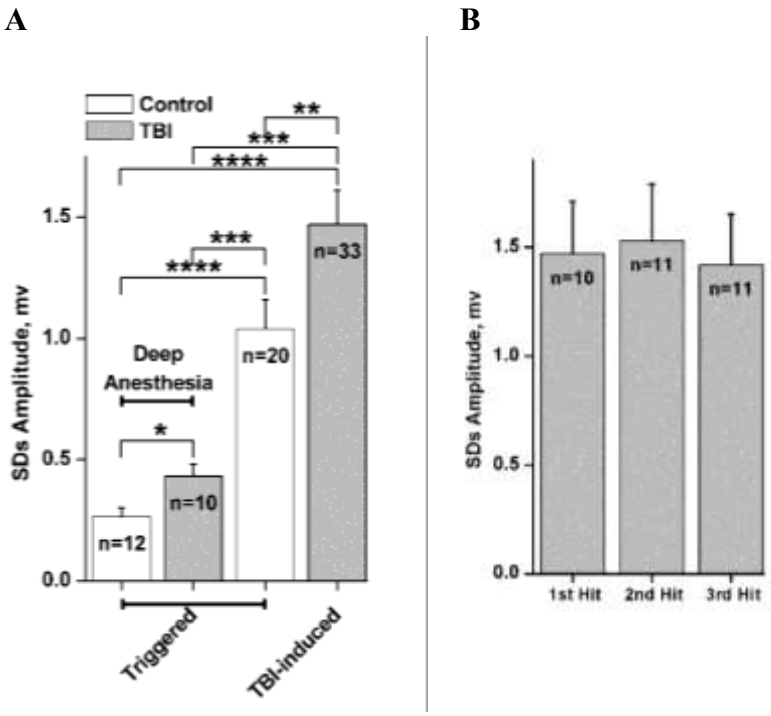

Figure 2.13. SD amplitude in awake and anesthetized rats.

(**A**) The lowest SD amplitudes were recorded in anesthetized groups, and the highest were in TBI-induced SDs. (**B**) No significant difference between SDs amplitude depending on the number of impacts. * $P < 0.05$, ** $P \leq 0.01$, *** $P \leq 0.001$, and **** $P \leq 0.0001$.

2.3.5 SDs Characteristics II: Duration

The duration of SDs was measured from the start of the deviation from baseline of DC shift of slow potential change of SDs to the return of DC shift to the baseline. No differences were found in SD duration between awake and anesthetized animals, or between electrically- and TBI-induced SDs (Figure 2.14).

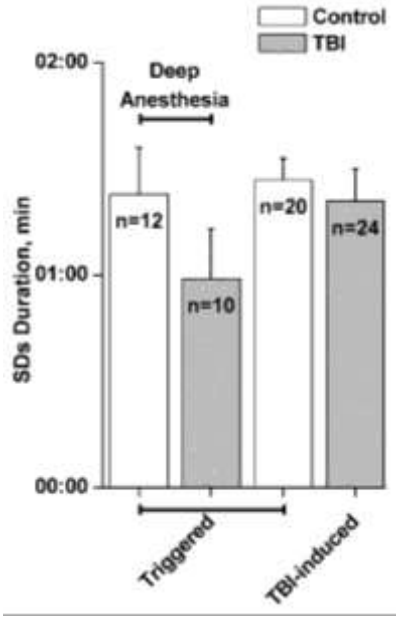

Figure 2.14. The duration of triggered SDs under anesthesia compared to slightly sedated or awake animals.

No differences in SD duration between anesthetized and awake animals who were exposed to TBI or electrically stimulated.

2.4 Discussion

We report here the common occurrence of SDs after mild TBI. SDs were recorded in > 50% of injured animals within 3 minutes after a direct impact in this closed-head rat model of mild TBI. Most rats with SDs required a longer time to resume spontaneous locomotion compared to injured animals with no SDs or sham controls. Our results are in agreement with those of Bouley and colleagues, who recently showed laser doppler flowmetry and intrinsic optical signaling changes consistent with SDs in a mouse model of closed brain injury (233), and with a previous study of a TBI model using anesthetized animals impacted directly on the dura (225).

SDs are characterized by abrupt, near-complete sustained depolarization of neurons and breakdown of the transmembrane ion gradient (48,51), observed as a large negative slow potential change (52,53). Spontaneous SDs have been described in sedated patients after severe brain injuries, including TBI (53,85,86), subarachnoid hemorrhage (52,87), and malignant stroke (54,88). Under these conditions, it has been shown that SDs may be associated with an impaired vascular response and worse clinical outcomes (54,89–91). SDs are also thought to underlie migraine aura with no evidence for neuronal injury,

perhaps due to normal vascular response and increased blood flow to the tissue (234,235). The known propagation velocity of SDs (2-9 mm/min) (236), and the observation that electrically-stimulated SDs at the site of injury (ca. 5 mm anterior to the recording site in the parietal cortex) resulted in a similar delay of SDs recorded in the parietal window. This suggests that SDs are initiated immediately following injury and slowly propagate throughout brain. In a recent study, direct impact to the dura mater of anesthetized mice showed a bilateral decrease in regional cerebral blood flow (rCBF), which was suggested to be the result of SDs (225). Our findings using direct recordings and analysis of intrinsic optical signaling confirm that SD initiation and propagation is common in a rodent model of mild TBI. Previous animal studies showed that electrically-induced SDs usually propagate ipsilaterally and do not cross to the contralateral hemisphere (237). The bilateral simultaneous SDs recorded in our animal model (Figure 2.7) could likely be the result of a bilateral induction of SDs in the parietal cortex, and the delay in recording could be the time needed for initiation of SDs.

While SDs were the most prevalent pathophysiological events following mild TBI, we occasionally also recorded seizures. The rare occurrence of electrophysiological seizures after mild TBI is consistent with clinical studies (238). Furthermore, while in most animals triggered SDs were associated with behavioral arrest (so-called “freezing behavior”) (239), we often noticed motor convulsions during SDs, suggesting the involvement of sub-cortical or spinal networks. Suppression of extrapyramidal tracts or basal ganglia cannot be excluded.

Rats that experienced SDs required a longer duration to resume spontaneous locomotion, consistent with the transient alteration in consciousness immediately following TBI, as often reported in concussed individuals. Published data does not have an hypothesis to explain these symptoms (92,95). We suggest that SD is the dominant and the primary factor in manufacturing the hallmark of concussion. Consistent with our results, immobility behavior that ranged from seconds to 10 minutes was the prominent behavioral change during triggered SDs (239). This requires further investigation to determine the difference between triggered and TBI-induced SDs. It has been found that the propagation of SDs through the cerebral hemisphere causes temporary sensory and motor dysfunction (240). In this study, the immobility during TBI-induced SDs could be explained also by the

involvement of the basal ganglia (240). However, the firing of dopamine neurons is under cortical regulation (241,242). The mechanisms by which SD modulates the dopaminergic synaptic network in the striatum are unknown (243). However, SDs change the neuronal activity (239) and modulate the dopamine release in subcortical structures, producing a decrease in dopamine release in the caudate nucleus. This may lead to inhibition of motor activity and termination of responses (240,244,245). Thus, the modulation of neurotransmitter release as a result of SD may have an impact on the voluntary locomotion of animals (240).

Although we performed near-DC recordings (with a high-pass filter of 0.02 Hz), and thus amplitude and duration measurements should be interpreted with caution (55), the larger amplitudes of injury-induced SDs compared to those induced by electrical stimulation are still interesting. This increase in amplitude is unlikely due to the effect of anesthesia, as isoflurane has been reported to suppress SDs (246). Furthermore, electrically-triggered SDs in awake rats were also lower in amplitude compared to TBI-induced SDs (Figure 2.13A). The larger amplitude of SDs following TBI may reflect a greater population of neurons involved in the SD process or a faster recruitment of these into the SD process. Interestingly, the electrically-induced SD amplitude was also larger in the traumatized brain, suggesting long-lasting changes in cortical circuitry function after SDs in this mild TBI model.

In humans, an impaired vascular response to SDs has been documented after severe brain injuries and has been suggested to underlie delayed cerebral ischemia after both traumatic and aneurysmal subarachnoid hemorrhage (54,100,247,248). The relative ischemia in response to the increased metabolic demand during SDs was shown to be associated with a longer duration of SD's negative DC shift (53). While the vascular response to SD was not monitored in the present study, no differences were found between the durations of the near-DC shifts in trauma-induced and electrically-induced SDs in the healthy or traumatized brain. This suggests that brain ischemia is not a prominent response to SDs after mild TBI.

Brain contusions are focal brain injuries that occur frequently at locations where the brain surfaces come in contact with protruded bony parts of skull, specifically the base of the skull. From a pathophysiological view, contusions result from damage to small cerebral

vessels. Our findings share similarities with a result of a previous study in which most contusions were seen in the inferior surface of temporal and frontal lobes (249). Indeed, contusions occur either directly beneath the location of impact or on the other side of it. Contusions can occur in the cortex or the white matter. In this study, the high occurrence rate (89.4%) of contusions after three impacts is consistent with a rodent model of repetitive mild TBI in which contusions were seen in all impacted animals (250). In another study, 50% of mild TBI patients (15 out of 30) were seen with BBB disruption around the area of the contusion (251).

In this study, we presented electrophysiological recordings confirming that SDs are a common, early cortical electrophysiological event in a model of mild TBI and are associated with a longer recovery time following injury. We suggest that SDs may be critically involved in brain dysfunction that results from a mild TBI. Additional studies are required to investigate the mechanisms underlying the initiation and propagation of SD in the traumatized brain, and the potential role of SDs in mediating delayed complications of concussive injury.

Chapter 3: Spreading Depolarization, Blood-Brain Barrier Integrity, and Neurovascular Coupling

3.1 Introduction

Spreading depolarizations (SDs) is a phenomenon discovered by Leão in 1944 (46). It is well known that SDs are initiated and propagated across the brain, but the mechanisms by which that occurs are unclear (46,47). SDs are known to occur in individuals with SAH (52,87), ischemic stroke (88), malignant hemispheric stroke (54), migraine (57,252), and TBI (53,85,86).

SD has a role in cytotoxic edema in the brain's gray matter (252), increased metabolic demands, and inverse neurovascular coupling (NVC) (52,197). The occurrence of SDs and the prolonged duration of silencing of the brain's spontaneous activity in TBI patients were considered as major factors that led to the formation of cortical lesions and impaired NVC (53,85,100).

In recent years, there has been considerable interest in BBB disruption and its relationship to various neurological disorders, including TBI and epilepsy. Regardless of the cause, BBB disruption is common, and it has important consequences for nervous tissue, leading to the generation of seizures and epilepsy, especially after TBI (8,123,126,253–255).

The relationship between SDs and the BBB is thought to be mediated by a family of proteolytic enzymes called matrix metalloproteinases (MMPs) (149), that are released and activated following intracerebral hemorrhage, stroke, brain tumor, and TBI (150,153–156), and will affect the integrity of the BBB.

The response of cerebral vessels to SDs differs between normal healthy and pathological tissue. In healthy tissue, the physiological hemodynamic response (hyperemia) is dominant, but an oligemia in tissue at risk for progressive damage is the inverse hemodynamic response (48,89,203–205). SDs are accompanied by the release of glutamate, arachidonic acid, and the production of NO metabolites that ultimately lead to vasodilation (209,210).

In TBI, NVC varied between patients, depending on the severity of the injuries. NVC can be physiological hyperemic, pathological inverse, or can alter from physiological to pathological coupling (89,202). In the previous chapter, we showed that SDs were the first

electrophysiological events that occurred following mild TBI. It is established that TBI is associated with BBB dysfunction (251)(255)(256), and repetitive TBI is associated with BBB disruption (250). Thus, the goal of this chapter is to shed light on the relationship between SDs and BBB permeability following repetitive mild TBI using a new technique for live continuous monitoring of pial vessels.

3.2 Materials and Methods

All experiments were performed following institutionally approved protocols in accordance with the Canadian Council on Animal Care and were approved by the Dalhousie University Committee on Laboratory Animals.

Sprague-Dawley rats (300-400 g) were randomly divided into two major groups, including control group (n=28) and TBI group (n=20). Depending on the method used for triggering SDs, each group was subdivided further into two subgroups, including KCl-triggered SDs and electrically-triggered SDs. Epidural ECoG recordings, rCBF monitoring, and vascular imaging were collected continuously during the experiment. To assess BBB integrity, the BBB-tracer Na-Fluorescein was injected before (baseline) and after triggering SDs (Figure 3.1). Triggering SDs was performed through the right frontal hole. Experimental design is summarized in Figure 3.1 and Figure 3.2.

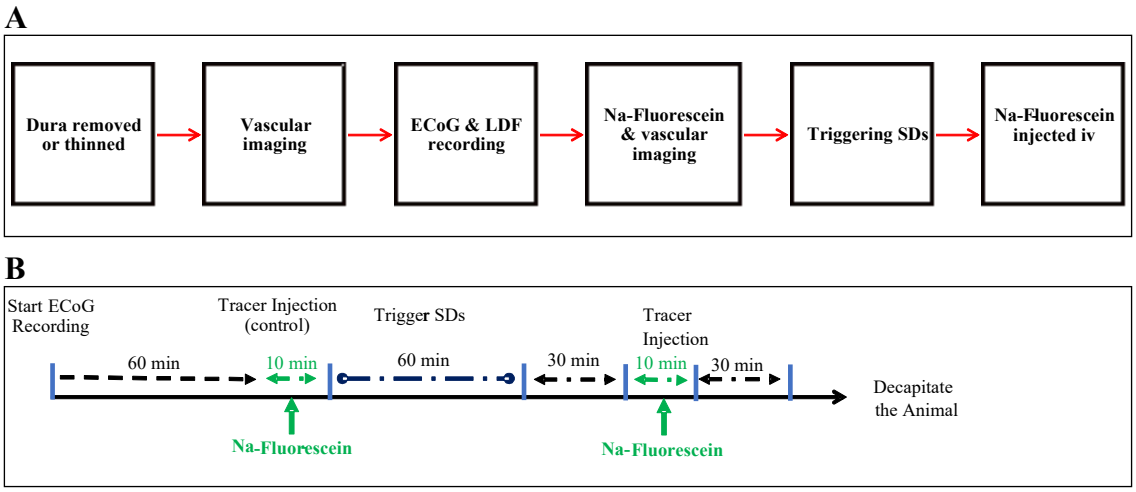

Figure 3.1. Monitoring of pial vessels and NVC of deeply anesthetized animals.

(**A**) Major steps included in the experiment design for vascular (pial) imaging. ECoG recording and rCBF monitoring (using laser doppler blood flowmetry (LDF)) are continuously recorded during the experiment. Na-Fluorescein (BBB-tracer) is injected before and after triggering SDs and is accompanied by video monitoring. (**B**) Schematic drawing for the timeline of procedures.

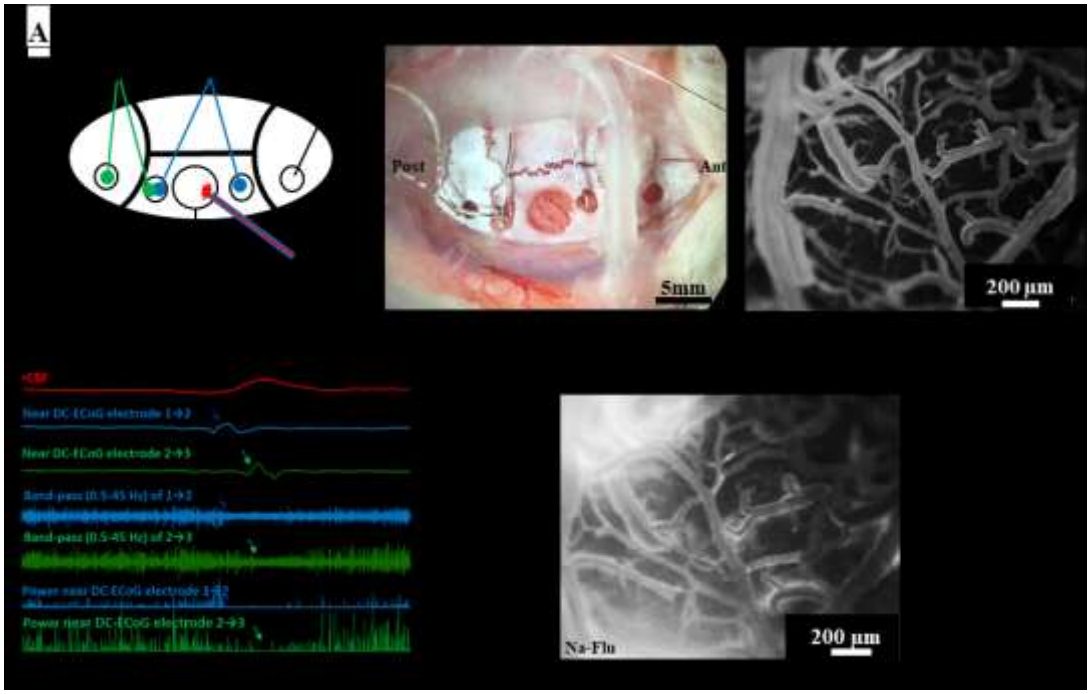

Figure 3.2. Major steps for acute brain monitoring and imaging.

(**A**) Schematic drawing for craniotomies including a small frontal hole for triggering SDs and other holes for ECoG recording. A large parietal window was drilled for acute cerebral vessel monitoring and imaging in addition to recording rCBF (**A** and **B**). ECoG recording and rCBF monitoring for 1 hour followed by vascular imaging and tracing dye injection (Na-Fluorescein) were performed for a baseline recording before triggering SDs (**C**). SDs were triggered electrically or using KCl through the right frontal hole, which is completely isolated from the rest of the skull by dental cement (**D**). Na-Fluorescein injected again after brain stimulation and pial vessels were monitored continuously (**E**). Notice the leakage from pial vessels to the extracellular space following induction of SDs.

3.2.1 Induction of Traumatic Brain Injury

The mild TBI induction is the same procedure as Chapter 2 (2.2.1.2) except with the following experiments the animal's skull and skin remained intact and the injury was induced using a 300 g weight dropped from a height of a meter directly onto the skin. These animals received a single mild TBI once per day for 5 consecutive days before undergoing a craniotomy and recording on day 6.

3.2.2 Craniotomy Protocol for Acute Brain Monitoring and Imaging

The surgical procedure is similar to that mentioned previously (Surgical Procedures 2.2.1.1). Three holes for bipolar ECoG recording were drilled, including two holes in the right parietal bone (2 mm posterior to bregma and 2 mm anterior to lambda, and both are 3 mm lateral to the midsagittal) and a third hole 3 mm posterior to lambda (Figure 3.2A and B). The ground was inserted in the subcutaneous tissue of the neck. Electrodes were made using Teflon insulated silver wire (A-M Systems, Inc. coated diameter is 280 µm). Electrodes were then fixed epidurally in bipolar fashion using dental cement (Figure 3.2B). To trigger SDs electrically, a right frontal hole (2x2 mm in diameter) was drilled 2 mm lateral and 2 mm anterior to bregma, and the dura was kept intact. The dura mater of the frontal hole was carefully opened. This opening was used to trigger SDs using KCl. For vascular imaging and monitoring, a right parietal window (4x5 mm in diameter, 2 mm posterior to bregma, 2 mm anterior to lambda, and 1 mm lateral to sagittal suture) was drilled as reported (135). However, the dura mater of parietal window was thinned and sometimes opened, and the exposed brain was perfused and continuously nourished by artificial cerebrospinal fluid (ACSF) at rate of 1.0 ml/min (257). The composition of the ACSF in mM was: NaCl: 124, KCl: 3, $CaCl_2$: 2, $MgSO_4$: 2, $NaHCO_3$: 26, glucose: 10, pH 7.4 at 34-36°C, osmolarity 300 ± 10 mOsmol/l and it was carbogenated with 95% O_2 and 5 % CO_2 (135,258).

3.2.3 Electrocorticographic (ECoG) Recording

Recordings were performed using the same equipment and configurations mentioned previously in Chapter 2. Recording of ECoG signals was carried out under deep anesthesia using isoflurane (1.5-2%) for three hours. The first hour was baseline recording followed by an hour of simultaneous ECoG and triggering of SDs either electrically or using KCl. The recording was continued for another hour after the triggering phase. The recordings were analyzed using the same method explained previously in Chapter 2.

3.2.4 Triggering of Spreading Depolarizations

Episodes of SDs were triggered for both control and TBI groups. Two different methods were used to trigger SDs.

3.2.4.1 KCl-Triggered SDs

SDs were triggered at the stimulation site (frontal hole) by application of 3 M KCl-soaked cotton ball to the pial surface of the frontal cortex for 30 seconds. The hole was continuously drained by ACSF. This process was repeated for three times with 10-15 minutes intervals.

3.2.4.2 Electrically-Triggered SDs

The electrical stimulation method was mentioned previously (2.2.1.4).

3.2.5 Evaluation of BBB Integrity

Before and 30 minutes after triggering SDs, Na-Fluorescein (Na-Flu, MW 376 Da), 0.6 ml/kg (1mg/ml in saline) was injected intravenously in the tail vein at a rate of 0.45 ml/min (135,259), Figure 3.1 and Figure 3.2C and E. During the entire procedure, pial vessels were monitored continuously through high resolution video recording (2560×2160, and 1 image/s) using an imaging-setup of a fluorescence microscope (Axio Zoom, V16, Zeiss GmbH; Konigsallee, Germany) with three built-in filters (580 nm wavelength) and scientific CMOS camera (PCO Edge 5.5 model, PCO-Tech Canada). Half an hour after the last injection of Na-Flu, the anesthetized animals were perfused, and the brains were quickly removed and kept in 4% formaldehyde solution.

3.2.6 Image Analysis

Using MATLAB codes designated by Prager and his colleagues (2010) (135), we analyzed the videos to assess the BBB-integrity. Images were rescaled to 256×256 pixels (135) and corrected for movement artifacts. To assess the vascular permeability, the extravascular space and vascular compartment were segmented and selected by points and dotted lines, using the MATLAB software, based on an arteriovenous anatomy. For each extravascular space pixel, the software compares the change in extravascular space signal intensity over time (reflecting tracer accumulation) before and after SDs in both TBI and control groups.

The difference in the signal intensity represents the BBB integrity and the amount of leakage in the extravascular space. This change is known as the 'blood-brain barrier permeability index' (135). If the value of permeability index (PI) is less than or equal to 1, there is no change or increase in BBB permeability

3.2.7 Measurement of Regional Cerebral Blood Flow (rCBF)

Cerebral blood flow was continuously recorded using an Oxyflo Probe (Oxford Optronix Ltd, MNP110XP, U.K) connected to a blood flowmeter (ADInstruments, INL191, wavelength 830 ± 10 nm) (135,204,225,260). The probe was fixed to a micromanipulator and positioned close to the parietal cortex. Laser Doppler flowmetry (LDF) measures the microvascular blood perfusion (relative blood cell flux) by utilizing the frequency changes reflected by blood cells. This varying signal content is converted into a voltage output that represents the percentage of backscattered light. Results are expressed as percentage of baseline (0-100%) providing relative blood flow values.

Statistical Analysis

Results are expressed as mean ± standard error of the mean, unless otherwise stated. Differences between more than two groups were determined by Kruskal Wallis test or Friedman test, and between two groups were determined by Wilcoxon signed-rank test or Mann-Whitney U test. Differences were statistically significant at $P<0.05$. All statistical analyses were performed using IBM SPSS Statistics (version 24.0).

3.3 Results

3.3.1 TBI Group Has More Vulnerability for an Increase in BBB Permeability under the Effect of SDs

SDs were triggered in control (n=18) and TBI (n=16) groups using two different methods, electrical stimulation (control: n= 9 vs. TBI: n=8) and using KCl (control: n=9 vs. TBI: n=8). BBB integrity change was assessed and evaluated before and after triggering SDs in both TBI and control groups. The degree of the change in BBB permeability was represented (arbitrary unit) as a permeability index (PI), and if the value of PI is less than or equal to 1, there is no change or increase in BBB permeability (135). In the present study, SDs may have no effect on the BBB of control groups within an hour after stimulation. On the other hand, in TBI groups, a significant increase in BBB-permeability index after SDs was observed following KCl (before SDs: 0.73 ± 0.1 vs. after SDs: 1.3 ± 0.24, n=8, P=0.01) and electrical stimulation (before SDs: 0.86 ± 0.06 vs. after SDs: 1.7 ± 0.43, n=8, P=0.03), Figure 3.3E.

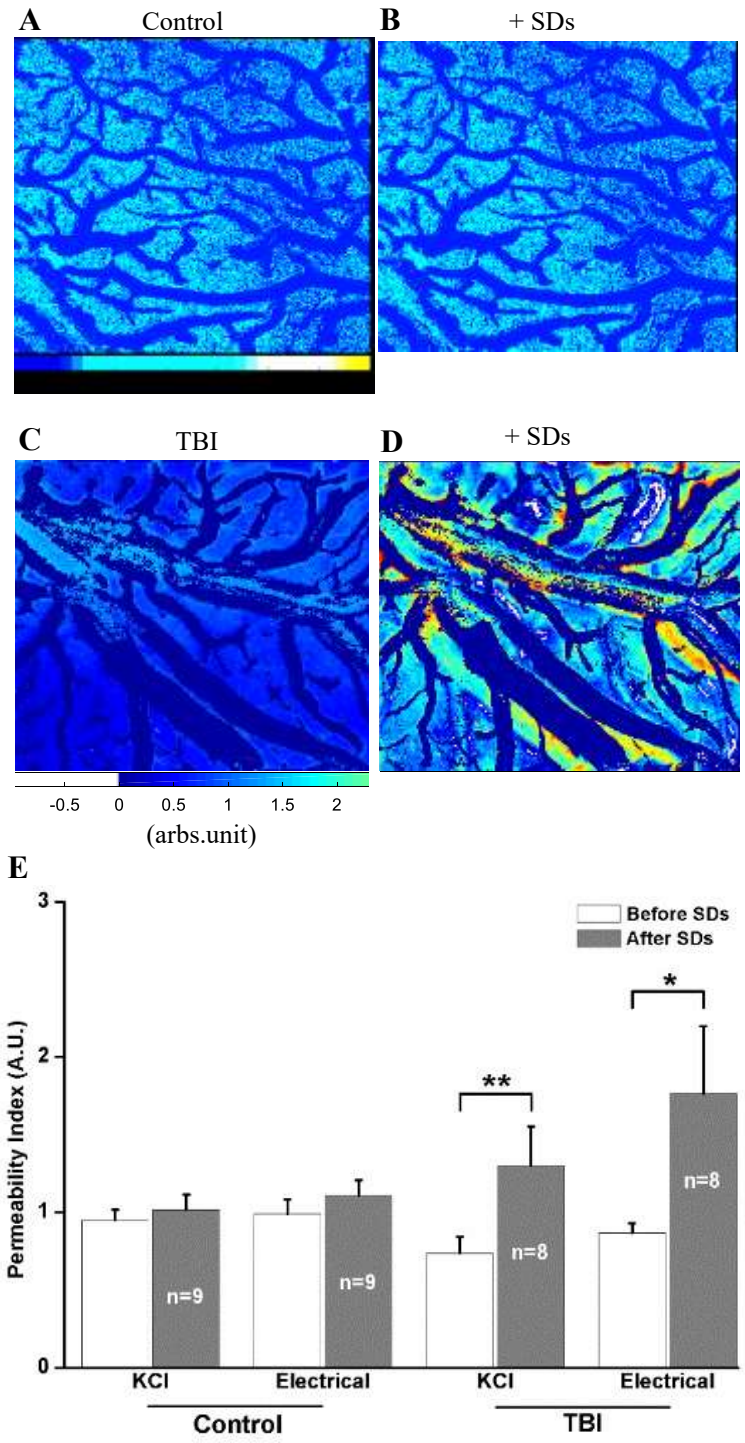

Figure 3.3. The effect of SDs on blood-brain barrier permeability in-vivo.

BBB permeability maps (arbs.unit) before (**A**) and after (**B**) triggering SDs in control animal. Permeability maps for a TBI animal (**C**) showing an increase in accumulation of Na-Fluorescein in the extravascular space after triggering SDs (**D**), suggesting an increase in BBB permeability. (**E**) Mean (±SEM) of PI for control and TBI groups before and after SDs. Chemical (KCl) and

electrical methods were used to trigger SDs. If the value of PI ≤ 1, then there is no increase in BBB permeability. * P < 0.05, ** P ≤ 0.01 (Mann-Whitney test and Wilcoxon signed ranks test).

3.3.2 Seizures Recorded in Control and TBI Groups

During ~3 hours of ECoG recording and triggering SDs, our results showed seizure events (Figure 3.4A) recorded in both control and TBI groups regardless of the method used to trigger SDs, Figure 3.4B. Seizure events (n=9) were recorded in control and TBI groups, and recordings from 7 rats showed that seizures came after SDs, and 2 rats showed seizure activities before and after SDs.

A

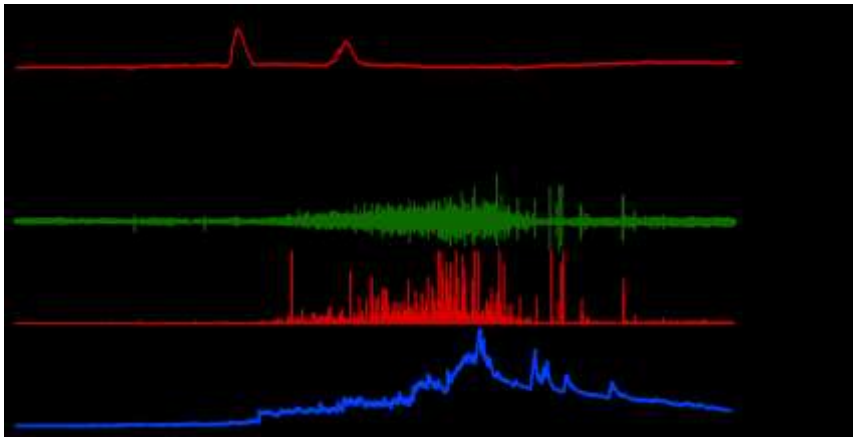

B

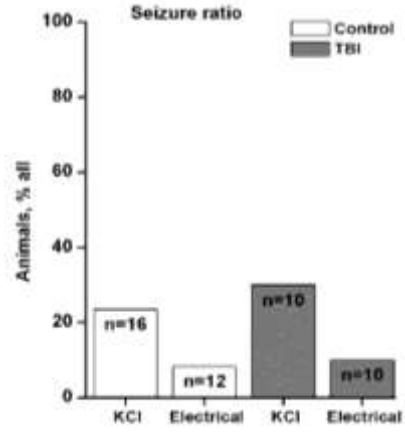

Figure 3.4. Seizures following SDs triggered at the frontal cortex.

(**A**) ECoG recording from the right parietal cortex following KCl application on the right frontal cortex to trigger SDs. After stimulation, there were seizures after SDs and these lasted for ~20

minutes duration, and these were accompanied by an increase in rCBF (hyperemia) as seen in the first upper trace. To show the spontaneous brain activity, a digital band-pass filter (0.5-45 Hz) was applied (green trace) to the raw ECoG recording (0.02-100 Hz). The recording shows an increase in squared spontaneous activity (power near DC-ECoG, 4th trace) during the seizures. (**B**) Seizure activities for control and TBI groups following KCl- and electrical-stimulation.

3.3.3 Spreading Depolarization Characteristics

3.3.3.1 SD Durations

SD durations were measured from the beginning of deviation from the baseline to the starting point of recovery and the return to baseline (55,206), Figure 3.5B. SD durations in control and TBI groups were almost similar and no significant difference was seen among KCl groups (control: n=16, 98 ± 10 s versus TBI: n=10, 96 ± 3 s) or using electrical stimulation (control: n=12, 83 ± 13 s versus TBI: n=10, 59 ± 14 s, Figure 3.5A).

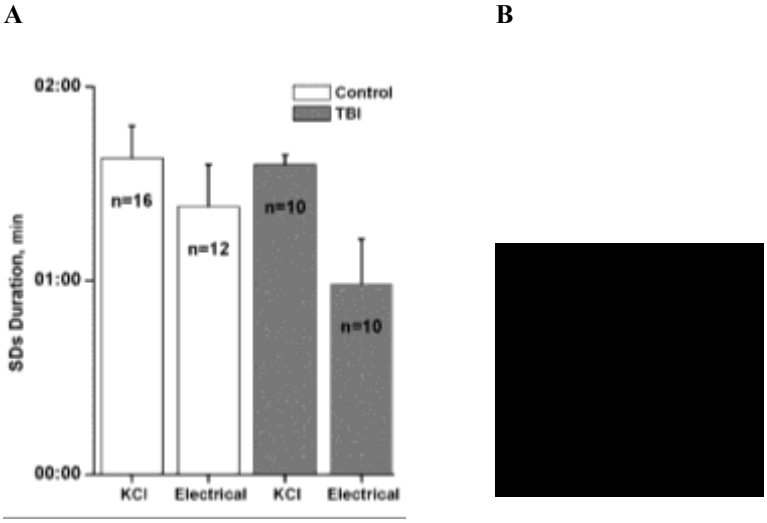

Figure 3.5. Spreading depolarization durations.
(**A**) The duration of triggered SDs for control and TBI groups. (**B**) Schematic drawing shows the duration of the SD phase measured from the start of deviation from the baseline level until the return to the baseline.

3.3.3.2 SDs Amplitude

The amplitudes of the slow potential changes of SD waves were measured from peak to peak as illustrated in the schematic drawing above (Figure 3.5B). In terms of SD amplitude, the results did not confirm any significant difference between control (n=16) and TBI (n=10) groups stimulated by KCl (control: 0.41 ± 0.07 mV vs. TBI: 0.38 ± 0.07 mV). However, significantly larger amplitudes were recorded in the electrically-triggered TBI group as compared to control (control: n=12, 0.26 ± 0.03 mV vs. TBI: n=10, 0.43 ± 0.04 mV, P = 0.02), Figure 3.6A.

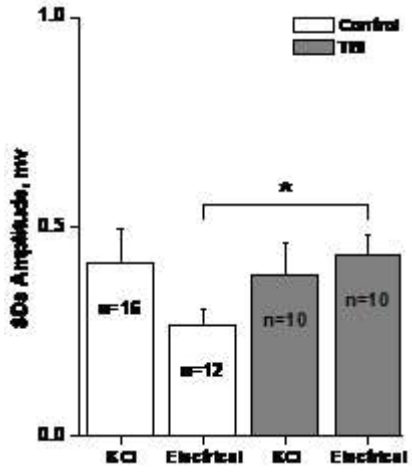

Figure 3.6. SDs amplitude in control and TBI groups.

Mean of SDs amplitude is higher in TBI group after electrical stimulation.

* P < 0.05, (Kruskal Wallis test and Mann-Whitney U test).

3.3.3.3 SDs Propagation

While the right frontal hole (~5 mm anterior to the recording site in the parietal cortex) is the location of the stimulation (Figure 3.7A), the propagation velocity of SDs was measured by dividing the total displacement (between frontal hole and first parietal electrode) by the total time needed to start SDs at the recording site (Figure 3.7A and B). The anesthetized groups showed no significant differences in SDs velocity neither between KCl-triggered groups (control: n=16, 3.1 ± 0.25 vs. TBI: n=10, 2.5 ± .35 mm/min) nor between electrically-stimulated groups (control: n=12, 3.0 ± 0.23 vs. TBI: n=10, 3.0 ± 0.18 mm/min), Figure 3.7C). To show the effect of anesthesia on SDs propagation velocity, SDs

were electrically triggered in unanesthetized non-traumatized animals. Interestingly, we found that SDs were significantly (P = 0.0003) propagated faster in the unanesthetized group (n=20, 5.07 ± 0.34 mm/min) compared to deeply anesthetized animals (n=12, 3.0 ± 0.23 mm/min), Figure 3.7D.

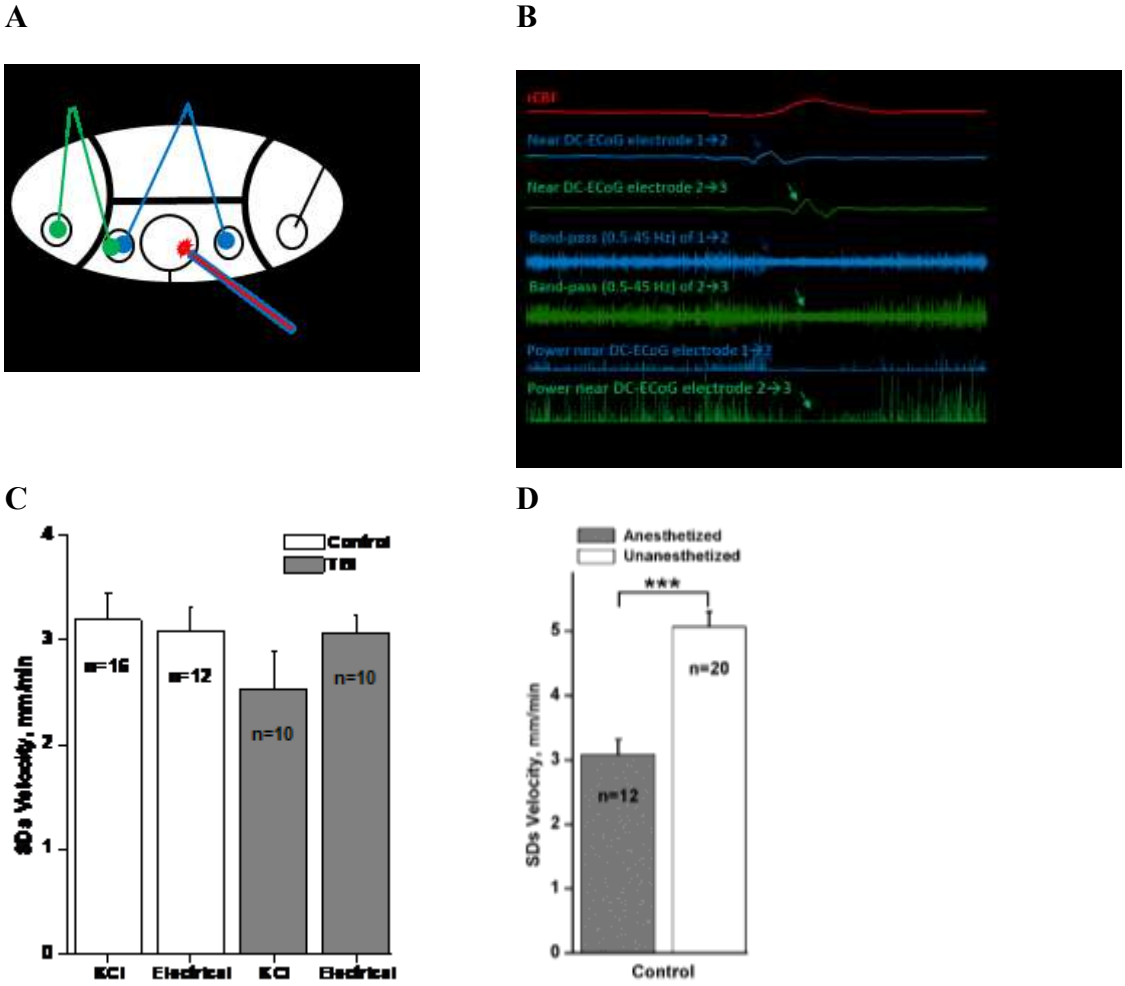

Figure 3.7. SD propagation velocities in control and TBI groups.

(**A**) The schematic drawing shows the location of stimulation and ECoG recording, in which SDs were triggered at the frontal hole and propagated toward the anterior electrode of channel 1. (**B**) Bipolar raw ECoG recordings (band-pass: 0.02-100 Hz, 2nd and 3rd traces). SD observed as a slow potential change (oblique arrows), that propagated across the right brain hemisphere from anterior electrodes (channel 1) to posterior electrodes (channel 2). (**C**) Regardless of the method used to trigger SDs (KCl or electrically) in deeply anesthetized rats, there was no difference between SDs velocity in control or TBI groups. (**D**) SDs propagated slower under anesthesia.

3.3.4 Regional Cerebral Blood Flow (rCBF) in Response to SDs

Neurovascular coupling is a phenomenon of an increase and decrease in rCBF in response to different neuronal activities (48,100,135,168). SDs were found to be accompanied by an increase in cerebral blood flow (Figure 3.8A) to compensate for the increase in energy demands, and occasionally reversed NVC and a decrease in the blood flow in pathological tissue (197). In this study and in response to triggered SDs, rCBF recordings were classified into three phases (214) depending on analysis of recordings acquired using laser doppler blood flowmetry (LDF), Figure 3.8B.

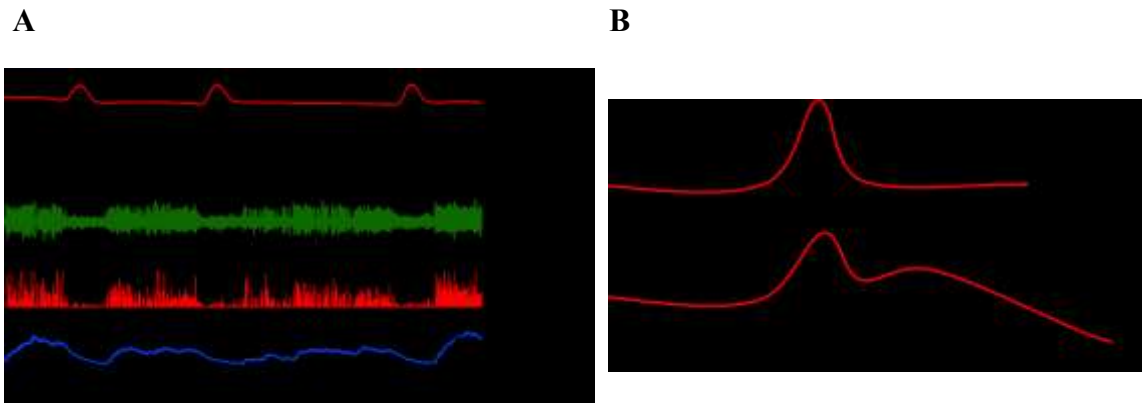

Figure 3.8. Neurovascular coupling in response to triggered SDs.
(**A**) ECoG recording from the right parietal cortex of a control animal associated with recording of rCBF from the same region of recording using LDF. SDs were triggered by 3M of KCl-soaked cotton ball applied to the right frontal cortex for 30 seconds. Vertical arrows of the first trace (rCBF) indicate the time of KCl application. rCBF shows that hyperemia (phase I) is the major response of pial vessels to SDs. Oblique arrows on the second trace indicate SDs. (**B**) Schematic drawings show three different phases of rCBF in response to SDs, in which I, II, and III represent hyperemic, late hyperemic, and oligemic phases respectively. It is noteworthy to mention that it is not necessary for all phases to exist in the same rCBF response.

3.3.4.1 Hyperemic Phase

The hyperemic phase (I) is the most common phase during SD (202,205,214). The duration of this phase is ~ 1-2 minutes, and it was measured from the point of deviation from baseline toward the peak until the point of returning to baseline or converted to the second phase (late hyperemia), Figure 3.9A. Phase I precedes the phase of late hyperemia (II), and it has a dome shape with a peak, and it represents the major rapid hyperemic phase in

response to SDs and seizures. However, the difference in duration for this phase was not significant among the different groups (control, KCl: 116 ± 5 s and electrical: 119 ± 15 s vs. TBI, KCl: 134 ± 14 s and electrical: 89 ± 18 s), and the majority had a duration of ~ 2 minutes (Figure 3.9B).

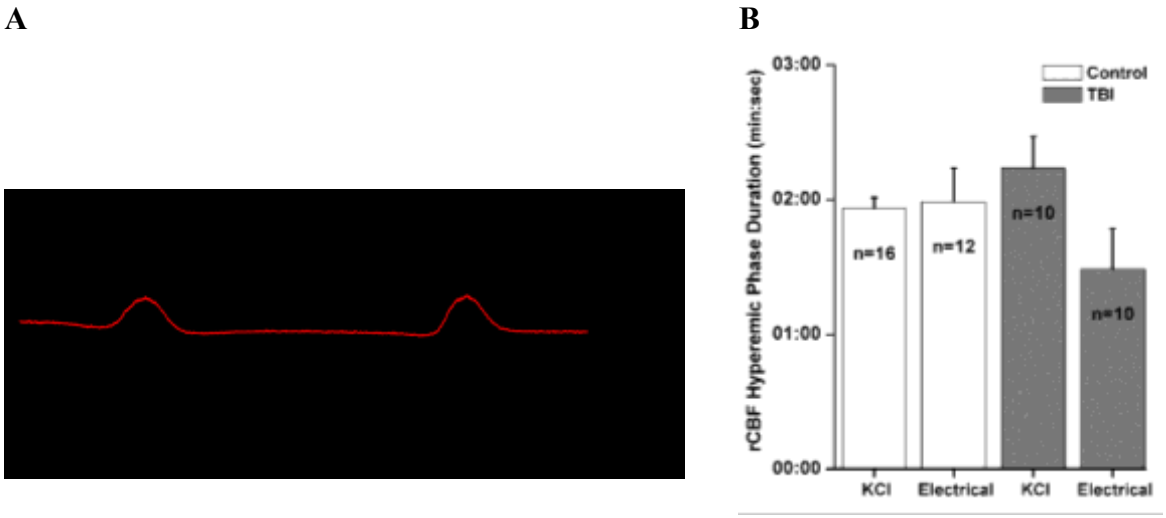

Figure 3.9. Hyperemic phase of rCBF (phase I) in response to SD.

(**A**) The recording of rCBF and ECoG from the right parietal cortex of a control animal. Hyperemia is seen in the rCBF recording (red trace) in response to KCl-triggered SD (arrow). (**B**) The durations of the hyperemic phase in both control and TBI groups after triggering SDs electrically and using KCl.

3.3.4.2 Late Hyperemic Phase

It is the second phase in the response to SD. The phase comes immediately or later after the hyperemic phase. Furthermore, the late hyperemic phase can start earlier, before the ending of the hyperemic phase and superimpose it (Figure 3.10A). Interestingly, the analysis revealed a significant shorter duration of late hyperemia in TBI (n=10, 47 ± 32 s) than control (n=12, 200 ± 41 s) in response to electrically-triggered SDs, but not using KCl (control: n=16, 110 ± 47 s vs. TBI: n=10, 87 ± 28 s), Figure 3.10C).

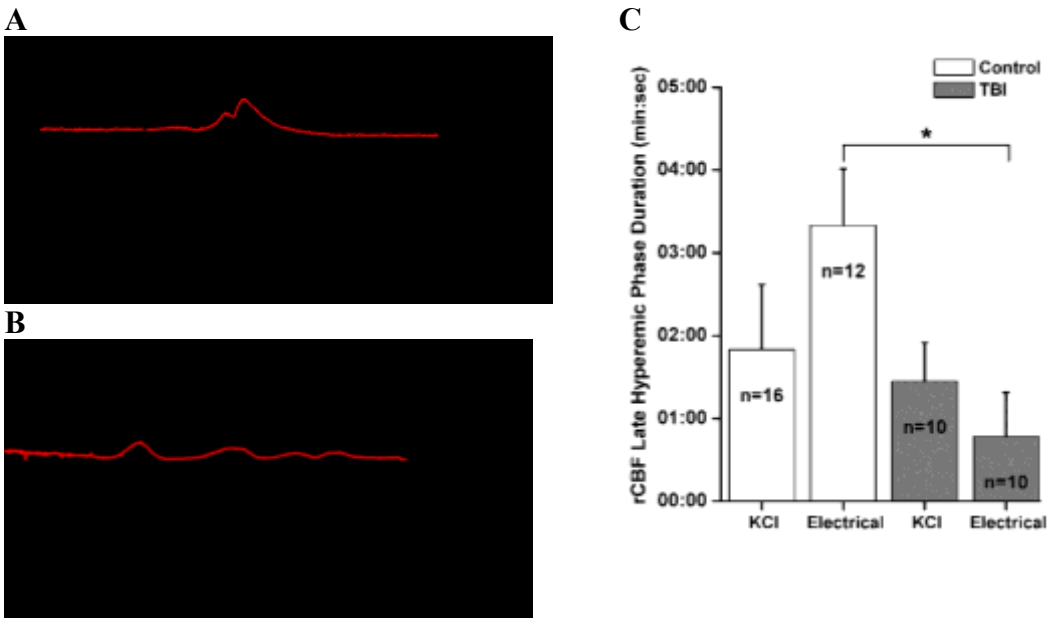

Figure 3.10. Late hyperemic phase (phase II) in response to SDs.

ECoG and rCBF recordings show the hyperemic phase (I) superimposed (**A**) or followed **(B)** by late hyperemic phase (II) in response to an electrically-triggered SD through the frontal hole. Late hyperemia started when the hyperemic phase was interrupted before returning to baseline. (**C**) The duration of late hyperemia is longer in control animals. * $P < 0.05$, (Kruskal Wallis test and Mann-Whitney U test).

3.3.4.3 Oligemia Phase

The oligemia (phase III) (Figure 3.11A) is associated with different neurological conditions such as TBI, SDs, and subarachnoid hemorrhage, and can last for hours or longer (53,89,202,205,214,216,217). Our stimulation results showed that control animals, exposed to electrical stimulation, has a significantly longer duration of oligemia (electrical: n=12, 181 ± 31 s vs. KCl: n=16, 42 ± 19 s), but in the TBI group the difference was not significant (Figure 3.11B). Contrary to expectation, there was no significant difference between control and TBI groups.

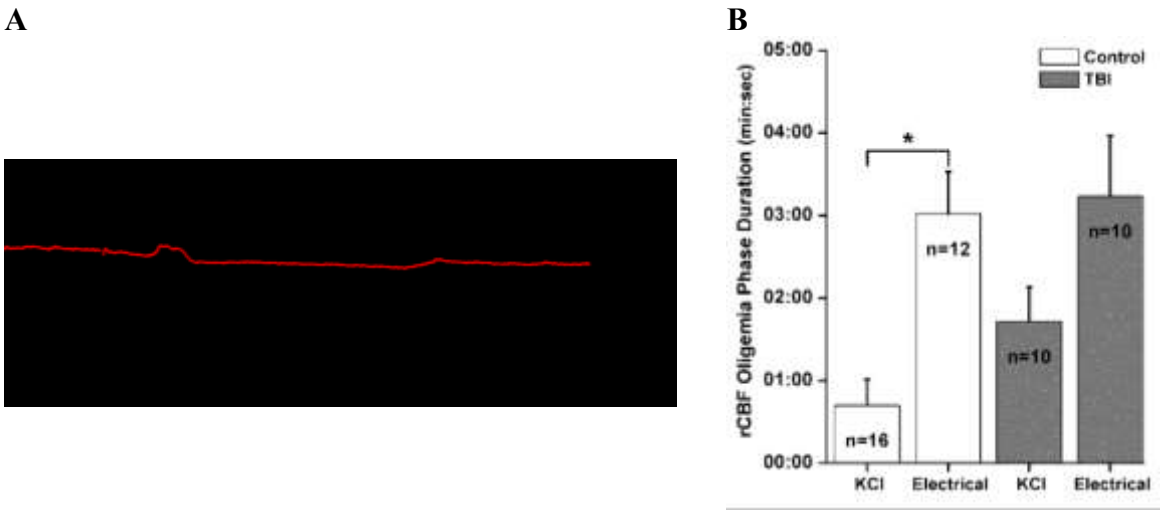

Figure 3.11. Oligemia phase (Phase III) of rCBF.

(**A**) In response to electrically-triggered SD (dotted arrow), oligemia (red trace) followed a short duration of hyperemia. However, animals started to recover gradually (asterisk) from oligemia. (**B**) The duration of oligemia in both control and TBI groups in response to electrically-and KCl-triggered SDs.

However, in this study, we calculated the occurrence rate of all rCBF components (I-III) in relation to the number of SDs in each group (Figure 3.12). Among the groups, the analysis showed that the late hyperemia (phase II) in the electrically-triggered TBI group (18.18%) has a lower occurrence rate compared to the electrically-triggered control group (80%). Phase I is the predominant rCBF response among all groups.

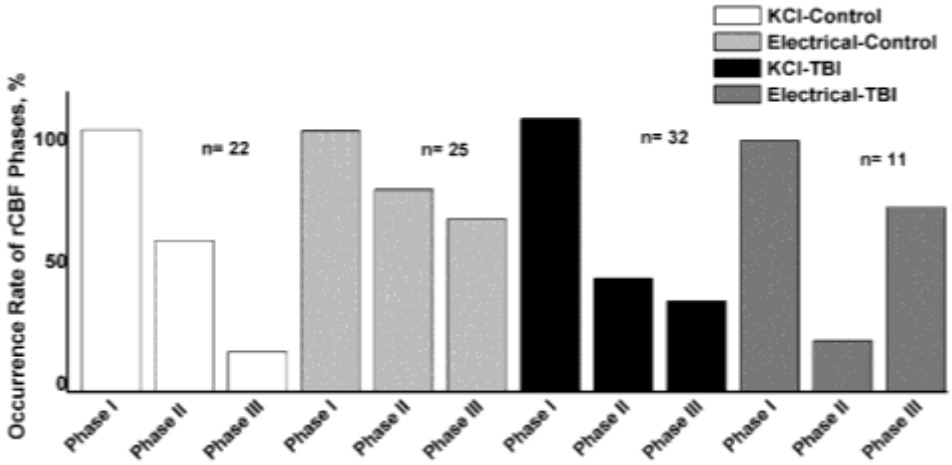

Figure 3.12. Occurrence rate of rCBF phases.

The occurrence rate of different rCBF phases in relation to the number of triggered SDs (indicated by “n”) either electrically or using KCl in TBI and control groups.

3.4 Discussion

In our previous study (Chapter 2), SDs were found to be the immediate pathophysiological event following mild TBI, and this suggested SDs as the hallmark of concussion. However, in TBI the effects of SDs are still unclear, and worse clinical outcomes are seen in patients who have SDs associated with TBI (53,85). Thus, we assumed that SDs could be one of the key factors in the relationship between TBI and BBB dysfunction.

This study has demonstrated that animals exposed to TBI have more vulnerability for an increase in BBB permeability within ~2 hours after triggering SDs. SDs occur spontaneously after ischemic, hemorrhagic and traumatic brain injury (85,88,206). BBB dysfunction may occur because of status epilepticus or TBI (117,118). There are very limited studies on the effect of SDs on BBB integrity.

Matrix metalloproteinases (MMPs) are members of an enzyme family (proteolytic enzymes) that digest components of the extracellular matrix (ECM) such as the interstitial and basement membrane collagens and cell surface receptors (150). In the literature, the effect of release and activation of MMPs were observed following intracerebral hemorrhage, stroke, brain tumor, and TBI (150,153–156) with a noticeable effect on the integrity of the BBB. Following 3-6 hours of triggering SDs in a rodent model, the level of MMP-9 was increased, and reaching the maximum at 24 hours. Furthermore, cerebral vascular leakage was reported after 3 hours of triggered SDs, but not in MMP-9-null mice, indicating that MMPs was a predisposing factor for the initiation of BBB disruption process (149).

In another study, after 30 minutes of intracortical injection of KCl, C-sucrose leaked to the cortex, resolved within 6 hours, with no change in tight junction proteins (occludin or claudin-5) expression (261). The increase in extravasation of plasma protein as a result of topical KCl itself was not excluded (158).

In our study, the increase in BBB permeability was noticed within ~2 hours of triggering SDs in TBI animals, suggesting that there may be a fast mechanism by which SDs affect BBB integrity following TBI. There is evidence that the permeability of the BBB increases following activation of NMDA receptors and excessive glutamate release (262). While SDs are accompanied by a massive increase in glutamate level, NMDAR antagonists had reduced the BBB permeability by decreasing the number of SDs (158). Furthermore, the

extracellular concentration of glutamate increased immediately following TBI and peaked within 4-5 minutes (263). In another study, the concentrations of glutamate and aspartate in the CSF of patients with head injuries were 2 to 8-fold higher than control, measured one hour after injuries and continued to be elevated for 3 days (264) and up to 9 days (265). In a rat model, the rise in the extracellular glutamate level was immediate and lasted up to 9 days following TBI (266). Thus, in our study, an increase in glutamate, that could last for days after mild TBI, may have enhanced the effect of triggered SDs on BBB integrity.

SDs triggered electrically or chemically using KCl (high K^+) have similar pharmacology, in which NMDA receptor antagonists block SDs triggered by both methods (75,267). In this study, the analysis did not confirm any significant difference between both methods of stimulation.

In the present study, BBB permeability and vascular leakage of Na-Fluorescein were significantly increased after triggering SDs in the TBI group, suggesting that pathological brain tissues are more vulnerable for further injuries.

Seizure activities were recorded from both control and TBI groups. Seizures and CSDs were reported following acutely injured human brain, and they have a role in exacerbation of tissue damage (58,98). In this study, the ratio of seizures to the number of SDs is very low. It had been reported that patients with an acute brain injury and aneurismal subarachnoid hemorrhage (ASH) had increased occurrence of SDs over that of ictal epileptic events, and were associated with worse outcomes (58,90,91). In this study, and after brain stimulation, seizures were recorded in 17.8% of the control group (5 out of 28), and 20% in the TBI group (4 out of 20). In the present study, most of seizures came after, but rarely before, triggered SDs. However, the relationship and interaction between SDs and seizures is still a controversy. An interrelationship between SDs and seizures is reported, in which SDs were preceded or followed seizures (103,268). While they are following each other interchangeably, this makes the explanation more difficult. It has been reported that triggered SDs enhanced neuronal excitability and facilitated seizure activity in epileptic human brain tissues (104–106,269), and in anesthetized rats, triggered seizure activities can lead to single and repetitive SDs (106).

It had been suggested that prolonged duration of SDs is one of the major factors in forming cortical lesions by inducing hypoperfusion and impaired NVC (53). Similar to the freely

behaving animals in this study (Chapter 2), SDs duration in deeply anesthetized animals was almost similar among all groups, and the durations were also relatively short. This consistency and short duration of SDs among the various groups may indicate an absence of brain ischemia (270,271) and cortical lesions (53) after the mild TBI, and sufficient cerebral perfusion and functional NVC (53,271,272). Consistent with our results, and under isoflurane anesthesia, KCl-triggered CSDs have short durations (273). Taken together, our results suggest that anesthesia and different stimulation methods may have no effect on SDs durations. This could be related to the brain tissue condition and sufficient cerebral perfusion for this energy demand situation.

SDs propagate at 1-9.5 mm/min in the brain of patients with SAH and malignant stroke (52,54,56). In previous studies, KCl-triggered SDs were propagated at ~2-2.5 mm/min (274,275), and at ~3.2 mm/min using electrical stimulation (276). Thus, this confirms our findings, in which the propagation velocity was ~3 mm/min in both KCl- and electrically-triggered SDs under the effect of anesthesia. The speed of propagation was greater (~5 mm/min) in unanesthetized animals, and an explanation for this could be the effect of anesthesia on SDs propagation speed. Although the mechanism of propagation of SDs across the brain is a controversy, it is still considered one of the most important characteristics of SDs wave (46,48). However, in our study, anesthesia reduced the speed of SDs propagation, but has no impact on SDs duration. Isoflurane is an anesthetic that causes modest inhibition of NMDA receptors (277,278). Thus, the effect of an increase in concentration of K^+ and glutamate in the extracellular space during SDs could be partially decreased under the effect of anesthesia, and that ultimately affected the excitability level in neighboring neurons and the propagation of SDs to the surrounding tissue across the brain (48,84).

Neurovascular coupling (NVC) is a phenomenon of increase or decrease in rCBF in response to physiological neuronal activation or deactivation respectively (135,165–167). The changes in cerebral blood flow in response to SDs, including hyperemia or oligemia, had been observed before (135,159,178,179,198–202). In previous studies, and using magnetic resonance imaging (MRI), BBB dysfunction was associated with impaired NVC in response to SDs and ictal epileptic events (52,197).

In our study, hyperemia and to a lesser extent oligemia, were recorded in response to

triggered SDs and seizures. While physiological hemodynamic response (hyperemia) was the dominant response of cerebral vessels to SDs in healthy tissue, inverse hemodynamic response (oligemia) was not uncommon in tissue at risk for progressive damage (48,89,203–205).

All three rCBF phases were recorded in our study. Most importantly, the duration of the late hyperemia phase was shorter in TBI group but longer in control. In a previous study (202), TBI-exposed animals had less rCBF before and even after SDs, suggesting a compromised NVC process. NVC was varied between TBI patients depending on the severity of the injuries. The variations in rCBF were between physiological hyperemic and pathological inverse coupling, and could switch from physiological to pathological coupling (89). SD usually accompanied by an increase in cerebral blood flow in well supplied tissue, but a decrease in cerebral blood flow and an inverse in NVC were recorded with SDs following SAH, TBI, and injured human brain (201,207,208), suggesting that inverse NVC leads to an exacerbation of existing ischemic conditions and increases the duration of SDs.

Consistent with our study, the hyperemic phase was reported during SDs (202,205,214) with approximately 1-2 minutes duration, reaching the peak within a minute from the beginning of SD. After 3-5 minutes of SD, the late hyperemia phase starts as reported previously, and it represents an increase of about 10 % in CBF (198,279). There are many factors that have a role in decreasing CBF, but it has been suggested that oligemia in response to SDs could be due to secretion of a pericyte constrictor (20-hydroxyeicosatetraenoic acid) (196) and a decrease in nitric oxide (280). Oligemia was reported following a transient increase in CBF and it lasted for around 1-2 hours (279). Unfortunately, following different neurological conditions such as TBI or SAH, oligemia was varied in duration and it may last for hours or longer (53,89,202,205,214,216,217).

Chapter 4: Spreading Depolarizations and Catastrophic Death Following Traumatic Brain Injury

4.1 Introduction

Traumatic brain injury (TBI) is the leading cause of death for infants and children. TBI-related deaths affect approximately 9000 people annually in the US (281), and cardiopulmonary resuscitation was not able to save lives in many of the cases of concussion. The immediate pathophysiological event that occurs and leads to death following TBI is unknown, although a central rather than peripheral mechanism accounting for respiratory depression was suggested (227). In Chapter 2 of this study, cortical spreading depolarization was found to be the common pathophysiological phenomenon recorded in both brain hemispheres within around two minutes immediately following concussion in almost half of the cases.

Nonspreading depression was described previously (271,282) as the simultaneous arrest of spontaneous brain activity of different brain regions as a result of oxygen depletion, circulatory arrest, and insufficient energy supply (234,271). Nonspreading depression was found concomitant with neuronal hyperpolarization probably due to a disturbance of vesicular transmitter release (glutamate and GABA) (283) and an increase in the conductance of K^+ (284,285). ATP-sensitive potassium (KATP) channels exist abundantly in the membrane of neurons in the brain and in the brain stem (286,287). Activation of KATP channels leads to hyperpolarization of the nerve cells, causing a higher threshold and decrease in the excitability (284,285). However, the hyperpolarization state is followed by an increase in spontaneous vesicular release of glutamate before generating a depolarization (284,288,289). Nonspreading depression is typically followed by a short lasting or terminal spreading depolarization (TSD) propagating across the brain (48,271,282,290). TSD occurs in the presence of severely noxious conditions such as anoxia, aglycemia, and severe focal or global ischemia (48). TSD defines the point at which repolarization will no longer occur (271,291). However, nonspreading depression and TSD have not been reported immediately following TBI. In this study, we provide for the first time direct electrophysiological evidence that spreading depolarization and nonspreading

depression occurs in the brain stem immediately following TBI and can lead to respiratory depression and is followed in some cases by TSD and death.

4.2 Materials and Methods

All experiments were performed following institutionally approved protocols in accordance with the Canadian Council on Animal Care and were approved by the Dalhousie University Committee on Laboratory Animals.

Briefly, in this rodent model, animals with pre-implanted electrodes were sedated for two minutes and exposed to TBI, and then connected immediately (less than 20 seconds) to the recording system. The brain signals from both hemispheres and brain stem were recorded simultaneously with electrocardiogram (ECG) and respiratory rate acquired before and immediately after TBI. Two animals in this study were intubated and connected to a ventilator after the impact.

4.2.1 Surgical Procedures

The surgical procedure is similar to that mentioned previously (2.2.1.1. Surgical Procedures 2.2.1.1). For recording from the brain hemispheres, four holes (2x2 mm in diameter) for screws (stainless steel bone screws, F.S.T, 0.86 mm x 4 mm) were drilled in the right and left parietal bones (2 mm posterior to bregma, and 2 mm anterior to lambda, and 3 mm lateral to sagittal suture). In addition, two holes (one in each side) in the occipital bone (12 mm posterior to bregma, and 3 mm lateral to midline) were drilled for recording from the brain stem at 9 mm depth. A ground electrode was inserted into the neck subcutaneous tissue. A round platform (1x1 cm) was formed above the skull (parietal bone) using a dental cement (Figure 4.1).

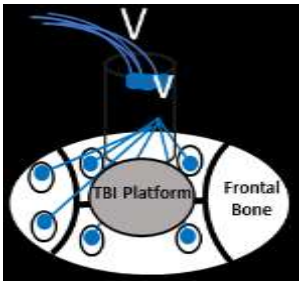

Figure 4.1. Schematic drawing shows the location of holes for ECoG and constructed platform for TBI.

4.2.2 Traumatic Brain Injury Model

We used the same weight-drop model of TBI mentioned previously in Chapter 2 (2.2.1.2) except that the TBI was induced using the weight travelling vertically (1 m), and directed to hit the dental cement-platform located above parietal bones.

4.2.3 Electrocorticographic (ECoG) Recordings

Recordings were performed using the same equipment and configurations mentioned previously in Chapter 2. In addition to recording signals from both brain hemispheres and brain stem, ECG and respiratory rate (RR) were recorded using subcutaneous stainless-steel cups (2 mm diameter) fixed laterally to the chest, connected to the silver wires and ultimately to the recording system.

Statistical analysis

Results are expressed as mean ± standard error of the mean, unless otherwise stated. Differences between two groups were determined by the Wilcoxon signed-rank test or the Mann-Whitney U test. Differences were deemed statistically significant at $P<0.05$. All statistical analyses were performed using IBM SPSS Statistics (version 25.0).

4.3 Results

Repetitive TBI can be associated with an immediate sudden death by an unknown mechanism. In this study, a repetitive TBI model was created to induce a concussion, which was followed occasionally by death, and to record the electrophysiological alterations in both brain hemispheres and brain stem immediately following TBI. It is ethically and practically not feasible to record invasively from a human immediately after TBI, and that makes it difficult to understand the pathophysiological mechanism of the catastrophic death following concussion.

In our previous study, SDs were the most common electrophysiological change following mild TBI to either one or both brain hemispheres. Importantly, most of the SDs were recorded within the first 3 minutes after the impact. However, in this study, the recordings were performed from both brain hemispheres and for the first time from the brain stem (Figure 4.2).

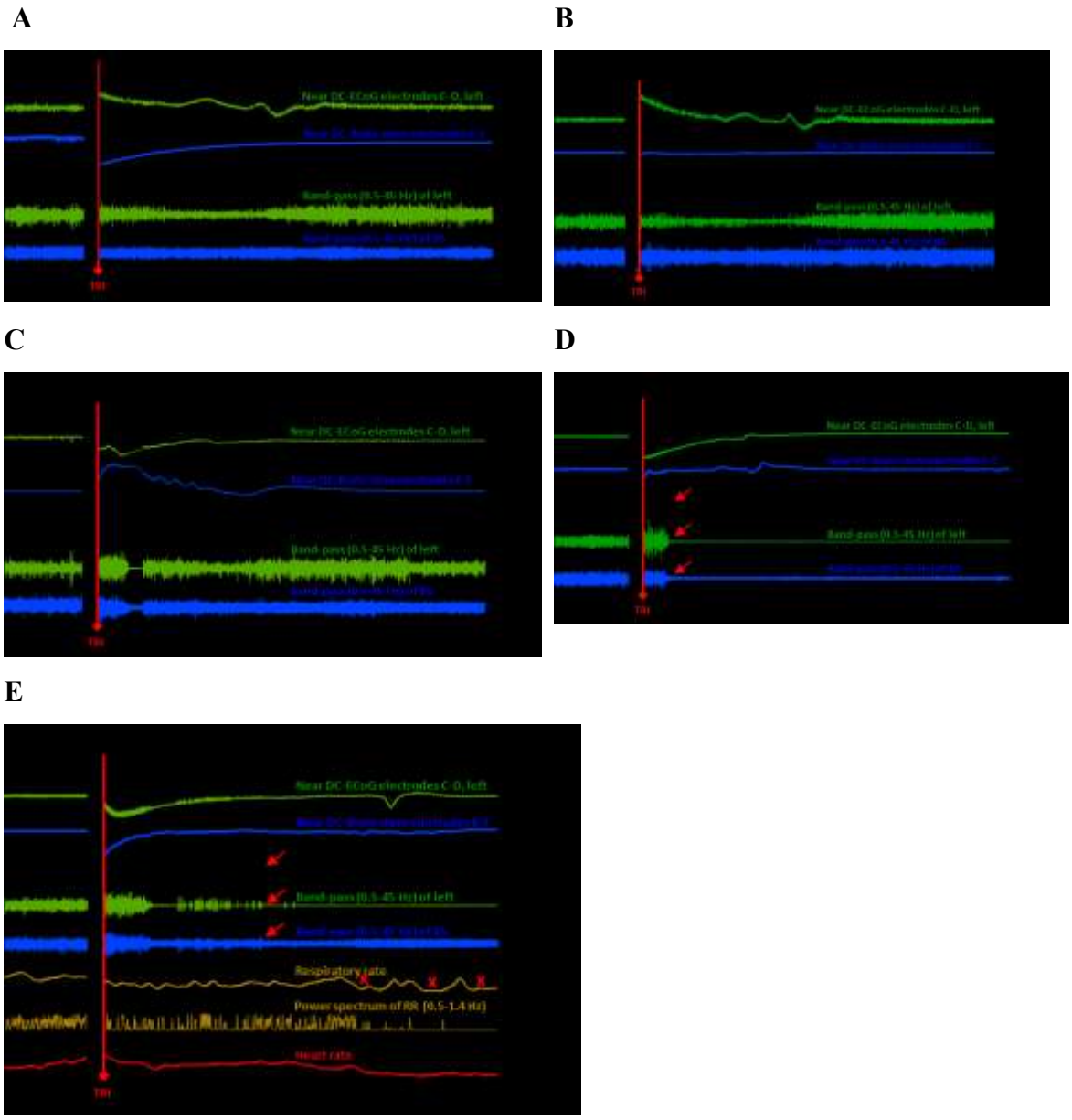

Figure 4.2. The electrophysiological changes following TBI.

In general, the first upper two traces represent the raw ECoG recordings (band-pass: 0.02-100 Hz) from both brain hemispheres, while the third trace represents near-DC recording from the brain stem (BS). Traces 4, 5, and 6 show the spontaneous brain activity (band-pass 0.5-45 Hz) of the first three raw traces respectively. Spreading depression of the brain activity recorded during TBI-induced SDs in **A**, **B**, **C**, and **E** (asterisk). Nonspreading depression (red arrows) followed by terminal spreading depolarization (TSD) was observed simultaneously in all traces following TBI (**D** and **E**). (**E**) Respiratory rate (RR) and ECG were monitored simultaneously with ECoG and BS recordings, in which respiration was interrupted during SDs. Respiratory depression (x) followed nonspreading depression of brain activity. Heart rate appears not to be significantly affected.

SDs and depression of brain activity were observed in 25 out of 37 (67.5%) impacts (Figure 4.3).

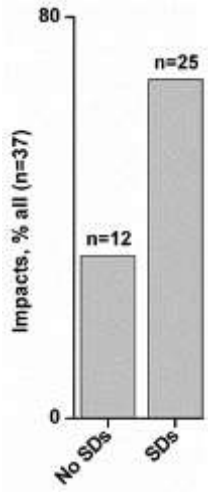

Figure 4.3. Occurrence rate of SDs following TBI.

Similar to our results in Chapter 2, SDs are common after TBI.

The depression of brain activity that accompanied either SDs, TSD, or both was recorded in the right hemispheres only (n=5), left hemisphere only (n=6), right and left hemispheres (n=4), and in both hemispheres and brain stem (n=14), Figure 4.2 and Figure 4.4.

All SDs and the associated spreading depression were recorded from survived animals (Figure 4.2A, B, and C) immediately after 146 ± 13 s (n=20) of TBI (Figure 4.4). Most importantly, all animals that died (n=9 out of 10) showed a nonspreading depression of spontaneous activity in both brain hemispheres and brain stem (Figure 4.2D and E). However, TSDs followed the occurrence of nonspreading depression and were recorded 204 ± 41 s (n=9) after TBI (Figure 4.2D).

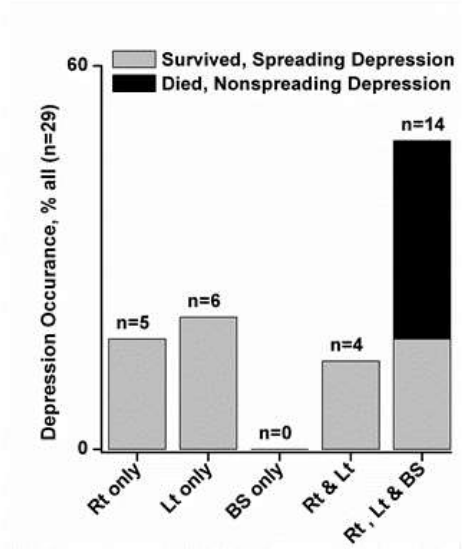

Figure 4.4. Occurrence rate of depression of brain activity in brain hemispheres and brain stem.

The mortality was in the group of animals with a nonspreading depression of activity in the brain stem. All animals with spreading depression even in the brain stem survived.

Rt: right brain hemisphere, **Lt**: left brain hemisphere, **BS**: brain stem.

Interestingly, regardless of the cause of depression of brain activity (whether it is spreading or nonspreading depression) after TBI, we found that the difference between animals that survived and those that died was the duration of the depression of activity in the brain stem (Figure 4.5). All animals with depression in the brain stem that was approximately 2 minutes in duration died (129 ± 11 s, n=9, Figure 4.2D and E), in contrast to those with half of that duration (Figure 4.2C) and survived (55 ± 8s, n=5, P=0.003).

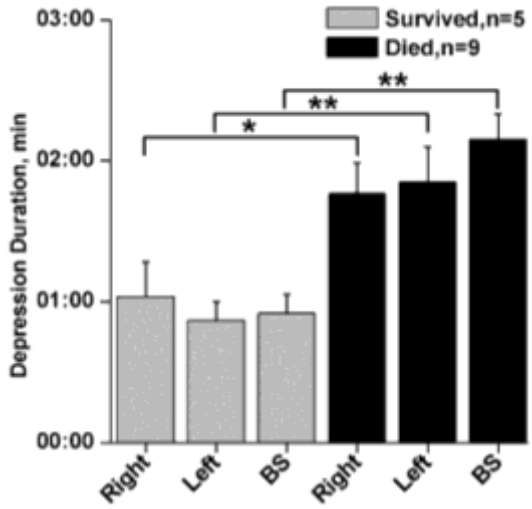

Figure 4.5. The duration of depression of brain activity in the brain stem (BS) and brain hemispheres.

Right: right brain hemisphere, **Left**: left brain hemisphere, **BS**: brain stem. * $P < 0.05$, ** $P \leq 0.01$.

It is worth noting that all animals with depression of spontaneous activity in the brain hemispheres (Figure 4.2A and B), that did not have a long duration of depression in the brain stem (Figure 4.2C), survived.

ECG and respiratory rates were monitored continuously and simultaneously during the ECoG recordings. Among the animals that died, respiration was interrupted and later stopped during and after the depression of brain stem activity following TBI (Figure 4.2E). The results showed that nonspreading depression in the brain stem and in both brain hemispheres is an earlier event that occurs 89 ± 34 s after impact, followed by respiratory arrest that occurs after 263 ± 87 s (Figure 4.6).

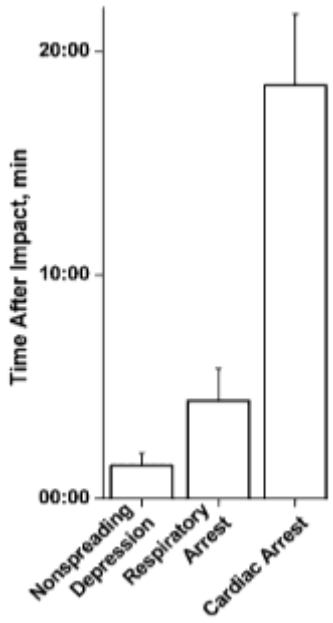

Figure 4.6. Nonspreading depression in the brain stem followed by respiratory depression and cardiac arrest following TBI.

In most of cases, respiratory interruption and arrest followed the nonspreading depression of electrical activity in brain stem.

Electrocardiographs (ECG) showed that the heart continued beating until approximately 18 minutes (1110 ± 190 s, n=7) after TBI (Figure 4.2E). Two animals were intubated immediately after TSDs and connected to a small animal ventilator for 30 minutes (RWD Life Science Inc, Model 407) with 1 ml tidal volume and 65 times/minute respiratory rate. Their ECG signals continued as a normal rhythm and recovered, but neither the activities of brain hemispheres and brain stem nor the spontaneous breathing recovered. Further work is needed to study the effect of intubation before the terminal SDs occurrence.

4.4 Discussion

In this study, the occurrence of SDs and depression of electrical spontaneous activity were recorded for the first time in the brain stem following TBI. Interestingly, all incidences of mortality were among animals that showed a nonspreading depression in their brain stem. We assume that death occurred because of a nonspreading depression that lasted for more than two minutes in the brain stem and was followed by a respiratory depression. Furthermore, we reported for the first time the occurrence of TSD within minutes after a TBI in the brain hemispheres and brain stem.

Depression of spontaneous brain activity across the cortex was observed previously (46,47). This phenomenon was considered as a disruption of normal brain activity following severe injuries to the brain, including TBI (53,85,86), subarachnoid hemorrhage (52,87), and malignant stroke (54,88).

The respiratory center in the medulla oblongata and pons of brain stem is the main region for generation of respiratory rhythm and control of breathing (292,293). The interruption and cessation of respiration following nonspreading depression after the impact could be due to depression of electrical activity in the brain stem, the center for controlling the respiration. Previously, respiratory depression was reported following TBI, and central respiratory depression was suggested as the cause of the death (227). A recent rodent study showed that local triggering of SDs (<10 min) in the brain stem causes apnea and sudden death (292). The recording of heart signals for about 18 minutes after TBI could be related to the anatomical and physiological properties of the heart, as it has its own pacemaker cells that make it independent of the brain stem (271,293).

This study shows for the first time the electrophysiological change in the brain stem seconds after TBI. In most of the animals that died, two minutes was the critical duration of depression of brain stem activity after the impact and before TSD. Although this seems very quick, we suggest that it is long enough to interrupt and arrest respiration and initiate toxic changes that eventually lead to death (271). In our study, TSDs were recorded 115 sec after the beginning of nonspreading depression, and this is consistent with a human study, in which TSDs were recorded from devastating brain injuries after withdrawal of life sustaining therapy (terminal extubation) (271). Furthermore, nonspreading depression followed by TSD was reported in a rodent study following global cerebral ischemia

(48,271,294). TSDs originated in severe noxious conditions, such as cardiac arrest, severe prolonged hypoxia, global cerebral ischemic, hypoglycemia, and tissue exposed to a high concentration of K^+ or glutamate (48,271,282,291,294) but it was not reported immediately after TBI. However, TSDs have recently been used to describe the reaching of a commitment point in which repolarization never occurs and to confirm neuronal death (271,291).

It is not known experimentally or clinically when TSD can be reversed (271). In a previous TBI model (227), death occurred within minutes following a TBI as a result of severe hypoxia, but tracheal intubation with a mechanical ventilator during and for few minutes after the impact reduced the mortality rate by more than 40%. In our study, intubation of two animals immediately after TSDs led to recovery of their normal heart rhythm but not recovery of respiration or spontaneous electrical activity of the brain hemispheres or brain stem. Further work is needed to determine if TSDs can be predicted in advance, and whether intubation before the occurrence of TSD can save the lives of injured people, including sport injuries, where medical intervention is available.

Chapter 5: Conclusion

In this study, electrophysiological recordings confirmed that SDs are a common early cortical electrophysiological event in a model of mild TBI. SDs were recorded in more than 50% of injured animals within ~ 2 minutes after a direct impact. Most rats with SDs required more time to resume spontaneous locomotion compared to injured animals with no SDs or the control group. This may explain the incomplete understanding of the etiology of signs and symptoms of concussion. While the explanation of the initiation and propagation of SDs is still a controversy, further studies are required to investigate the mechanisms underlying the initiation and propagation of SD in the traumatized brain, and the potential role of SDs in mediating delayed complications of concussive injury. Interestingly, in this study TBI-induced SDs had a larger amplitude compared to triggered SDs, and about 90% of animals exposed to repetitive (but not single) mild TBI had brain contusions and cerebral vascular damage.

The relationship between SDs and BBB dysfunction is not well known. In our study, a significant increase in BBB permeability was noticed less than 2 hours following triggered SDs in TBI animals, suggesting that there may be a rapid mechanism by which SDs affect BBB integrity following TBI. Furthermore, the short duration of late hyperemia in TBI-exposed animals, as compared to controls, may indicate a compromised neurovascular coupling process. However, further work is needed to investigate the mechanism by which a

REFERENCES

1. Menon DK, Schwab K, Wright DW, Maas AI. Position statement: Definition of traumatic brain injury. Arch Phys Med Rehabil [Internet]. 2010;91(11):1637–40. Available from: http://dx.doi.org/10.1016/j.apmr.2010.05.017

2. Taylor CA, Bell JM, Breiding MJ, Xu L. Traumatic Brain Injury–Related Emergency Department Visits, Hospitalizations, and Deaths — United States, 2007 and 2013. MMWR Surveill Summ [Internet]. 2017 Mar 17 [cited 2017 Jul 30];66(9):1–16. Available from: http://www.cdc.gov/mmwr/volumes/66/ss/ss6609a1.htm

3. Brain Injury Canada: Education, Awareness, Advocacy [Internet]. [cited 2018 Dec 4]. Available from: https://www.braininjurycanada.ca/

4. Government of Canada PHA of C. 3. Scope (Prevalence and Incidence) of Neurological Conditions - Mapping Connections - An understanding of neurological conditions in Canada - Public Health Agency of Canada. [cited 2017 Jul 30]; Available from: http://www.phac-aspc.gc.ca/publicat/cd-mc/mc-ec/section-3-eng.php

5. Gardner RC, Yaffe K. Epidemiology of mild traumatic brain injury and neurodegenerative disease HHS Public Access. Mol Cell Neurosci [Internet]. 2015 [cited 2019 Jun 26];66:75–80. Available from: https://www.ncbi.nlm.nih.gov/pmc/articles/PMC4461453/pdf/nihms669609.pdf

6. Cassidy JD, Carroll LJ, Peloso PM, Borg J, von Holst H, Holm L, et al. Incidence, risk factors and prevention of mild traumatic brain injury: Results of the WHO Collaborating Centre Task Force on Mild Traumatic Brain Injury. Journal of Rehabilitation Medicine, Supplement. 2004. p. 28–60.

7. Horn JD Van, Bhattrai A, Irimia A. Multimodal Imaging of Neurometabolic Pathology due to Traumatic Brain Injury. Trends Neurosci [Internet]. 2017;40(1):39–59. Available from: http://dx.doi.org/10.1016/j.tins.2016.10.007

8. Agrawal A, Timothy J, Pandit L, Manju M. Post-traumatic epilepsy: An overview. Clin Neurol Neurosurg. 2006;108(5):433–9.

9. Julien J, Joubert S, Ferland MC, Frenette LC, Boudreau-Duhaime MM, Malo-Véronneau L, et al. Association of traumatic brain injury and Alzheimer disease onset: A systematic review. Ann Phys Rehabil Med. 2017;60(5):347–56.

10. Mortimer JA, van Duijn CM, Chandra V, Fratiglioni L, Graves AB, Heyman A, et al. Head trauma as a risk factor for Alzheimer's disease: a collaborative re-analysis of case-control studies. EURODEM Risk Factors Research Group. Int J Epidemiol [Internet]. 1991 [cited 2018 Nov 20];20 Suppl 2:S28-35. Available from: http://www.ncbi.nlm.nih.gov/pubmed/1833351

11. Freberg L. Discovering Biological Psychology. Second edi. Potter J, editor. California: Cengage learning; 2010. 147 p.

12. Kanamori A, Catrinescu M-M, Belisle JM, Costantino S, Levin LA. Retrograde and Wallerian axonal degeneration occur synchronously after retinal ganglion cell axotomy. Am J Pathol [Internet]. 2012 Jul [cited 2019 Jan 27];181(1):62–73. Available from: http://www.ncbi.nlm.nih.gov/pubmed/22642911

13. Kerschensteiner M, Schwab ME, Lichtman JW, Misgeld T. In vivo imaging of axonal degeneration and regeneration in the injured spinal cord. Nat Med [Internet]. 2005 May 10 [cited 2019 Jan 27];11(5):572–7. Available from: http://www.ncbi.nlm.nih.gov/pubmed/15821747

14. Valk J, van der Knaap MS. Wallerian Degeneration and Demyelination Secondary to Neuronal and Axonal Degeneration. Magn Reson Myelin, Myelination, Myelin Disord. 2013;319–26.

15. XX. Experiments on the section of the glossopharyngeal and hypoglossal nerves of the frog, and observations of the alterations produced thereby in the structure of their primitive fibres. Philos Trans R Soc London [Internet]. 1850 Jan [cited 2019 Mar 26];140:423–9. Available from: http://www.royalsocietypublishing.org/doi/10.1098/rstl.1850.0021

16. Buss A, Pech K, Merkler D, Kakulas BA, Martin D, Schoenen J, et al. Sequential loss of myelin proteins during Wallerian degeneration in the human spinal cord. Brain. 2005;128(2):356–64.

17. George EB, Glass JD, Griffin JW. Axotomy-Induced Axonal Degeneration Is Mediated by Calcium Influx Through Ion-Specific Channels [Internet]. Vol. 75, The Journal of Neuroscience. 1995 [cited 2019 Mar 26]. Available from: http://www.jneurosci.org/content/jneuro/15/10/6445.full.pdf

18. Fenrich K, Gordon T. Canadian Association of Neuroscience Review: Axonal Regeneration in the Peripheral and Central Nervous Systems – Current Issues and Advances. Can J Neurol Sci [Internet]. 2004 May 16 [cited 2019 Jan 27];31(02):142–56. Available from: http://www.journals.cambridge.org/abstract_S0317167100053798

19. George R, Griffin JW. Delayed Macrophage Responses and Myelin Clearance during Wallerian Degeneration in the Central Nervous System: The Dorsal Radiculotomy Model. Exp Neurol [Internet]. 1994 Oct [cited 2019 Mar 26];129(2):225–36. Available from: http://www.ncbi.nlm.nih.gov/pubmed/7957737

20. Wang JT, Medress ZA, Barres BA. Axon degeneration: Molecular mechanisms of a self-destruction pathway. J Cell Biol. 2012;196(1):7–18.

21. Billger M, Wallin M, Karlsson JO. Proteolysis of tubulin and microtubule-associated proteins 1 and 2 by calpain I and II. Difference in sensitivity of assembled and disassembled microtubules. Cell Calcium [Internet]. 1988 Feb [cited 2019 Jun 26];9(1):33–44. Available from: http://www.ncbi.nlm.nih.gov/pubmed/2834062

22. Knöferle J, Koch JC, Ostendorf T, Michel U, Planchamp V, Vutova P, et al. Mechanisms of acute axonal degeneration in the optic nerve in vivo. Proc Natl Acad Sci U S A [Internet]. 2010 Mar 30 [cited 2019 Jun 26];107(13):6064–9. Available from: http://www.ncbi.nlm.nih.gov/pubmed/20231460

23. Vargas ME, Barres BA. Why Is Wallerian Degeneration in the CNS So Slow? Annu Rev Neurosci [Internet]. 2007 Jul [cited 2019 Mar 26];30(1):153–79. Available from: http://www.annualreviews.org/doi/10.1146/annurev.neuro.30.051606.094354

24. Lunn ER, Perry VH, Brown MC, Rosen H, Gordon S. Absence of Wallerian Degeneration does not Hinder Regeneration in Peripheral Nerve. Eur J Neurosci [Internet]. 1989 [cited 2019 Mar 27];1(1):27–33. Available from: http://www.ncbi.nlm.nih.gov/pubmed/12106171

25. Kerschensteiner M, Schwab ME, Lichtman JW, Misgeld T. In vivo imaging of axonal degeneration and regeneration in the injured spinal cord. Nat Med [Internet]. 2005 May 10 [cited 2019 Mar 26];11(5):572–7. Available from: http://www.nature.com/articles/nm1229

26. Stys PK, Sontheimer H, Ransom BR, Waxman SG. Noninactivating, tetrodotoxin-sensitive Na+ conductance in rat optic nerve axons. Proc Natl Acad Sci U S A. 1993;90(15):6976–80.

27. Taylor CP. Na+ currents that fail to inactivate. Trends Neurosci [Internet]. 1993 Nov [cited 2020 Mar 23];16(11):455–60. Available from: http://www.ncbi.nlm.nih.gov/pubmed/7507618

28. Stirling DP, Stys PK. Mechanisms of axonal injury: internodal nanocomplexes and calcium deregulation. Trends Mol Med [Internet]. 2010 Apr [cited 2019 Jun 26];16(4):160–70. Available from: http://www.ncbi.nlm.nih.gov/pubmed/20207196

29. Stone MC, Albertson RM, Chen L, Rolls MM. Dendrite injury triggers DLK-independent regeneration. Cell Rep [Internet]. 2014 Jan 30 [cited 2019 Jan 27];6(2):247–53. Available from: http://www.ncbi.nlm.nih.gov/pubmed/24412365

30. Gersh I, Bodian D. Some chemical mechanisms in chromatolysis. J Cell Comp Physiol [Internet]. 1943 Jun [cited 2019 Jan 27];21(3):253–79. Available from: http://doi.wiley.com/10.1002/jcp.1030210305

31. Gonatas NK, Stieber A, Mourelatos Z, Chen Y, Gonatas J 0, Appel SH, et al. Fragmentation of the Golgi Apparatus of Motor Neurons in Amyotrophic Lateral Sclerosis [Internet]. Vol. 140, American Journal of Pathology. 1992 [cited 2019 Jan 27]. Available from: https://europepmc.org/backend/ptpmcrender.fcgi?accid=PMC1886164&blobtype=pdf

32. Holtzman E, Novikoff AB, Villaverde H. Lysosomes and GERL in normal and chromatolytic neurons of the rat ganglion nodosum. J Cell Biol [Internet]. 1967

May [cited 2019 Jan 27];33(2):419–35. Available from: http://www.ncbi.nlm.nih.gov/pubmed/4292314

33. Griffin JW, George R, Lobato C, Tyor WR, Yan LC, Glass JD. Macrophage responses and myelin clearance during Wallerian degeneration: relevance to immune-mediated demyelination. J Neuroimmunol [Internet]. 1992 Oct [cited 2019 Mar 26];40(2–3):153–65. Available from: http://www.ncbi.nlm.nih.gov/pubmed/1430148

34. Gordon T. Nerve regeneration in the peripheral and central nervous systems. J Physiol [Internet]. 2016 [cited 2019 Jan 27];594(13):3517–20. Available from: http://www.ncbi.nlm.nih.gov/pubmed/27365158

35. Gordon T, Gordon K. Nerve regeneration in the peripheral nervous system versus the central nervous system and the relevance to speech and hearing after nerve injuries. J Commun Disord [Internet]. 2010 Jul [cited 2019 Jan 27];43(4):274–85. Available from: http://www.ncbi.nlm.nih.gov/pubmed/20510423

36. Busch SA, Silver J. The role of extracellular matrix in CNS regeneration. Curr Opin Neurobiol [Internet]. 2007 Feb [cited 2019 Jan 27];17(1):120–7. Available from: http://www.ncbi.nlm.nih.gov/pubmed/17223033

37. Guertin AD, Zhang DP, Mak KS, Alberta JA, Kim HA. Microanatomy of Axon/Glial Signaling during Wallerian Degeneration. J Neurosci [Internet]. 2005 Mar 30 [cited 2019 Mar 26];25(13):3478–87. Available from: http://www.ncbi.nlm.nih.gov/pubmed/15800203

38. Brück W. The role of macrophages in Wallerian degeneration. Brain Pathol [Internet]. 1997 Apr [cited 2019 Mar 26];7(2):741–52. Available from: http://www.ncbi.nlm.nih.gov/pubmed/9161725

39. S. B, M. R, de Lima S V., T. S, B. Martinez AM. Wallerian Degeneration in Injury and Diseases: Concepts and Prevention. In: Advanced Understanding of Neurodegenerative Diseases [Internet]. InTech; 2011 [cited 2019 Jan 27]. Available from: http://www.intechopen.com/books/advanced-understanding-of-neurodegenerative-diseases/wallerian-degeneration-in-injury-and-diseases-concepts-and-prevention

40. Coleman M. Axon degeneration mechanisms: commonality amid diversity. Nat Rev Neurosci [Internet]. 2005 Nov 14 [cited 2019 Jan 27];6(11):889–98. Available from: http://www.ncbi.nlm.nih.gov/pubmed/16224497

41. Muramatsu R, Ueno M, Yamashita T. Intrinsic regenerative mechanisms of central nervous system neurons. Biosci Trends [Internet]. 2009 Oct [cited 2019 Jan 27];3(5):179–83. Available from: http://www.ncbi.nlm.nih.gov/pubmed/20103844

42. Dong X, Wang Y, Qin Z. Molecular mechanisms of excitotoxicity and their relevance to pathogenesis of neurodegenerative diseases. Acta Pharmacol Sin [Internet]. 2009 Apr [cited 2019 Jan 28];30(4):379–87. Available from: http://www.ncbi.nlm.nih.gov/pubmed/19343058

43. Manev H, Favaron M, Guidotti A, Costa E. Delayed increase of Ca2+ influx elicited by glutamate: role in neuronal death. Mol Pharmacol [Internet]. 1989 Jul [cited 2019 Jan 28];36(1):106–12. Available from: http://www.ncbi.nlm.nih.gov/pubmed/2568579

44. Rosa AO, Rapoport SI. Intracellular- and extracellular-derived Ca(2+) influence phospholipase A(2)-mediated fatty acid release from brain phospholipids. Biochim Biophys Acta [Internet]. 2009 Aug [cited 2019 Jan 28];1791(8):697–705. Available from: http://www.ncbi.nlm.nih.gov/pubmed/19327408

45. Misslin C, Velasco-Estevez M, Albert M, O'Sullivan SA, Dev KK. Phospholipase A2 is involved in galactosylsphingosine-induced astrocyte toxicity, neuronal damage and demyelination. Eugenin EA, editor. PLoS One [Internet]. 2017 Nov 2 [cited 2019 Jan 28];12(11):e0187217. Available from: https://dx.plos.org/10.1371/journal.pone.0187217

46. Leão AAP. Spreading depression of activity in the cerebral cortex. J Physiol. 1944;7(6):359–90.

47. Leão AAP. The slow voltage variation of cortical spreading depression of activity. Electroencephalogr Clin Neurophysiol [Internet]. 1951 Aug [cited 2017 Aug 25];3(3):315–21. Available from: http://linkinghub.elsevier.com/retrieve/pii/001346945190079X

48. Dreier JP. The role of spreading depression, spreading depolarization and spreading ischemia in neurological disease. Nat Med [Internet]. 2011;17(4):439–47. Available from: http://www.nature.com/doifinder/10.1038/nm.2333

49. Kraio RP, Nicholson C. Extracellular ionic variations during spreading depression. Neuroscience [Internet]. 1978 Nov [cited 2017 Aug 25];3(11):1045–59. Available from: http://linkinghub.elsevier.com/retrieve/pii/0306452278901227

50. Takano K, Latour LL, Formato JE, Carano RAD, Helmer KG, Hasegawa Y, et al. The role of spreading depression in focal ischemia evaluated bv dffusion mapping. Ann Neurol [Internet]. 1996 Mar 1 [cited 2017 Aug 25];39(3):308–18. Available from: http://doi.wiley.com/10.1002/ana.410390307

51. Canals S. Longitudinal Depolarization Gradients Along the Somatodendritic Axis of CA1 Pyramidal Cells: A Novel Feature of Spreading Depression. J Neurophysiol [Internet]. 2005;94(2):943–51. Available from: http://jn.physiology.org/cgi/doi/10.1152/jn.01145.2004

52. Dreier JP, Woitzik J, Fabricius M, Bhatia R, Major S, Drenckhahn C, et al. Delayed ischaemic neurological deficits after subarachnoid haemorrhage are associated with clusters of spreading depolarizations. Brain. 2006;129(12):3224–37.

53. Hartings JA, Watanabe T, Bullock MR, Okonkwo DO, Fabricius M, Woitzik J, et al. Spreading depolarizations have prolonged direct current shifts and are associated with poor outcome in brain trauma. Brain. 2011;134(5):1529–40.

54. Woitzik J, Hecht N, Pinczolits A, Sandow N, Major S, Winkler MKL, et al. Propagation of cortical spreading depolarization in the human cortex after malignant stroke. Neurology [Internet]. 2013 Mar 19 [cited 2019 Mar 4];80(12):1095–102. Available from: https://n.neurology.org/content/80/12/1095

55. Dreier JP, Fabricius M, Ayata C, Sakowitz OW, William Shuttleworth C, Dohmen C, et al. Recording, analysis, and interpretation of spreading depolarizations in neurointensive care: Review and recommendations of the COSBID research group. J Cereb Blood Flow Metab. 2017;37(5):1595–625.

56. Kager H, Wadman WJ, Somjen GG. Conditions for the Triggering of Spreading Depression Studied With Computer Simulations. J Neurophysiol [Internet]. 2002 [cited 2017 Aug 25];88(5). Available from: http://jn.physiology.org/content/88/5/2700.long

57. LASHLEY KS. PATTERNS OF CEREBRAL INTEGRATION INDICATED BY THE SCOTOMAS OF MIGRAINE. Arch Neurol Psychiatry [Internet]. 1941 Aug 1 [cited 2018 Dec 7];46(2):331. Available from: http://archneurpsyc.jamanetwork.com/article.aspx?doi=10.1001/archneurpsyc.1941.02280200137007

58. Fabricius M, Fuhr S, Willumsen L, Dreier JP, Bhatia R, Boutelle MG, et al. Association of seizures with cortical spreading depression and peri-infarct depolarisations in the acutely injured human brain. Clin Neurophysiol Author Manuscr Clin Neurophysiol [Internet]. 2009 [cited 2017 Aug 25];119(9):1973–198405. Available from: https://www.ncbi.nlm.nih.gov/pmc/articles/PMC2573967/pdf/nihms65668.pdf

59. Strong AJ, Fabricius M, Boutelle MG, Hibbins SJ, Hopwood SE, Jones R, et al. Spreading and synchronous depressions of cortical activity in acutely injured human brain. Stroke. 2002;33(12):2738–43.

60. Woods RP, Iacoboni M, Mazziotta JC. Bilateral Spreading Cerebral Hypoperfusion during Spontaneous Migraine Headache. N Engl J Med [Internet]. 1994 Dec 22 [cited 2017 Aug 25];331(25):1689–92. Available from: http://www.ncbi.nlm.nih.gov/pubmed/7969360

61. Kreisman NR, Lamanna JC. Rapid and Slow Swelling During Hypoxia in the CA1 Region of Rat Hippocampal Slices [Internet]. 1999 [cited 2018 Dec 12]. Available from: www.physiology.org/journal/jn

62. Lauritzen M, Rice ME, Okada Y, Nicholson C. Quisqualate, kainate and NMDA can initiate spreading depression in the turtle cerebellum. Brain Res [Internet]. 1988 Dec 20 [cited 2018 Dec 12];475(2):317–27. Available from: https://www.sciencedirect.com/science/article/pii/0006899388906208

63. Roitbak AI, Bobrov A V. SPREADING DEPRESSION RESULTING FROM CORTICAL PUNCTURES [Internet]. [cited 2018 Dec 12]. Available from: https://www.ane.pl/pdf/3559.pdf

64. Strong AJ. Dr. Bernice Grafstein's paper on the mechanism of spreading depression. J Neurophysiol [Internet]. 2005;94(1):5–7. Available from: http://www.physiology.org/doi/10.1152/classicessays.00032.2005

65. Herreras O, Somjen GG. Analysis of potential shifts associated with recurrent spreading depression and prolonged unstable spreading depression induced by microdialysis of elevated K+ in hippocampus of anesthetized rats. Brain Res [Internet]. 1993 May 7 [cited 2018 Dec 12];610(2):283–94. Available from: http://www.ncbi.nlm.nih.gov/pubmed/8319090

66. Hü Bel N, Hosseini-Zare MS, Iburkus JZˇ, Ullah G. The role of glutamate in neuronal ion homeostasis: A case study of spreading depolarization. 2017 [cited 2018 Dec 12]; Available from: https://doi.org/10.1371/journal.pcbi.1005804

67. Kramer DR, Fujii T, Ohiorhenuan I, Liu CY. Cortical spreading depolarization: Pathophysiology, implications, and future directions. J Clin Neurosci [Internet]. 2016;24:22–7. Available from: http://dx.doi.org/10.1016/j.jocn.2015.08.004

68. Herreras O, Somjen GG. Effects of prolonged elevation of potassium on hippocampus of anesthetized rats. Brain Res [Internet]. 1993 Jul 23 [cited 2018 Dec 12];617(2):194–204. Available from: http://www.ncbi.nlm.nih.gov/pubmed/8402147

69. Pietrobon D, Moskowitz MA. Chaos and commotion in the wake of cortical spreading depression and spreading depolarizations. Nat Rev Neurosci [Internet]. 2014;15(6):379–93. Available from: http://www.nature.com/doifinder/10.1038/nrn3770

70. Mclachlan RS. Suppression of Spreading Depression of Leao in Neocortex by an N-Methyl-D-Aspartate Receptor Antagonist. J Neurol Sci [Internet]. 1992 [cited 2018 Dec 16];19:487–91. Available from: https://doi.org/10.1017/S0317167100041688

71. Tang YT, Mendez JM, Theriot JJ, Sawant PM, López-Valdés HE, Ju YS, et al. Minimum conditions for the induction of cortical spreading depression in brain slices. J Neurophysiol [Internet]. 2014 [cited 2017 Aug 25];112(10). Available from: http://jn.physiology.org/content/112/10/2572

72. HANSEN AJ, ZEUTHEN T. Extracellular ion concentrations during spreading depression and ischemia in the rat brain cortex. Acta Physiol Scand. 1981;113(4):437–45.

73. Tottene A, Urbani A, Pietrobon D. Role of different voltage-gated Ca2+channels in cortical spreading depression: Specific requirement of P/Q-type Ca2+channels. Channels. 2011;5(2).

74. Hill MP, Brotchie JM. Control of glutamate release by calcium channels and k - opioid receptors in rodent and primate striatum. 1999;275–83.

75. Lauritzen M, Hansen AJ. The effect of glutamate receptor blockade on anoxic

depolarization and cortical spreading depression. J Cereb Blood Flow Metab. 1992;12:223–9.

76. Almeida A, Bolaños JP, Medina JM. Nitric oxide mediates glutamate-induced mitochondrial depolarization in rat cortical neurons. Brain Res [Internet]. 1999 Jan 23 [cited 2018 Dec 17];816(2):580–6. Available from: http://www.ncbi.nlm.nih.gov/pubmed/9878883

77. Shuttleworth CW, Connor JA. Strain-dependent differences in calcium signaling predict excitotoxicity in murine hippocampal neurons. J Neurosci [Internet]. 2001 Jun 15 [cited 2018 Dec 18];21(12):4225–36. Available from: http://www.ncbi.nlm.nih.gov/pubmed/11404408

78. Aiba I, Shuttleworth CW. Sustained NMDA receptor activation by spreading depolarizations can initiate excitotoxic injury in metabolically compromised neurons. J Physiol [Internet]. 2012 Nov 15 [cited 2018 Dec 18];590(22):5877–93. Available from: http://www.ncbi.nlm.nih.gov/pubmed/22907056

79. Ambrosio RD, Gordon DS, Winn HR, Ambrosio D, Gordon DS, Richard H. Differential Role of KIR Channel and Na ☺ / K ☺ -Pump in the Regulation of Extracellular K ☺ in Rat Hippocampus. 2018;98104:87–102.

80. Schousboe A, Scafidi S, Bak LK, Waagepetersen HS, Mckenna MC. Glutamate Metabolism in the Brain Focusing on Astrocytes HHS Public Access. Adv Neurobiol [Internet]. 2014 [cited 2018 Dec 17];11:13–30. Available from: https://www.ncbi.nlm.nih.gov/pmc/articles/PMC4667713/pdf/nihms665428.pdf

81. Hernández-Cáceres J, Macias-González R, Brozek G, Bures J. Systemic ketamine blocks cortical spreading depression but does not delay the onset of terminal anoxic depolarization in rats. Brain Res [Internet]. 1987 Dec 29 [cited 2018 Dec 16];437(2):360–4. Available from: http://www.ncbi.nlm.nih.gov/pubmed/3435842

82. Hertle DN, Dreier JP, Woitzik J, Hartings JA, Bullock R, Okonkwo DO, et al. Effect of analgesics and sedatives on the occurrence of spreading depolarizations accompanying acute brain injury. Brain. 2012;135(8):2390–8.

83. Sanchez-Porras R, Sakowitz OW, Ludwigsburg K. Pharmacological Modulation of Spreading Depolarizations Therapy to block Spreading Depolarizations in translational model of neurologic diseases View project. 2015 [cited 2018 Dec 18]; Available from: https://www.researchgate.net/publication/267740733

84. Zhou N, Gordon GRJ, Feighan D, MacVicar BA. Transient Swelling, Acidification, and Mitochondrial Depolarization Occurs in Neurons but not Astrocytes during Spreading Depression. Cereb Cortex [Internet]. 2010 Nov 1 [cited 2017 Aug 25];20(11):2614–24. Available from: https://academic.oup.com/cercor/article-lookup/doi/10.1093/cercor/bhq018

85. Hartings JA, Strong AJ, Fabricius M, Manning A, Bhatia R, Dreier JP, et al. Spreading Depolarizations and Late Secondary Insults after Traumatic Brain Injury. J Neurotrauma [Internet]. 2009;26(11):1857–66. Available from:

http://www.liebertonline.com/doi/abs/10.1089/neu.2009.0961

86. Fabricius M, Fuhr S, Bhatia R, Boutelle M, Hashemi P, Strong AJ, et al. Cortical spreading depression and peri-infarct depolarization in acutely injured human cerebral cortex. Brain. 2006;129(3):778–90.

87. Lückl J, Lemale CL, Kola V, Horst V, Khojasteh U, Oliveira-Ferreira AI, et al. The negative ultraslow potential, electrophysiological correlate of infarction in the human cortex. Brain [Internet]. 2018 Jun 1 [cited 2019 Jun 20];141(6):1734–52. Available from: http://www.ncbi.nlm.nih.gov/pubmed/29668855

88. Dohmen C, Sakowitz OW, Fabricius M, Bosche B, Reithmeier T, Ernestus RI, et al. Spreading depolarizations occur in human ischemic stroke with high incidence. Ann Neurol. 2008;63(6):720–8.

89. Hinzman JM, Andaluz N, Shutter LA, Okonkwo DO, Pahl C, Strong AJ, et al. Inverse neurovascular coupling to cortical spreading depolarizations in severe brain trauma. Brain. 2014;137(11):2960–72.

90. Dreier JP, Major S, Pannek HW, Woitzik J, Scheel M, Wiesenthal D, et al. Spreading convulsions, spreading depolarization and epileptogenesis in human cerebral cortex. Brain. 2012;135(1):259–75.

91. Hartings JA, Bullock MR, Okonkwo DO, Murray LS, Murray GD, Fabricius M, et al. Spreading depolarisations and outcome after traumatic brain injury: A prospective observational study. Lancet Neurol [Internet]. 2011;10(12):1058–64. Available from: http://dx.doi.org/10.1016/S1474-4422(11)70243-5

92. Blyth BJ, Bazarian JJ. Traumatic alterations in consciousness: traumatic brain injury. Emerg Med Clin North Am [Internet]. 2010 Aug [cited 2018 May 1];28(3):571–94. Available from: http://www.ncbi.nlm.nih.gov/pubmed/20709244

93. Van Horn JD, Bhattrai A, Irimia A. Multimodal Imaging of Neurometabolic Pathology due to Traumatic Brain Injury. Trends Neurosci [Internet]. 2017;40(1):39–59. Available from: http://dx.doi.org/10.1016/j.tins.2016.10.007

94. McCrory P, Feddermann-Demont N, Dvoøák J, Cassidy JD, McIntosh A, Vos PE, et al. What is the definition of sports-related concussion: A systematic review. Br J Sports Med. 2017;51(11):877–87.

95. VA/DoD CLINICAL PRACTICE GUIDELINE FOR MANAGEMENT OF CONCUSSION/ MILD TRAUMATIC BRAIN INJURY The Management of Concussion/mTBI Working Group VA/DoD Clinical Practice Guideline For Management of Concussion/mTBI. 2009 [cited 2018 May 1]; Available from: https://www.rehab.research.va.gov/jour/09/46/6/pdf/cpg.pdf

96. Jiruska P, de Curtis M, Jefferys JGR, Schevon CA, Schiff SJ, Schindler K. Synchronization and desynchronization in epilepsy: controversies and hypotheses. J Physiol [Internet]. 2013 Feb 15 [cited 2018 Jun 4];591(4):787–97. Available from: http://www.ncbi.nlm.nih.gov/pubmed/23184516

97. Mayevsky A, Doron A, Manor T, Meilin S, Zarchin N, Ouaknine GE. Cortical spreading depression recorded from the human brain using a multiparametric monitoring system. Brain Res. 1996;740(1–2):268–74.

98. Vespa PM, O'Phelan K, Shah M, Mirabelli J, Starkman S, Kidwell C, et al. Acute seizures after intracerebral hemorrhage: a factor in progressive midline shift and outcome. Neurology [Internet]. 2003 May 13 [cited 2017 Aug 26];60(9):1441–6. Available from: http://www.ncbi.nlm.nih.gov/pubmed/12743228

99. Claassen J, Mayer SA, Kowalski RG, Emerson RG, Hirsch LJ. Detection of electrographic seizures with continuous EEG monitoring in critically ill patients. Neurology [Internet]. 2004 May 25 [cited 2017 Aug 26];62(10):1743–8. Available from: http://www.ncbi.nlm.nih.gov/pubmed/15159471

100. Hinzman JM, Andaluz N, Shutter LA, Okonkwo DO, Pahl C, Strong AJ, et al. Inverse neurovascular coupling to cortical spreading depolarizations in severe brain trauma. Brain [Internet]. 2014 Nov [cited 2019 Jun 20];137(11):2960–72. Available from: http://www.ncbi.nlm.nih.gov/pubmed/25154387

101. Fabricius M, Fuhr S, Willumsen L, Dreier JP, Bhatia R, Boutelle MG, et al. Association of seizures with cortical spreading depression and peri-infarct depolarisations in the acutely injured human brain. Clin Neurophysiol [Internet]. 2008 [cited 2018 Nov 1];119(9):1973–84. Available from: https://www.ncbi.nlm.nih.gov/pmc/articles/PMC2573967/pdf/nihms65668.pdf

102. Hartings JA, Shuttleworth CW, Kirov SA, Ayata C, Hinzman JM, Foreman B, et al. The continuum of spreading depolarizations in acute cortical lesion development: Examining Leão's legacy. J Cereb Blood Flow Metab. 2017;37(5):1571–94.

103. Fabricius M, Fuhr S, Willumsen L, Dreier JP, Bhatia R, Boutelle MG, et al. Association of seizures with cortical spreading depression and peri-infarct depolarisations in the acutely injured human brain. Clin Neurophysiol. 2008;119(9):1973–84.

104. Gorji A, Speckmann E-J. Spreading depression enhances the spontaneous epileptiform activity in human neocortical tissues. Eur J Neurosci [Internet]. 2004 Jun 1 [cited 2017 Aug 26];19(12):3371–4. Available from: http://doi.wiley.com/10.1111/j.0953-816X.2004.03436.x

105. Eickhoff M, Kovac S, Shahabi P, Khaleghi Ghadiri M, Dreier JP, Stummer W, et al. Spreading depression triggers ictaform activity in partially disinhibited neuronal tissues. Exp Neurol [Internet]. 2014;253:1–15. Available from: http://dx.doi.org/10.1016/j.expneurol.2013.12.008

106. Koroleva VI, Bures J. Cortical penicillin focus as a generator of repetitive spike-triggered waves of spreading depression in rats. Exp brain Res [Internet]. 1983 [cited 2017 Aug 26];51(2):291–7. Available from: http://www.ncbi.nlm.nih.gov/pubmed/6617798

107. Marrannes R, Willems R, De Prins E, Wauquier A. Evidence for a role of the N-methyl-d-aspartate (NMDA) receptor in cortical spreading depression in the rat. Brain Res [Internet]. 1988 Aug 9 [cited 2019 Aug 18];457(2):226–40. Available from: http://www.ncbi.nlm.nih.gov/pubmed/2851364

108. Serlin Y, Shelef I, Knyazer B, Friedman A. Anatomy and physiology of the blood-brain barrier. Seminars in Cell and Developmental Biology. 2015.

109. Abbott NJ, Patabendige AAK, Dolman DEM, Yusof SR, Begley DJ. Structure and function of the blood-brain barrier. Neurobiol Dis [Internet]. 2010;37(1):13–25. Available from: http://dx.doi.org/10.1016/j.nbd.2009.07.030

110. Hawkins BT, Davis TP. The Blood-Brain Barrier/Neurovascular Unit in Health and Disease. Pharmacol Rev [Internet]. 2005 [cited 2017 Jul 31];57(2). Available from: http://pharmrev.aspetjournals.org/content/57/2/173.long

111. van Vliet EA, Aronica E, Gorter JA. Blood-brain barrier dysfunction, seizures and epilepsy. Semin Cell Dev Biol [Internet]. 2015;38:26–34. Available from: http://dx.doi.org/10.1016/j.semcdb.2014.10.003

112. Keaney J, Campbell M. The dynamic blood-brain barrier. FEBS J. 2015;282(21):4067–79.

113. Daneman R, Prat A. The Blood-Brain Barrier. [cited 2019 Jun 29]; Available from: www.cshperspectives.org

114. Coomber BL, Stewart PA. Morphometric analysis of CNS microvascular endothelium. Microvasc Res. 1985;30(1):99–115.

115. Brightman MW, Reese TS. Junctions between intimately apposed cell membranes in the vertebrate brain. J Cell Biol [Internet]. 1969 Mar [cited 2018 Jun 13];40(3):648–77. Available from: http://www.ncbi.nlm.nih.gov/pubmed/5765759

116. Oldendorf WH, Cornford ME, Brown WJ. Large apparent work capability of blood-brain-barrier - study of mitochondrial content of capillary endothelial cells in brain and other tissues of rat. Ann Neurol. 1977;1:409–17.

117. Marchi N, Granata T, Ghosh C, Janigro D. Blood-brain barrier dysfunction and epilepsy: pathophysiologic role and therapeutic approaches. Epilepsia [Internet]. 2012 Nov [cited 2019 Jan 30];53(11):1877–86. Available from: http://www.ncbi.nlm.nih.gov/pubmed/22905812

118. Shlosberg D, Benifla M, Kaufer D, Friedman A. Blood–brain barrier breakdown as a therapeutic target in traumatic brain injury. [cited 2018 Jun 14]; Available from: https://www.ncbi.nlm.nih.gov/pmc/articles/PMC3625732/pdf/nihms452815.pdf

119. Heinemann U, Kaufer D, Friedman A. Blood-brain barrier dysfunction, TGFβ signaling, and astrocyte dysfunction in epilepsy. Glia. 2012;60(8):1251–7.

120. Friedman A. Blood-brain barrier dysfunction, status epilepticus, seizures and epilepsy: a puzzle of a chicken and egg? 2011 [cited 2018 Jun 14];52:19–20.

Available from:
https://www.ncbi.nlm.nih.gov/pmc/articles/PMC3234990/pdf/nihms311179.pdf

121. Bar-Klein G, Cacheaux LP, Kamintsky L, Prager O, Weissberg I, Schoknecht K, et al. Losartan prevents acquired epilepsy via TGF-β signaling suppression. Ann Neurol [Internet]. 2014 Jun [cited 2019 Jun 29];75(6):864–75. Available from: http://www.ncbi.nlm.nih.gov/pubmed/24659129

122. Banks WA, Farr SA, Morley JE. Permeability of the Blood-Brain Barrier to Albumin and Insulin in the Young and Aged SAMP8 Mouse. J Gerontol Biol Sci Public Domain [Internet]. 2000 [cited 2018 Jun 15];55(12):601–6. Available from: https://pdfs.semanticscholar.org/2b1e/771dcd7ba3bcd8feb2b8e86833e16adf05d2.pdf?_ga=2.177568742.2130920457.1529031704-850426803.1529031704

123. Seiffert E. Lasting Blood-Brain Barrier Disruption Induces Epileptic Focus in the Rat Somatosensory Cortex. J Neurosci [Internet]. 2004;24(36):7829–36. Available from: http://www.jneurosci.org/cgi/doi/10.1523/JNEUROSCI.1751-04.2004

124. Van Vliet EA, Araújo SDC, Redeker S, Van Schaik R, Aronica E, Gorter JA. Blood-brain barrier leakage may lead to progression of temporal lobe epilepsy. Brain. 2007;130(2):521–34.

125. Cornford EM, Hyman S. Blood–brain barrier permeability to small and large molecules. Adv Drug Deliv Rev [Internet]. 1999 Apr [cited 2017 Aug 16];36(2–3):145–63. Available from: http://linkinghub.elsevier.com/retrieve/pii/S0169409X98000829

126. Schmitz AK, Grote A, Raabe A, Urbach H, Friedman A, Von Lehe M, et al. Albumin storage in neoplastic astroglial elements of gangliogliomas. 2013 [cited 2017 Aug 16]; Available from: https://pdfs.semanticscholar.org/01c7/8134c5d6150d01a5082daef312bb897fd94e.pdf

127. Prabowo AS, Iyer AM, Anink JJ, Spliet WG, Van Rijen PC, Aronica E. Differential expression of major histocompatibility complex class I in developmental glioneuronal lesions. [cited 2017 Aug 16]; Available from: https://jneuroinflammation.biomedcentral.com/track/pdf/10.1186/1742-2094-10-12?site=jneuroinflammation.biomedcentral.com

128. Dobolyi A, Vincze C, Pál G, Lovas G. The Neuroprotective Functions of Transforming Growth Factor Beta Proteins. OPEN ACCESS Int J Mol Sci [Internet]. 2012 [cited 2019 Jun 29];13:13. Available from: www.mdpi.com/journal/ijms

129. Fee DB, Sewell DL, Andresen K, Jacques TJ, Piaskowski S, Barger BA, et al. Traumatic brain injury increases TGFβRII expression on endothelial cells. Brain Res [Internet]. 2004 Jun 25 [cited 2019 Jun 29];1012(1–2):52–9. Available from: http://www.ncbi.nlm.nih.gov/pubmed/15158160

130. Friedman A, Kaufer D, Heinemann U. Blood-brain barrier breakdown-inducing

astrocytic transformation: novel targets for the prevention of epilepsy. Epilepsy Res [Internet]. 2009 Aug [cited 2019 Jun 29];85(2–3):142–9. Available from: http://www.ncbi.nlm.nih.gov/pubmed/19362806

131. Perillan PR, Chen M, Potts EA, Simard JM. Transforming growth factor-beta 1 regulates Kir2.3 inward rectifier K+ channels via phospholipase C and protein kinase C-delta in reactive astrocytes from adult rat brain. J Biol Chem [Internet]. 2002 Jan 18 [cited 2019 Jun 29];277(3):1974–80. Available from: http://www.ncbi.nlm.nih.gov/pubmed/11713246

132. Flores LP, Zumsteg D, Bechmann I, Heinemann U, Seiffert E, Friedman A, et al. TGF- receptor-mediated albumin uptake into astrocytes is involved in neocortical epileptogenesis. Brain. 2006;130(2):535–47.

133. Tanaka K, Watase K, Manabe T, Yamada K, Watanabe M, Takahashi K, et al. Epilepsy and Exacerbation of Brain Injury in Mice Lacking the Glutamate Transporter GLT-1. Science (80-) [Internet]. 1997 Jun 13 [cited 2019 Jun 29];276(5319):1699–702. Available from: http://www.ncbi.nlm.nih.gov/pubmed/9180080

134. Kozler P, Pokorný J. Altered Blood-Brain Barrier Permeability and Its Effect on the Distribution of Evans Blue and Sodium Fluorescein in the Rat Brain Applied by Intracarotid Injection. Physiol Res. 2003;52(5):607–14.

135. Prager O, Chassidim Y, Klein C, Levi H, Shelef I, Friedman A. Dynamic in vivo imaging of cerebral blood flow and blood-brain barrier permeability. Neuroimage [Internet]. 2010;49(1):337–44. Available from: http://dx.doi.org/10.1016/j.neuroimage.2009.08.009

136. Kaya M, Ahishali B. Assessment of Permeability in Barrier Type of Endothelium in Brain Using Tracers: Evans Blue, Sodium Fluorescein, and Horseradish Peroxidase. In: Methods in molecular biology (Clifton, NJ) [Internet]. 2011 [cited 2017 Aug 16]. p. 369–82. Available from: http://www.ncbi.nlm.nih.gov/pubmed/21874465

137. Hoffmann A, Bredno J, Wendland M, Derugin N, Ohara P, Wintermark M. High and Low Molecular Weight Fluorescein Isothiocyanate (FITC)-Dextrans to Assess Blood-Brain Barrier Disruption: Technical Considerations. Transl Stroke Res [Internet]. 2011 Mar [cited 2017 Aug 16];2(1):106–11. Available from: http://www.ncbi.nlm.nih.gov/pubmed/21423333

138. Saunders NR, Dziegielewska KM, M??llg??rd K, Habgood MD. Markers for blood-brain barrier integrity: How appropriate is Evans blue in the twenty-first century and what are the alternatives? Front Neurosci. 2015;9(OCT):1–16.

139. UJIIE M, DICKSTEIN DL, CARLOW DA, JEFFERIES WA. Blood–Brain Barrier Permeability Precedes Senile Plaque Formation in an Alzheimer Disease Model. Microcirculation [Internet]. 2003 Jan [cited 2017 Aug 16];10(6):463–70. Available from: http://doi.wiley.com/10.1080/mic.10.6.463.470

140. HOFFMAN HJ, OLSZEWSKI J. Spread of sodium fluorescein in normal brain tissue. A study of the mechanism of the blood-brain barrier. Neurology [Internet]. 1961 Dec [cited 2017 Aug 24];11:1081–5. Available from: http://www.ncbi.nlm.nih.gov/pubmed/13908102

141. Malmgren LT, Olsson Y. Differences between the peripheral and the central nervous system in permeability to sodium fluorescein. J Comp Neurol [Internet]. 1980 May 1 [cited 2017 Aug 24];191(1):103–17. Available from: http://www.ncbi.nlm.nih.gov/pubmed/7400388

142. BROMAN T. Supravital Analysis of Disorders in the Cerebral Vascular Permeability in Man. Acta Med Scand [Internet]. 2009 Apr 24 [cited 2018 Jun 16];118(1–3):79–83. Available from: http://doi.wiley.com/10.1111/j.0954-6820.1944.tb17793.x

143. Wolman M, Klatzo I, Chui E, Wilmes F, Nishimoto K, Fujiwara K, et al. Evaluation of the dye-protein tracers in pathophysiology of the blood-brain barrier. Acta Neuropathol [Internet]. 1981 [cited 2017 Aug 24];54(1):55–61. Available from: http://www.ncbi.nlm.nih.gov/pubmed/7234328

144. Saunders NR, Dziegielewska KM, Møllgård K, Habgood MD. Markers for blood-brain barrier integrity: how appropriate is Evans blue in the twenty-first century and what are the alternatives? Front Neurosci [Internet]. 2015 Oct 29 [cited 2017 Aug 24];9:385. Available from: http://journal.frontiersin.org/Article/10.3389/fnins.2015.00385/abstract

145. Tsopelas C, Sutton R. Why certain dyes are useful for localizing the sentinel lymph node. J Nucl Med. 2002;43(10):1377–82.

146. Wolman M, Klatzo I, Chui E, Wilmes F, Nishimoto K, Fujiwara K, et al. Evaluation of the dye-protein tracers in pathophysiology of the blood-brain barrier. Acta Neuropathol [Internet]. 1981 [cited 2017 Dec 11];54(1):55–61. Available from: http://www.ncbi.nlm.nih.gov/pubmed/7234328

147. VanWert AL, Gionfriddo MR, Sweet DH. Organic anion transporters: discovery, pharmacology, regulation and roles in pathophysiology. Biopharm Drug Dispos [Internet]. 2009 [cited 2019 Jan 30];n/a-n/a. Available from: http://doi.wiley.com/10.1002/bdd.693

148. Chassidim Y, Veksler R, Lublinsky S, Pell GS, Friedman A, Shelef I. Quantitative imaging assessment of blood-brain barrier permeability in humans. Vol. 10, Fluids and Barriers of the CNS. 2013.

149. Gursoy-Ozdemir Y, Qiu J, Matsuoka N, Bolay H, Bermpohl D, Jin H, et al. Cortical spreading depression activates and upregulates MMP-9. J Clin Invest. 2004;113(10):1447–55.

150. Malemud CJ. Matrix metalloproteinases (MMPs) in health and disease: an overview. Front Biosci [Internet]. 2006 May 1 [cited 2018 Jun 11];11:1696–701. Available from: http://www.ncbi.nlm.nih.gov/pubmed/16368548

151. Van Lint P, Libert C. Chemokine and cytokine processing by matrix metalloproteinases and its effect on leukocyte migration and inflammation. J Leukoc Biol [Internet]. 2007 Jul 25 [cited 2018 Jun 11];82(6):1375–81. Available from: http://doi.wiley.com/10.1189/jlb.0607338

152. Elkington PTG, O'Kane CM, Friedland JS. The paradox of matrix metalloproteinases in infectious disease. Clin Exp Immunol [Internet]. 2005 Oct [cited 2018 Jun 11];142(1):12–20. Available from: http://www.ncbi.nlm.nih.gov/pubmed/16178851

153. Rosenberg GA, Kornfeld M, Estrada E, Kelley RO, Liotta LA, Stetler-Stevenson WG. TIMP-2 reduces proteolytic opening of blood-brain barrier by type IV collagenase. Brain Res [Internet]. 1992 Apr [cited 2018 Jun 11];576(2):203–7. Available from: http://linkinghub.elsevier.com/retrieve/pii/000689939290681X

154. Romanic AM, White RF, Arleth AJ, Ohlstein EH, Barone FC. Matrix Metalloproteinase Expression Increases After Cerebral Focal Ischemia in Rats Inhibition of Matrix Metalloproteinase-9 Reduces Infarct Size. 1998;1020–31.

155. Rosell A, Ortega-Aznar A, Alvarez-Sabín J, Fernández-Cadenas I, Ribó M, Molina CA, et al. Increased brain expression of matrix metalloproteinase-9 after ischemic and hemorrhagic human stroke. Stroke. 2006;37(6):1399–406.

156. Guilfoyle MR, Carpenter KLH, Helmy A, Pickard JD, Menon DK, Hutchinson PJA. Matrix Metalloproteinase Expression in Contusional Traumatic Brain Injury: A Paired Microdialysis Study. J Neurotrauma [Internet]. 2015;32(20):1553–9. Available from: http://online.liebertpub.com/doi/10.1089/neu.2014.3764

157. Yisarakun W, Supornsilpchai W, Chantong C, Srikiatkhachorn A, Maneesri-le Grand S. Chronic paracetamol treatment increases alterations in cerebral vessels in cortical spreading depression model. Microvasc Res [Internet]. 2014;94:36–46. Available from: http://dx.doi.org/10.1016/j.mvr.2014.04.012

158. Gáspár O, Herédi J, Menyhárt Á, Zsolt C, Nagy D, Fuzik J, et al. Unexpected effects of peripherally administered kynurenic acid on cortical spreading depression and related blood-brain barrier permeability. Drug Des Devel Ther. 2013;7:981–7.

159. Roy CS, Sherrington CS. On the Regulation of the Blood-supply of the Brain. J Physiol [Internet]. 1890;11(1–2):85-158.17. Available from: http://www.ncbi.nlm.nih.gov/pubmed/16991945%0Ahttp://www.pubmedcentral.nih.gov/articlerender.fcgi?artid=PMC1514242

160. CRAIGIE EH. THE ARCHITECTURE OF THE CEREBRAL CAPILLARY BED. Biol Rev [Internet]. 1945 Oct [cited 2019 Nov 6];20(4):133–46. Available from: http://doi.wiley.com/10.1111/j.1469-185X.1945.tb00446.x

161. Iadecola C. The Neurovascular Unit Coming of Age: A Journey through Neurovascular Coupling in Health and Disease. Vol. 96, Neuron. Cell Press; 2017. p. 17–42.

162. Raichle ME, Mintun MA. BRAIN WORK AND BRAIN IMAGING. Annu Rev Neurosci. 2006 Jul 21;29(1):449–76.

163. Dienel GA, Hertz L. Glucose and lactate metabolism during brain activation. J Neurosci Res [Internet]. 2001 Dec 1 [cited 2018 Jun 17];66(5):824–38. Available from: http://doi.wiley.com/10.1002/jnr.10079

164. Cremer JE, Braun LD, Oldendorf WH. Changes during development in transport processes of the blood-brain barrier. Biochim Biophys Acta [Internet]. 1976 Nov 2 [cited 2018 Jun 17];448(4):633–7. Available from: http://www.ncbi.nlm.nih.gov/pubmed/823975

165. Muoio V, Persson PB, Sendeski MM. The neurovascular unit - concept review. Acta Physiol. 2014;210(4):790–8.

166. Hillman EMC. Coupling mechanism and significance of the BOLD signal: a status report. Annu Rev Neurosci [Internet]. 2014 [cited 2018 Oct 29];37:161–81. Available from: http://www.ncbi.nlm.nih.gov/pubmed/25032494

167. Østergaard L, Dreier JP, Hadjikhani N, Jespersen SN, Dirnagl U, Dalkara T. Neurovascular Coupling during Cortical Spreading Depolarization and - Depression. Stroke. 2015;46(5):1392–401.

168. Phillips AA, Chan FH, Zheng MMZ, Krassioukov A V., Ainslie PN. Neurovascular coupling in humans: Physiology, methodological advances and clinical implications. J Cereb Blood Flow Metab. 2015;36(4):647–64.

169. Hamilton NB. Pericyte-mediated regulation of capillary diameter: a component of neurovascular coupling in health and disease. Front Neuroenergetics [Internet]. 2010;2(May):1–14. Available from: http://journal.frontiersin.org/article/10.3389/fnene.2010.00005/abstract

170. Staddon JM, Rubin LL. Cell adhesion, cell junctions and the blood-brain barrier. Curr Opin Neurobiol [Internet]. 1996 Oct [cited 2018 Jun 20];6(5):622–7. Available from: http://www.ncbi.nlm.nih.gov/pubmed/8937826

171. Attwell D, Buchan A, Charpak S, Lauritzen M, MacVicar B, Newman E. Glian and neuronal control of brain blood flow. Nature. 2011;468(7321):232–43.

172. Busija DW, Bari F, Domoki F, Louis T. Mechanisms Involved in the Cerebrovascular Dilator Effects of N- methyl-D-aspartate in Cerebral Cortex. [cited 2018 Jun 20]; Available from: https://www.ncbi.nlm.nih.gov/pmc/articles/PMC2174154/pdf/nihms35335.pdf

173. Golanov E V, Christensen JRC, Reis DJ. Neurons of a Limited Subthalamic Area Mediate Elevations in Cortical Cerebral Blood Flow Evoked by Hypoxia and Excitation of Neurons of the Rostral Ventrolateral Medulla. [cited 2018 Jun 20]; Available from: http://www.jneurosci.org/content/jneuro/21/11/4032.full.pdf

174. Rancillac A, Rossier J, Guille M, Tong X-K, Geoffroy H, Amatore C, et al. Glutamatergic Control of Microvascular Tone by Distinct GABA Neurons in the

Cerebellum. [cited 2018 Jun 20]; Available from: http://www.jneurosci.org/content/jneuro/26/26/6997.full.pdf

175. Yang G, Huard JMT, Beitz AJ, Ross ME, Iadecola C. Stellate Neurons Mediate Functional Hyperemia in the Cerebellar Molecular Layer. [cited 2018 Jun 20]; Available from: http://www.jneurosci.org/content/jneuro/20/18/6968.full.pdf

176. Zonta M, Angulo MC, Gobbo S, Rosengarten B, Hossmann KA, Pozzan T, et al. Neuron-to-astrocyte signaling is central to the dynamic control of brain microcirculation. Nat Neurosci. 2003;6(1):43–50.

177. Ma J, Ayata C, Huang PL, Fishman MC, Moskowitz MA. Regional cerebral blood flow response to vibrissal stimulation in mice lacking type I NOS gene expression. Am J Physiol Circ Physiol [Internet]. 1996 Mar [cited 2018 Jun 26];270(3):H1085–90. Available from: http://www.ncbi.nlm.nih.gov/pubmed/8780207

178. Akgören N, Fabricius M, Lauritzen M. Importance of nitric oxide for local increases of blood flow in rat cerebellar cortex during electrical stimulation. Proc Natl Acad Sci U S A. 1994;91(13):5903–7.

179. Pereira de Vasconcelos a, Baldwin R a, Wasterlain CG. Nitric oxide mediates the increase in local cerebral blood flow during focal seizures. Proc Natl Acad Sci U S A [Internet]. 1995;92(8):3175–9. Available from: http://www.pubmedcentral.nih.gov/articlerender.fcgi?artid=42128&tool=pmcentrez&rendertype=abstract

180. Armstead WM. Role of nitric oxide, cyclic nucleotides, and the activation of ATP-sensitive K+channels in the contribution of adenosine to hypoxia-induced pial artery dilation. J Cereb Blood Flow Metab. 1997;17(1):100–8.

181. Miyata N, Roman RJ. Role of 20-hydroxyeicosatetraenoic acid (20-HETE) in vascular system. J Smooth Muscle Res. 2005;41(4):175–93.

182. Harder DR, Lange AR, Birks EK, Roman RJ. Cytochrome P450 Metabolites of Arachidonic Acid as Intracellular Signaling Molecules in Vascular Tissue iripnm r. 1997;53226.

183. Niwa K, Araki E, Morham SG, Ross ME, Iadecola C. Cyclooxygenase-2 contributes to functional hyperemia in whisker-barrel cortex. J Neurosci. 2000;20(2):763–70.

184. Behm DJ, Ogbonna A, Wu C, Burns-Kurtis CL, Douglas SA. Epoxyeicosatrienoic Acids Function as Selective, Endogenous Antagonists of Native Thromboxane Receptors: Identification of a Novel Mechanism of Vasodilation. J Pharmacol Exp Ther [Internet]. 2009;328(1):231–9. Available from: http://jpet.aspetjournals.org/cgi/doi/10.1124/jpet.108.145102

185. Mathiisen TM, Lehre KP, Danbolt NC, Ottersen OP. The perivascular astroglial sheath provides a complete covering of the brain microvessels: An electron

microscopic 3D reconstruction. Glia. 2010;58(9):1094–103.

186. Girouard H, Bonev AD, Hannah RM, Meredith A, Aldrich RW, Nelson MT. Astrocytic endfoot Ca2+ and BK channels determine both arteriolar dilation and constriction. Proc Natl Acad Sci U S A [Internet]. 2010 Feb 23 [cited 2018 Jun 27];107(8):3811–6. Available from: http://www.ncbi.nlm.nih.gov/pubmed/20133576

187. Filosa JA, Bonev AD, Straub S V., Meredith AL, Wilkerson MK, Aldrich RW, et al. Local potassium signaling couples neuronal activity to vasodilation in the brain. Nat Neurosci. 2006;9(11):1397–403.

188. Longden TA, Nelson MT. Vascular inward rectifier K+ channels as external K+ sensors in the control of cerebral blood flow. Microcirculation [Internet]. 2015 Apr [cited 2018 Jun 27];22(3):183–96. Available from: http://www.ncbi.nlm.nih.gov/pubmed/25641345

189. Hill MA, Yang Y, Ella SR, Davis MJ, Braun AP. Large conductance, Ca2+-activated K+ channels (BKCa) and arteriolar myogenic signaling. FEBS Lett [Internet]. 2010 May 17 [cited 2018 Jun 27];584(10):2033–42. Available from: http://www.ncbi.nlm.nih.gov/pubmed/20178789

190. Orie NN, Fry CH, Clapp LH. Evidence that inward rectifier K+channels mediate relaxation by the PGI2receptor agonist cicaprost via a cyclic AMP-independent mechanism. Cardiovasc Res. 2006;69(1):107–15.

191. Nizar K, Uhlirova H, Tian P, Saisan PA, Cheng Q, Reznichenko L, et al. In vivo Stimulus-Induced Vasodilation Occurs without IP3 Receptor Activation and May Precede Astrocytic Calcium Increase. J Neurosci [Internet]. 2013;33(19):8411–22. Available from: http://www.jneurosci.org/cgi/doi/10.1523/JNEUROSCI.3285-12.2013

192. McCaslin AFH, Chen BR, Radosevich AJ, Cauli B, Hillman EMC. In vivo 3D morphology of astrocyte-vasculature interactions in the somatosensory cortex: implications for neurovascular coupling. J Cereb Blood Flow Metab [Internet]. 2011 Mar [cited 2019 Jan 31];31(3):795–806. Available from: http://www.ncbi.nlm.nih.gov/pubmed/21139630

193. Clark JF, Pyne-Geithman G. Vascular smooth muscle function: The physiology and pathology of vasoconstriction. Pathophysiology. 2005;12(1):35–45.

194. Attwell D, Mishra A, Hall CN, O'Farrell FM, Dalkara T. What is a pericyte? J Cereb Blood Flow Metab [Internet]. 2016 Feb [cited 2019 Jan 31];36(2):451–5. Available from: http://www.ncbi.nlm.nih.gov/pubmed/26661200

195. Dalkara T, Gursoy-Ozdemir Y, Yemisci M. Brain microvascular pericytes in health and disease. Acta Neuropathol [Internet]. 2011 Jul 9 [cited 2019 Jan 31];122(1):1–9. Available from: http://www.ncbi.nlm.nih.gov/pubmed/21656168

196. Hall CN, Reynell C, Gesslein B, Hamilton NB, Mishra A, Sutherland BA, et al.

Capillary pericytes regulate cerebral blood flow in health and disease. Nature [Internet]. 2014 Apr 3 [cited 2019 Jan 31];508(7494):55–60. Available from: http://www.ncbi.nlm.nih.gov/pubmed/24670647

197. Winkler MKL, Chassidim Y, Lublinsky S, Revankar GS, Major S, Kang E-J, et al. Impaired neurovascular coupling to ictal epileptic activity and spreading depolarization in a patient with subarachnoid hemorrhage: Possible link to blood-brain barrier dysfunction. Epilepsia [Internet]. 2012 Nov 1 [cited 2017 Aug 25];53(s6):22–30. Available from: http://doi.wiley.com/10.1111/j.1528-1167.2012.03699.x

198. Hoffmann U, Ayata C. Cerebral Vasospasm: Neurovascular Events After Subarachnoid Hemorrhage. 2013;115. Available from: http://link.springer.com/10.1007/978-3-7091-1192-5

199. de Crespigny A, Rother J, van Bruggen N, Beaulieu C, Moseley ME. Magnetic resonance imaging assessment of cerebral hemodynamics during spreading depression in rats. J Cereb Blood Flow Metab. 1998;18(9):1008–17.

200. Faraci FM, Sobey CG. Role of potassium channels in regulation of cerebral vascular tone. J Cereb Blood Flow Metab. 1998;18(10):1047–63.

201. Nielsen AN, Fabricius M, Lauritzen M. Scanning laser-Doppler flowmetry of rat cerebral circulation during cortical spreading depression. J Vasc Res. 2000;37(6):513–22.

202. Balança B, Meiller A, Bezin L, Dreier JP, Marinesco S, Lieutaud T. Altered hypermetabolic response to cortical spreading depolarizations after traumatic brain injury in rats. J Cereb Blood Flow Metab. 2017;37(5):1670–86.

203. Lauritzen M. Pathophysiology of the migraine aura. Brain [Internet]. 1994 Feb 1 [cited 2017 Aug 25];117(1):199–210. Available from: https://academic.oup.com/brain/article-lookup/doi/10.1093/brain/117.1.199

204. Piilgaard H, Lauritzen M. Persistent Increase in Oxygen Consumption and Impaired Neurovascular Coupling after Spreading Depression in Rat Neocortex. J Cereb Blood Flow Metab [Internet]. 2009;29(9):1517–27. Available from: http://journals.sagepub.com/doi/10.1038/jcbfm.2009.73

205. Ayata C, Shin HK, Salomone S, Ozdemir-Gursoy Y, Boas DA, Dunn AK, et al. Pronounced Hypoperfusion During Spreading Depression in Mouse Cortex. J Cereb Blood Flow Metab [Internet]. 2004;1172–82. Available from: http://jcb.sagepub.com/lookup/doi/10.1097/01.WCB.0000137057.92786.F3

206. Jeffcote T, Hinzman JM, Jewell SL, Learney RM, Pahl C, Tolias C, et al. Detection of spreading depolarization with intraparenchymal electrodes in the injured human brain. Neurocrit Care. 2014;20(1):21–31.

207. Shin HK, Dunn AK, Jones PB, Boas DA, Moskowitz MA, Ayata C. Vasoconstrictive neurovascular coupling during focal ischemic depolarizations. J

Cereb Blood Flow Metab. 2006;26(8):1018–30.

208. Koide M, Sukhotinsky I, Ayata C, Wellman GC. Subarachnoid hemorrhage, spreading depolarizations and impaired neurovascular coupling. Stroke Res Treat. 2013;2013.

209. Lauritzen M, Hansen AJ, Kronborg D, Wieloch T. Cortical Spreading Depression is Associated with Arachidonic Acid Accumulation and Preservation of Energy Charge. J Cereb Blood Flow Metab [Internet]. 1990 Jan 29 [cited 2017 Aug 25];10(1):115–22. Available from: http://journals.sagepub.com/doi/10.1038/jcbfm.1990.14

210. Windmuller O, Lindauer U, Foddis M, Einhäupl KM, Dirnagl U, Heinemann U, et al. Ion changes in spreading ischaemia induce rat middle cerebral artery constriction in the absence of NO. Brain [Internet]. 2005 Sep 1 [cited 2017 Aug 25];128(9):2042–51. Available from: https://academic.oup.com/brain/article-lookup/doi/10.1093/brain/awh545

211. Mutch WAC, Hansen AJ. Extracellular pH Changes during Spreading Depression and Cerebral Ischemia: Mechanisms of Brain pH Regulation. J Cereb Blood Flow Metab [Internet]. 1984 Mar 28 [cited 2017 Aug 25];4(1):17–27. Available from: http://www.ncbi.nlm.nih.gov/pubmed/6693512

212. Somjen GG. Ions in the brain : normal function, seizures, and stroke [Internet]. Oxford University Press; 2004 [cited 2017 Aug 25]. 470 p. Available from: https://global.oup.com/academic/product/ions-in-the-brain-9780195151718?cc=ca&lang=en&

213. Takano T, Tian G-F, Peng W, Lou N, Lovatt D, Hansen AJ, et al. Cortical spreading depression causes and coincides with tissue hypoxia. Nat Neurosci [Internet]. 2007 Jun 29 [cited 2017 Aug 25];10(6):754–62. Available from: http://www.ncbi.nlm.nih.gov/pubmed/17468748

214. Ayata C, Lauritzen M. Spreading Depression, Spreading Depolarizations, and the Cerebral Vasculature. Physiol Rev [Internet]. 2015;95(3):953–93. Available from: http://physrev.physiology.org/lookup/doi/10.1152/physrev.00027.2014

215. Fabricius M, Akgoren N, Lauritzen M. Arginine-nitric oxide pathway and cerebrovascular regulation in cortical spreading depression. Am J Physiol Circ Physiol [Internet]. 1995 Jul [cited 2019 Jul 1];269(1):H23–9. Available from: http://www.physiology.org/doi/10.1152/ajpheart.1995.269.1.H23

216. Bosche B, Graf R, Ernestus RI, Dohmen C, Reithmeier T, Brinker G, et al. Recurrent spreading depolarizations after subarachnoid hemorrhage decreases oxygen availability in human cerebral cortex. Ann Neurol. 2010;67(5):607–17.

217. SCHECKENBACH K, DREIER J, DIRNAGL U, LINDAUER U. Impaired cerebrovascular reactivity after cortical spreading depression in rats: Restoration by nitric oxide or cGMP. Exp Neurol [Internet]. 2006 Dec [cited 2017 Aug 25];202(2):449–55. Available from:

http://linkinghub.elsevier.com/retrieve/pii/S0014488606004249

218. Laker SR. Epidemiology of Concussion and Mild Traumatic Brain Injury. PM&R. 2011 Oct;3(10):S354–8.

219. Sharp DJ, Jenkins PO. Concussion is confusing us all. Pract Neurol. 2015;15(3):172–86.

220. Shaw N.A. The neurophysiology of concussion. Prog Neurobiol. 2002;67(September 2001):281–344.

221. Schoenhuber R, Gentilini M. Anxiety and depression after mild head injury: a case control study. J Neurol Neurosurg Psychiatry [Internet]. 1988 [cited 2019 Mar 31];51:722–4. Available from: http://jnnp.bmj.com/

222. Christensen J. Traumatic brain injury: Risks of epilepsy and implications for medicolegal assessment. Vol. 53, Epilepsia. 2012. p. 43–7.

223. Stein TD, Alvarez VE, McKee AC. Concussion in Chronic Traumatic Encephalopathy. Curr Pain Headache Rep. 2015;19(10):2–7.

224. Jafari S, Etminan M, Aminzadeh F, Samii A. Head injury and risk of Parkinson disease: A systematic review and meta-analysis. Mov Disord [Internet]. 2013 Aug [cited 2018 Nov 20];28(9):1222–9. Available from: http://www.ncbi.nlm.nih.gov/pubmed/23609436

225. von Baumgarten L, Trabold R, Thal S, Back T, Plesnila N. Role of cortical spreading depressions for secondary brain damage after traumatic brain injury in mice. J Cereb Blood Flow Metab [Internet]. 2008;28(7):1353–60. Available from: http://www.nature.com/doifinder/10.1038/jcbfm.2008.30%5Cnhttp://www.ncbi.nlm.nih.gov/pubmed/18414497

226. Mychasiuk R, Farran A, Esser MJ. Assessment of an experimental rodent model of pediatric mild traumatic brain injury. J Neurotrauma [Internet]. 2014 Apr 15 [cited 2020 Feb 7];31(8):749–57. Available from: http://www.liebertpub.com/doi/10.1089/neu.2013.3132

227. Marmarou a, Foda M a, van den Brink W, Campbell J, Kita H, Demetriadou K. A new model of diffuse brain injury in rats. Part I: Pathophysiology and biomechanics. J Neurosurg. 1994;80(2):291–300.

228. Kane MJ, Angoa-Pérez M, Briggs DI, Viano DC, Kreipke CW, Kuhn DM. A mouse model of human repetitive mild traumatic brain injury. J Neurosci Methods [Internet]. 2012 Jan 15 [cited 2018 Nov 17];203(1):41–9. Available from: http://www.ncbi.nlm.nih.gov/pubmed/21930157

229. Zheng Z, Cao Z, Luo J, Lv J. Characterization of Intrinsic Optical Signal during Spreading Depolarization. Neuropsychiatry (London). 2018;08(01):302–9.

230. Bogdanov VB, Middleton NA, Theriot JJ, Parker PD, Abdullah OM, Ju YS, et al. Susceptibility of Primary Sensory Cortex to Spreading Depolarizations. J Neurosci

[Internet]. 2016 Apr 27 [cited 2019 May 29];36(17):4733–43. Available from: http://www.jneurosci.org/content/36/17/4733

231. Dreier JP, Fabricius M, Ayata C, Sakowitz OW, William Shuttleworth C, Dohmen C, et al. Recording, analysis, and interpretation of spreading depolarizations in neurointensive care: Review and recommendations of the COSBID research group. Vol. 37, Journal of Cerebral Blood Flow and Metabolism. Nature Publishing Group; 2017. p. 1595–625.

232. Maslarova A, Alam M, Reiffurth C, Lapilover E, Gorji A, Dreier JP. Chronically Epileptic Human and Rat Neocortex Display a Similar Resistance Against Spreading Depolarization In Vitro. Stroke [Internet]. 2011 Oct [cited 2019 Jun 20];42(10):2917–22. Available from: http://www.ncbi.nlm.nih.gov/pubmed/21836085

233. Bouley J, Chung DY, Ayata C, Brown RH, Henninger N. Cortical Spreading Depression Denotes Concussion Injury. J Neurotrauma [Internet]. 2019 Apr 1 [cited 2019 Aug 2];36(7):1008–17. Available from: http://www.ncbi.nlm.nih.gov/pubmed/29999455

234. Dreier JP, Reiffurth C. The Stroke-Migraine Depolarization Continuum. Neuron [Internet]. 2015;86(4):902–22. Available from: http://dx.doi.org/10.1016/j.neuron.2015.04.004

235. Lauritzen M, Dreier JP, Fabricius M, Hartings JA, Graf R, Strong AJ. Clinical relevance of cortical spreading depression in neurological disorders: migraine, malignant stroke, subarachnoid and intracranial hemorrhage, and traumatic brain injury. J Cereb Blood Flow Metab [Internet]. 2011 Jan [cited 2019 Jun 20];31(1):17–35. Available from: http://www.ncbi.nlm.nih.gov/pubmed/21045864

236. Kager H, Wadman WJ, Somjen GG. Conditions for the Triggering of Spreading Depression Studied With Computer Simulations Downloaded from. J Neurophysiol [Internet]. 2002 [cited 2019 Dec 24];88:2700–12. Available from: www.jn.org

237. Hartings JA, York J, Carroll CP, Hinzman JM, Mahoney E, Krueger B, et al. Subarachnoid blood acutely induces spreading depolarizations and early cortical infarction. Brain [Internet]. 2017 [cited 2018 Oct 25];140(10):2673–90. Available from: http://www.ncbi.nlm.nih.gov/pubmed/28969382

238. Teasell R, Bayona N, Lippert C, Villamere J, Hellings C. Post-traumatic seizure disorder following acquired brain injury. Brain Inj. 2007;21(2):201–14.

239. Akcali D, Sayin A, Sara Y, Bolay H. Does single cortical spreading depression elicit pain behaviour in freely moving rats? Cephalalgia. 2010;30(10):1195–206.

240. Yavich L, Ylinen A. Spreading depression in the cortex differently modulates dopamine release in rat mesolimbic and nigrostriatal terminal fields. Exp Neurol. 2005;196(1):47–53.

241. Leviel V, Gobert A, Guibert B. The glutamate-mediated release of dopamine in the rat striatum: further characterization of the dual excitatory-inhibitory function. Neuroscience [Internet]. 1990 [cited 2019 Jul 7];39(2):305–12. Available from: http://www.ncbi.nlm.nih.gov/pubmed/1982344

242. Krebs MO, Desce JM, Kemel ML, Gauchy C, Godeheu G, Cheramy A, et al. Glutamatergic Control of Dopamine Release in the Rat Striatum: Evidence for Presynaptic N-Methyl-D-Aspartate Receptors on Dopaminergic Nerve Terminals. J Neurochem [Internet]. 1991 Jan [cited 2019 Jul 7];56(1):81–5. Available from: http://www.ncbi.nlm.nih.gov/pubmed/1824785

243. Haarmann AM, Jafarian M, Karimzadeh F, Gorji A. Modulatory Effects of Dopamine D2 Receptors on Spreading Depression in Rat Somatosensory Neocortex. Basic Clin Neurosci [Internet]. 2014 Oct [cited 2019 Jul 7];5(4):246–52. Available from: http://www.ncbi.nlm.nih.gov/pubmed/27284388

244. Taber MT, Fibiger HC. Electrical stimulation of the prefrontal cortex increases dopamine release in the nucleus accumbens of the rat: modulation by metabotropic glutamate receptors. J Neurosci [Internet]. 1995 May [cited 2019 Jul 7];15(5 Pt 2):3896–904. Available from: http://www.ncbi.nlm.nih.gov/pubmed/7751954

245. Karreman M, Moghaddam B. The Prefrontal Cortex Regulates the Basal Release of Dopamine in the Limbic Striatum: An Effect Mediated by Ventral Tegmental Area. J Neurochem [Internet]. 2002 Nov 23 [cited 2019 Jul 7];66(2):589–98. Available from: http://www.ncbi.nlm.nih.gov/pubmed/8592128

246. Takagaki M, Feuerstein D, Kumagai T, Gramer M, Yoshimine T, Graf R. Isoflurane suppresses cortical spreading depolarizations compared to propofol - Implications for sedation of neurocritical care patients. Exp Neurol [Internet]. 2014;252:12–7. Available from: http://dx.doi.org/10.1016/j.expneurol.2013.11.003

247. Dreier JP, Major S, Manning A, Woitzik J, Drenckhahn C, Steinbrink J, et al. Cortical spreading ischaemia is a novel process involved in ischaemic damage in patients with aneurysmal subarachnoid haemorrhage. Brain. 2009;132(7):1866–81.

248. Schinke C, Schlemm L, Wawra M, Dreier JP, Horst V, Scheel M, et al. A case report of delayed cortical infarction adjacent to sulcal clots after traumatic subarachnoid hemorrhage in the absence of proximal vasospasm. BMC Neurol. 2018;18(1):1–5.

249. Mckee AC, Daneshvar DH. The neuropathology of traumatic brain injury. Handb Clin Neurol [Internet]. 2015 [cited 2019 Feb 27];127:45–66. Available from: http://www.ncbi.nlm.nih.gov/pubmed/25702209

250. McAteer KM, Corrigan F, Thornton E, Turner RJ, Vink R. Short and long term behavioral and pathological changes in a novel rodent model of repetitive mild traumatic brain injury. PLoS One. 2016;11(8):1–18.

251. Cohen A, Shelef I, Benifla M, Friedman A, Feintuch A, Tomkins O. Blood-Brain Barrier Breakdown Following Traumatic Brain Injury: A Possible Role in

Posttraumatic Epilepsy. Cardiovasc Psychiatry Neurol. 2011;2011:1–11.

252. A.I. O-F, M.K.L. W, C. R, D. M, J. W, J.P. D. Spreading depolarization, a pathophysiological mechanism of stroke and migraine aura. Future Neurol [Internet]. 2012;7(1):45–64. Available from: http://www.embase.com/search/results?subaction=viewrecord&from=export&id=L363101109%0Ahttp://dx.doi.org/10.2217/fnl.11.69%0Ahttp://sfx.library.uu.nl/utrecht?sid=EMBASE&issn=14796708&id=doi:10.2217%2Ffnl.11.69&atitle=Spreading+depolarization%2C+a+pathophys

253. Schiering IAM, De Haan TR, Niermeijer J-MF, Koelman JH, Majoie CBLM, Reneman L, et al. Correlation Between Clinical and Histologic Findings in the Human Neonatal Hippocampus After Perinatal Asphyxia. [cited 2017 Aug 16]; Available from: http://www.sectionz.nl/cms/LIESBETHRENEMAN/media/pdf/62.pdf

254. Abbott NJ, Friedman A. Overview and introduction: the blood-brain barrier in health and disease. Epilepsia [Internet]. 2012;53 Suppl 6:1–6. Available from: http://www.pubmedcentral.nih.gov/articlerender.fcgi?artid=3625728&tool=pmcentrez&rendertype=abstract

255. Schoknecht K, Shalev Y. Blood–brain barrier dysfunction in brain diseases: Clinical experience. [cited 2018 Jun 9]; Available from: https://onlinelibrary.wiley.com/doi/pdf/10.1111/j.1528-1167.2012.03697.x

256. Lublinsky S, Major S, Kola V, Horst V, Santos E, Platz J, et al. Early blood-brain barrier dysfunction predicts neurological outcome following aneurysmal subarachnoid hemorrhage. EBioMedicine. 2019 May 1;43:460–72.

257. Masuda H, Ushiyama A, Hirota S, Lawlor GF, Ohkubo C. Long-term observation of pial microcirculatory parameters using an implanted cranial window method in the rat. In Vivo (Brooklyn). 2007;21(3):471–80.

258. Lapilover EG, Lippmann K, Salar S, Maslarova A, Dreier JP, Heinemann U, et al. Peri-infarct blood-brain barrier dysfunction facilitates induction of spreading depolarization associated with epileptiform discharges. Neurobiol Dis [Internet]. 2012;48(3):495–506. Available from: http://dx.doi.org/10.1016/j.nbd.2012.06.024

259. Manaenko A, Chen H, Kammer J, Zhang JH, Tang J. Comparison Evans Blue injection routes: Intravenous versus intraperitoneal, for measurement of blood-brain barrier in a mice hemorrhage model. J Neurosci Methods [Internet]. 2011;195(2):206–10. Available from: http://dx.doi.org/10.1016/j.jneumeth.2010.12.013

260. Dirnagl U, Kaplan B, Jacewicz M, Pulsinelli W. Continuous measurement of cerebral cortical blood flow by laser-Doppler flowmetry in a rat stroke model. J Cereb Blood Flow Metab. 1989;9(5):589–96.

261. Davis TP, Cottier KE, Liktor-Busa E, Calabrese EC, Vanderah TW, Kim J, et al. Loss of Blood-Brain Barrier Integrity in a KCl-Induced Model of Episodic

Headache Enhances CNS Drug Delivery. Eneuro. 2018;5(4):ENEURO.0116-18.2018.

262. Vazana U, Veksler R, Pell GS, Prager O, Fassler M, Chassidim Y, et al. Glutamate-Mediated Blood-Brain Barrier Opening: Implications for Neuroprotection and Drug Delivery. J Neurosci [Internet]. 2016;36(29):7727–39. Available from: http://www.jneurosci.org/cgi/doi/10.1523/JNEUROSCI.0587-16.2016

263. Nilsson P, Ronne-Engström E, Flink R, Ungerstedt U, Carlson H, Hillered L. Epileptic seizure activity in the acute phase following cortical impact trauma in rat. Brain Res. 1994;637(1–2):227–32.

264. Palmer AM, Marion DW, Botscheller ML, Bowen DM, Dekosky ST. Increased transmitter amino acid concentration in human ventricular CSF after brain trauma. Vol. 6, NeuroReport. 1994. p. 153–6.

265. Martin NA, Ronne-Engstrom E, Caron M, Becker DP, Hovda DA, Shalmon E, et al. Increase in extracellular glutamate caused by reduced cerebral perfusion pressure and seizures after human traumatic brain injury: a microdialysis study. J Neurosurg. 2009;89:971–82.

266. Folkersma H, Foster Dingley JC, Nm Van Berckel B, Rozemuller A, Boellaard R, Huisman MC, et al. Increased cerebral (R)-[11 C]PK11195 uptake and glutamate release in a rat model of traumatic brain injury: a longitudinal pilot study [Internet]. 2011 [cited 2019 Mar 21]. Available from: http://www.jneuroinflammation.com/content/8/1/67

267. Krüger H, Heinemann U, Luhmann HJ. Effects of ionotropic glutamate receptor blockade and 5-HT1A receptor activation on spreading depression in rat neocortical slices. Neuroreport [Internet]. 1999 Aug 20 [cited 2019 Mar 2];10(12):2651–6. Available from: http://www.ncbi.nlm.nih.gov/pubmed/10574386

268. Kramer DR, Fujii T, Ohiorhenuan I, Liu CY. Interplay between Cortical Spreading Depolarization and Seizures. Stereotact Funct Neurosurg. 2017;95(1):1–5.

269. Gorji A, Speckmann E. Spreading depression enhances the spontaneous epileptiform activity in human neocortical tissues. 2004;19:3371–4. Available from: http://apps.webofknowledge.com/full_record.do?product=UA&search_mode=GeneralSearch&qid=2&SID=2Eib@39kfeANoPp2jal&page=3&doc=22

270. Back T, Ginsberg MD, Dietrich WD, Watson BD. Journal of Cerebral Blood Flow and Metabolism Induction of Spreading Depression in the Ischemic Hemisphere Following Experimental Middle Cerebral Artery Occlusion: Effect on Infarct Morphology [Internet]. [cited 2018 Oct 28]. Available from: http://journals.sagepub.com/doi/pdf/10.1097/00004647-199603000-00004

271. Dreier JP, Major S, Foreman B, Winkler MKL, Kang EJ, Milakara D, et al.

Terminal spreading depolarization and electrical silence in death of human cerebral cortex. Ann Neurol. 2018;83(2):295–310.

272. Chung DY, Oka F, Ayata C. Spreading Depolarizations: A Therapeutic Target Against Delayed Cerebral Ischemia After Subarachnoid Hemorrhage. J Clin Neurophysiol [Internet]. 2016 Jun [cited 2018 Oct 27];33(3):196–202. Available from: http://www.ncbi.nlm.nih.gov/pubmed/27258442

273. Kudo C, Nozari A, Moskowitz MA, Ayata C. The impact of anesthetics and hyperoxia on cortical spreading depression. Exp Neurol. 2008;212(1):201–6.

274. Zandt B-J, Ten Haken B, Van Putten MJAM. Neurobiology of Disease Diffusing Substances during Spreading Depolarization: Analytical Expressions for Propagation Speed, Triggering, and Concentration Time Courses. 2013 [cited 2019 Mar 4]; Available from: http://www.jneurosci.org/content/jneuro/33/14/5915.full.pdf

275. Aiba I, Carlson AP, Sheline CT, Shuttleworth CW. Synaptic release and extracellular actions of Zn2+ limit propagation of spreading depression and related events in vitro and in vivo. J Neurophysiol [Internet]. 2012 Feb [cited 2019 Mar 4];107(3):1032–41. Available from: http://www.ncbi.nlm.nih.gov/pubmed/22131381

276. Van Den Maagdenberg AMJM, Pietrobon D, Pizzorusso T, Kaja S, Broos LAM, Cesetti T, et al. A Cacna1a knockin migraine mouse model with increased susceptibility to cortical spreading depression. Neuron. 2004;41(5):701–10.

277. Carlà V, Moroni F. General anaesthetics inhibit the responses induced by glutamate receptor agonists in the mouse cortex. Neurosci Lett [Internet]. 1992 Oct 26 [cited 2019 Apr 20];146(1):21–4. Available from: http://www.ncbi.nlm.nih.gov/pubmed/1282227

278. Dickinson R, Peterson BK, Banks P, Simillis C, Martin JCS, Valenzuela CA, et al. Competitive Inhibition at the Glycine Site of the N-Methyl-d-aspartate Receptor by the Anesthetics Xenon and Isoflurane. Anesthesiology [Internet]. 2007 Nov [cited 2019 Apr 20];107(5):756–67. Available from: http://www.ncbi.nlm.nih.gov/pubmed/18073551

279. Piper RD, Lambert GA, Duckworth JW. Cortical blood flow changes during spreading depression in cats. Am J Physiol Circ Physiol [Internet]. 1991 Jul [cited 2019 Mar 9];261(1):H96–102. Available from: http://www.ncbi.nlm.nih.gov/pubmed/1858935

280. Dreier JP, K??rner K, Ebert N, G??rner A, Rubin I, Back T, et al. Nitric Oxide Scavenging by Hemoglobin or Nitric Oxide Synthase Inhibition by N-Nitro-L-Arginine Induces Cortical Spreading Ischemia When K+ Is Increased in the Subarachnoid Space. J Cereb Blood Flow Metab [Internet]. 1998 Sep [cited 2017 Aug 25];978–90. Available from: http://jcb.sagepub.com/lookup/doi/10.1097/00004647-199809000-00007

281. Taylor CA, Bell JM, Breiding MJ, Xu L. Traumatic Brain Injury–Related Emergency Department Visits, Hospitalizations, and Deaths — United States, 2007 and 2013. MMWR Surveill Summ. 2017;66(9):1–16.

282. Leo AAP. FURTHER OBSERVATIONS ON THE SPREADING DEPRESSION OF ACTIVITY IN THE CEREBRAL CORTEX. J Neurophysiol [Internet]. 1947 Nov [cited 2019 Jun 3];10(6):409–14. Available from: http://www.physiology.org/doi/10.1152/jn.1947.10.6.409

283. Fleidervish IA, Gebhardt C, Astman N, Gutnick MJ, Heinemann U. Enhanced Spontaneous Transmitter Release Is the Earliest Consequence of Neocortical Hypoxia That Can Explain the Disruption of Normal Circuit Function. J Neurosci. 2018;21(13):4600–8.

284. HANSEN AJ, HOUNSGAARD J, JAHNSEN H. Anoxia increases potassium conductance in hippocampal nerve cells. Acta Physiol Scand. 1982;115(3):301–10.

285. Fujimura N, Tanaka E, Yamamoto S, Shigemori M, Higashi H. Contribution of ATP-Sensitive Potassium Channels to Hypoxic Hyperpolarization in Rat Hippocampal CA1 Neurons In Vitro. J Neurophysiol [Internet]. 1997 Jan [cited 2019 Jun 4];77(1):378–85. Available from: http://www.ncbi.nlm.nih.gov/pubmed/9120578

286. Karschin C, Ecke C, Ashcroft FM, Karschin A. Overlapping distribution of K(ATP) channel-forming Kir6.2 subunit and the sulfonylurea receptor SUR1 in rodent brain. FEBS Lett [Internet]. 1997 Jan 13 [cited 2019 Jun 4];401(1):59–64. Available from: http://www.ncbi.nlm.nih.gov/pubmed/9003806

287. Pelletier MR, Pahapill PA, Pennefather PS, Carlen PL. Analysis of Single K_{ATP} Channels in Mammalian Dentate Gyrus Granule Cells. J Neurophysiol [Internet]. 2000 Nov [cited 2019 Jun 4];84(5):2291–301. Available from: http://www.ncbi.nlm.nih.gov/pubmed/11067973

288. Martin RL, Lloyd HG, Cowan AI. The early events of oxygen and glucose deprivation: setting the scene for neuronal death? Trends Neurosci [Internet]. 1994 Jun [cited 2019 Jun 3];17(6):251–7. Available from: http://www.ncbi.nlm.nih.gov/pubmed/7521086

289. Tanaka E, Yamamoto S, Kudo Y, Mihara S, Higashi H. Mechanisms Underlying the Rapid Depolarization Produced by Deprivation of Oxygen and Glucose in Rat Hippocampal CA1 Neurons In Vitro. J Neurophysiol [Internet]. 1997 Aug [cited 2019 Jun 3];78(2):891–902. Available from: http://www.physiology.org/doi/10.1152/jn.1997.78.2.891

290. Hossmann K-A. Viability thresholds and the penumbra of focal ischemia. Ann Neurol [Internet]. 1994 Oct [cited 2017 Aug 24];36(4):557–65. Available from: http://doi.wiley.com/10.1002/ana.410360404

291. Saito R, Graf R, Hübel K, Fujita T, Rosner G, Heiss W-D. Reduction of Infarct Volume by Halothane: Effect on Cerebral Blood Flow or Perifocal Spreading

Depression-Like Depolarizations. J Cereb Blood Flow Metab [Internet]. 1997 Aug [cited 2019 Jul 13];17(8):857–64. Available from: http://www.ncbi.nlm.nih.gov/pubmed/9290583

292. I. A, J.L. N. Spreading depolarization in the brainstem mediates sudden cardiorespiratory arrest in mouse SUDEP models. Sci Transl Med [Internet]. 2015;7(282). Available from: http://www.embase.com/search/results?subaction=viewrecord&from=export&id=L603773324%0Ahttp://dx.doi.org/10.1126/scitranslmed.aaa4050%0Ahttp://sfx.library.uu.nl/utrecht?sid=EMBASE&issn=19466242&id=doi:10.1126%2Fscitranslmed.aaa4050&atitle=Spreading+depolar

293. Ikeda K, Kawakami K, Onimaru H, Okada Y, Yokota S, Koshiya N, et al. The respiratory control mechanisms in the brainstem and spinal cord: integrative views of the neuroanatomy and neurophysiology. J Physiol Sci. 2017;67(1):45–62.

294. Farkas E, Pratt R, Sengpiel F, Obrenovitch TP. Direct, live imaging of cortical spreading depression and anoxic depolarisation using a fluorescent, voltage-sensitive dye. 2008 [cited 2019 Jul 13]; Available from: https://www.ncbi.nlm.nih.gov/pmc/articles/PMC2653938/pdf/ukmss-2706.pdf